THE
PHYSICAL REVIEW
A Journal of Experimental and Theoretical Physics Established by E. L. Nichols in 1893
VOL. 57, No. 8 APRIL 15, 1940 SECOND SERIES

The Relative Probability for the Loss of Neutrons and Alpha-Particles from an Excited Nucleus

J. M. CORK AND J. HALPERN
University of Michigan, Ann Arbor, Michigan
(Received February 15, 1940)

A stack of foils of very pure iron was bombarded with deuterons of energy 10 Mev. Excitation curves are thus obtained for a radioactive manganese of half-life 21 minutes made by a (D,α) reaction and a radioactive cobalt of half-life 18 hours, made by a (D,n) reaction. These radioactive isotopes are both derived from the same parent iron isotope. Hence the radioactive yields reveal the relative probability of the escape of a neutron and the escape of an alpha-particle from the same excited nucleus. As the energy of the incident deuterons is increased the intensity of the 18-hour (D,n) cobalt attains a maximum value at about 7.5 Mev. There is a progressive increase with energy in the activity of the 21-minute (D,α) radioactive manganese. At 10 Mev the escape of a neutron is about three times as probable as the escape of an alpha-particle.

WHEN iron is bombarded with deuterons, radioactive isotopes of manganese and cobalt are formed. Two of these radioactivities have half-lives of 21 minutes and 18 hours, respectively, and decay by the emission of positrons. They have been assigned[1] with a reasonable degree of certainty to Mn^{52} and Co^{55}, respectively, both being derived from the same parent isotope, Fe^{54}, whose abundance in iron is only 6.5 percent. These reactions are therefore as follows:

$$_{26}Fe^{54}+{}_{1}H^{2}+E\rightarrow{}_{27}Co^{56*}\rightarrow{}_{27}Co^{55}+{}_{0}n^{1}$$

or

$$_{27}Co^{56*}\rightarrow{}_{25}Mn^{52}+{}_{2}He^{4}.$$

It was previously suggested that this would allow a unique observation of the relative escape probability for a neutron and for an alpha-particle from the same excited nucleus and a preliminary report[2] of results was made.

In the present investigation a stack of foils of very pure iron was exposed to the deuteron beam of range 64 cm in air. Each foil had a stopping power equivalent to about 3 cm of air, experimentally determined. After a bombardment of about 100 microampere minutes, at a current of 15 microamperes, the activity in each foil was studied by the use of a freon-filled ionization chamber connected to a string electrometer. With pure iron, no other radioactivities are produced in sufficient amounts to confuse the analysis of the decay curves. It was thus possible to determine the mean energy for the deuterons passing through any foil and the total yields of the cobalt isotope of half-life 18 hours and the manganese isotope of half-life 21 minutes in every foil.

These yields were first expressed in terms of divisions per second of the electrometer at the end of the bombardment. It is now possible to convert these observed intensities actually to the total number of activated nuclei formed. This was done by collecting on a small clean metallic surface a small quantity of actinon gas. In decaying to Pb^{207} every actinium B atom emits one

[1] B. T. Darling, B. R. Curtis and J. M. Cork, Phys. Rev. **51**, 1010 (1937); J. Livingood and G. T. Seaborg, Phys. Rev. **54**, 51 (1938).
[2] J. M. Cork and B. R. Curtis, Phys. Rev. **53**, 946 1938); **55**, 1264 (1939).

alpha-particle and two beta-particles. The half-life of 36 minutes associated with the beta-decay of actinium B is long compared to the half-lives of the subsequent emitters. The alpha-particles could be completely counted by an appropriate ionization chamber and linear amplifier. This then became an exact source of beta-particles, which could be used to calibrate the electrometer. It is assumed that the energies of the beta-particles are such that the number that do not enter the thin window and completely traverse the ionization chamber is negligibly small. It is also necessary to cover the actinon with a very thin absorbing layer sufficient to prevent the escape of the heavy nuclei by recoil upon disintegration, yet not enough to stop the 6.6-Mev alpha-particles.

The data obtained with such a stack of foils, with the energy expressed in Mev are shown in Fig. 1. Four such sets of foils were studied giving in each case results similar to that shown. The ordinates, while labeled relative cross sections, may be made absolute by the fact that at the number 100 the cross section is about 1×10^{-27} cm². The cover foil was in each case rejected as it appeared to have too little activity. This is due to the fact that some of the recoil atoms from every foil are driven into the next underlying foil. Even after rejecting the cover foil there still

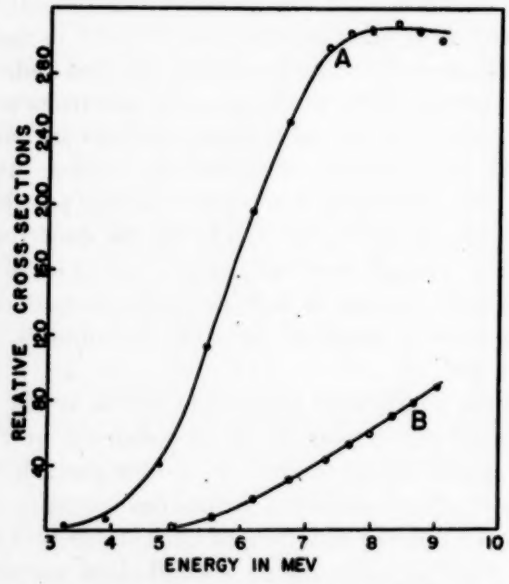

FIG. 1. Excitation curves for (*A*) $Fe(D,n)Co$ and (*B*) $Fe(D,\alpha)Mn$ expressed in terms of cross section. At 100, σ equals 1×10^{-27} cm².

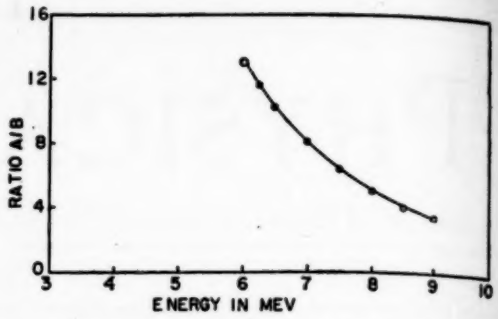

FIG. 2. Variation with energy of the ratio of escape probability of neutron to escape probability of an alpha-particle.

seems to be a very slight increase in the 18-hour cobalt activity in going to deeper foils before a rapid decrease is observed. No such saturation was observed for the 21-minute manganese activity.

In Fig. 2 is shown the ratio of the yield of the 18-hour (D,n) cobalt to the corresponding yield for the 21-minute (D,α) manganese. In both processes the deuteron as a whole has entered the nucleus through the potential barrier; that is, the Oppenheimer-Phillips splitting of the deuteron in the external field would play no part in these reactions. If the masses of the incoming deuteron and its incident energy be compared with (*a*) the mass of the escaping neutron and (*b*) the mass of the escaping alpha-particle, and if we assume the same nuclear defect for original and final atoms the limiting energy of the escaping particles can be determined. For an incident deuteron of 10 Mev the neutron could have a maximum energy of 15 Mev and the alpha-particle an energy of 20 Mev.

It may perhaps be reasonable that the observed yield of 18-hour (D,n) cobalt attain a maximum value and then fall off slightly as the energy of the incident particles is increased. This would be the case, if with increasing energy the probability of the competing (D,α) process became greater and the total number of excited atoms remained the same. Since the incident deuteron energies are much in excess of the nuclear barrier it might be expected that the number of excited nuclei would be constant. At 10 Mev the possibility of a neutron being emitted is about three times as probable as the emission of an alpha-particle.

This investigation is made possible by a grant from the Horace H. Rackham Fund.

Anomalous Scattering of Fast Neutrons

M. R. MacPhail
*Palmer Physical Laboratory, Princeton University, Princeton, New Jersey**
(Received January 20, 1940)

The cross sections of a number of elements for neutron scattering were measured as a function of neutron energy throughout a range of 0.5 Mev. Anomalous cross sections were found in the cases of magnesium and aluminum. It was possible to account quantitatively for the anomaly in magnesium on the assumption that the effect was due to resonance in Mg^{25}.

Introduction

THE first measurements of nuclear cross sections for fast neutron scattering were made by Dunning in 1934.[1] Using neutrons from a mixture of radon and beryllium whose energies ranged from about 0.1 to nearly 14 Mev, he concluded that the cross section of a nucleus of atomic weight A was proportional to $A^{\frac{1}{3}}$. This cross section was, of course, an average with respect to neutron energy. More recently, Ladenburg and Kanner,[2] and Kikuchi and Aoki[2a] remeasured the cross sections of a large number of nuclei, using the nearly homogeneous neutrons produced in the deuteron-deuteron reaction. They found that the cross section for these neutrons was not proportional to $A^{\frac{1}{3}}$, and in fact was not a monotonic function of the atomic weight. Evidently then, even for fast neutrons, nuclear cross sections must have been appreciably dependent on neutron energy. It therefore seemed worth while to measure throughout as wide an energy range as possible the cross sections of a number of elements in order to verify the expected energy dependence, and, more important, to see if there were anomalous scattering. The experimental results were reported some time ago.[3] Aoki[4] had previously reported a similar effect in silicon, and recently in more extended experiments[5] found a number of additional anomalies. Other work has also been reported by Zinn, Seely, and Cohen.[6]

The Apparatus

The neutrons were produced by the action of 100-kv deuterons on targets of heavy ice. The deuteron source and discharge tube were similar to the source and discharge tube described by Zinn and Seely.[7, 8] The ion beam was unanalyzed because it was thought undesirable to have a contamination target of variable strength formed where the discarded beam would hit the walls of the discharge tube. Ion currents used were from 600 to 1000 microamperes, the upper limit being set by the amount of heat which could be dissipated at the target. This was a cylindrical copper box cooled with liquid air, on the front face of which heavy water was condensed. The 100-kv accelerating voltage was supplied by an x-ray transformer-rectifier set.

For counting neutrons, a system consisting of a paraffin-lined ionization chamber, linear amplifier,[9] and thyratron counter[10] was used. The ionization chamber and linear amplifier were mounted on a light table which could be easily rolled about on wheels. A Lauritsen electroscope[11] lined with paraffin was used to measure the neutron intensity.

The arrangement of the apparatus is shown schematically in Fig. 1. The target, scatterer, ionization chamber, and electroscope are represented, respectively, by T, S, I, and E. Scatterers were cylindrical and were slightly larger in di-

* Now with the Standard Oil Company of Venezuela, Caracas.

[1] J. R. Dunning, Phys. Rev. **45**, 586 (1934).
[2] R. Ladenburg and M. H. Kanner, Phys. Rev. **52**, 911 (1937).
[2a] S. Kikuchi and H. Aoki, Sci. Papers of the Inst. of Phys. and Chem. Research **34**, 865 (1938).
[3] M. MacPhail and J. Giarratana, Phys. Rev. **56**, 207 (1939).
[4] H. Aoki, Phys. Rev. **55**, 795 (1939).
[5] H. Aoki, Proc. Phys. Math. Soc. Japan **21**, 232 (1939).
[6] Zinn, Seely, and Cohen, Phys. Rev. **56**, 260 (1939).
[7] W. H. Zinn, Phys. Rev. **52**, 655 (1937).
[8] W. H. Zinn and S. Seely, Phys. Rev. **52**, 919 (1937).
[9] J. R. Dunning, Rev. Sci. Inst. **5**, 387 (1934).
[10] J. Giarratana, Rev. Sci. Inst. **8**, 390 (1937).
[11] C. C. Lauritsen and T. Lauritsen, Rev. Sci. Inst. **8**, 438 (1937).

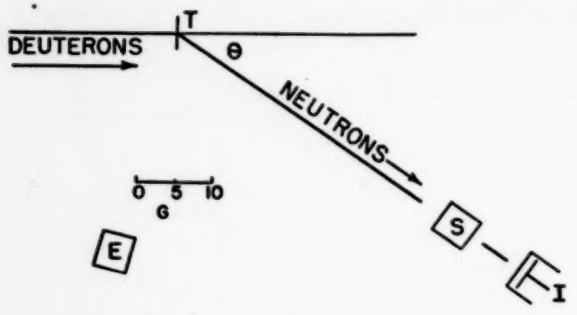

FIG. 1. Arrangement of neutron source T, electroscope E, scatterer S, and ionization chamber I.

ameter than the ionization chamber (4.2 cm) and between 4 and 6 cm in length.

The neutron energy was varied by rotating the counter and scatterer about the target, that is, by varying the angle θ between the paths of the neutrons and the deuterons. The following relation obtained from the equations of conservation of energy and momentum gives the dependence of neutron energy E_n on the deuteron energy E_D and angle θ:

$$E_n-(E_DE_n/2)^{\frac{1}{2}}\cos\theta-(E_D+3Q)/4=0.$$

Q, the energy released in the reaction $D^2+D^2\rightarrow He^3+n^1+Q$, was taken to be 3.32 Mev.[12] The dependence of the neutron energy on θ is shown graphically in Fig. 2 for deuteron energies of 0.10 and 0.05 Mev which are the energies of the D^+ and D_2^+ ions, respectively. Because of the presence of both kinds in the beam and because of the slowing down of the deuterons in the ice target, the neutrons will have a spread of energy corresponding to that of the deuterons from 0 to 0.10 Mev.

EXPERIMENTAL PROCEDURE

The cross section for a particular scatterer was calculated from the measured transmission, i.e., the ratio of the number of neutrons indicated by the counter with the scatterer in front of it to that indicated with the scatterer removed, the times being such that the electroscope deflections in each case were the same. A correction was made for the number of neutrons deflected by the scatterer into the ionization chamber on the assumption that the scattering was isotropic. For the dimensions indicated in Fig. 1 and a measured transmission t, this was $0.01(1-t)$ and was to be subtracted from t. A second small correction due to the finite width of the neutron energy spectrum will be given later. From the corrected transmission t_0 thus obtained, the cross section σ was calculated by means of the formula $\sigma=(MA/Nm)\log(1/t_0)$ where A is the area of a face of the scatterer, m its mass, M its atomic or molecular weight, and N Avogadro's number. The exponential law of absorption on which this formula rests was tested by measuring the transmission as a function of length through scatterers of aluminum. The results of two tests are given in Fig. 3.

The intensity of scattered neutrons coming from the walls and floor of the room was estimated by measuring neutron intensity as a function of the distance D of the counter from the target. The results of two tests made at 0° and 90° to the deuteron beam are shown graphically in Fig. 4. All measurements of transmissions were done at a distance of 56 cm from the target for which $D^{-2}=320\times10^{-6}$ cm^{-2}. The intercept at $D^{-2}=0$, i.e., the proportion of neutrons scattered by the walls and floor, is less than 3 percent of the number at 56 cm coming from the target. The effect of these scattered neutrons would be to decrease the cross section from 0 to 3 percent depending on their intensity. But as the intenisty

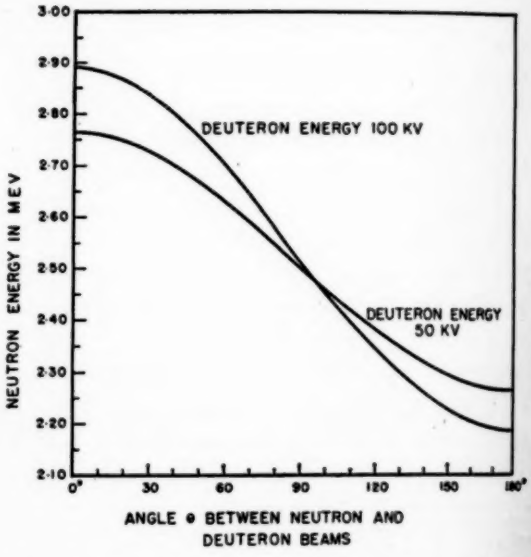

FIG. 2. Neutron energy as a function of the angle of emission for a thin target.

[12] L. G. Bonner, Nature **143**, 681 (1939).

of the scattered neutrons is probably about the same for all values of θ, a correction, if it could be made, would only increase the cross sections at each energy by a small amount.

Because of the finite width of the energy spectrum and the finite angle subtended at the target by the neutron counter, the measured transmission is an average value, the average being taken first with respect to neutron energy and then over the face of the ionization chamber. A simple calculation gives

$$t(\theta)=t_0(E_0)+\frac{1}{2}\left[\frac{\eta^2}{4}\frac{d^2E_0}{d\theta^2}\cdot\frac{dt_0}{dE_0}+(h^2+k^2)\frac{d^2t_0}{dE_0^2}\right]+\cdots \quad (1)$$

where $t(\theta)$ is the transmission measured at angle θ (the angle between the direction of the deuterons and the line through the target and the center of the ionization chamber), $t_0(E_0)$ the transmission for homogeneous neutrons of energy E_0, E_0 the average energy of the neutrons emitted at angle θ, η the angle subtended by the radius of the ionization chamber at the target,

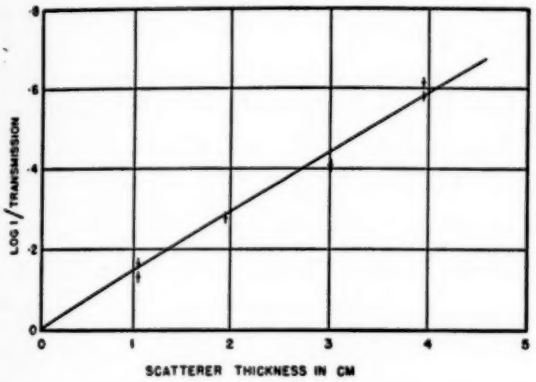

FIG. 3. Experimental test of the exponential law of absorption for the case of aluminum.

$h=\frac{1}{2}\eta dE_0/d\theta$ the root-mean-square variation of neutron energy across the ionization chamber, and k the root-mean-square variation of the neutron energy about the average, E_0, due to the lack of homogeneity of the neutron beam at a given angle θ. The term in square brackets is to a first approximation the effect on the transmission of finite resolving power determined by h and k. We shall neglect terms beyond it which is equivalent to assuming that the transmission-

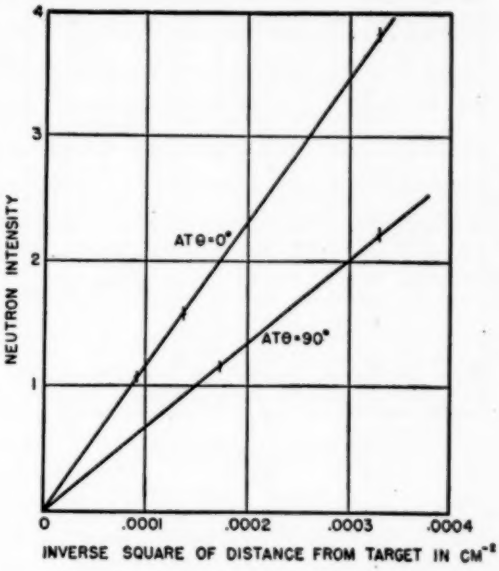

FIG. 4. Testing of the inverse square law; if scattering from the walls of the room were appreciable, the lines would not pass through the origin.

energy curves show no fine structure. Replacing t_0 by t in the square brackets, we can then solve (1) for t_0 in terms of the measurable quantities, $t(\theta)$ and its first two derivatives; i.e.,

$$t_0(E_0)=t(\theta)-\left[\frac{\eta^2}{8}\frac{d^2E_0}{d\theta^2}\cdot\frac{dt}{dE_0}+\frac{1}{2}(h^2+k^2)\frac{d^2t}{dE_0^2}\right]. \quad (2)$$

The first term in the square brackets turns out to be 10^{-4} or less, so is negligible. The other term represents the combined effects of an ionization chamber of finite size and of inhomogeneous neutrons. It is seen to sharpen the transmission curves by raising the peaks and lowering the hollows where d^2t/dE_0^2 is, respectively, negative and positive. This is of course what one would expect.

To obtain E_0 and k as functions of θ, it is necessary to calculate the neutron spectrum. Thus, if the number of neutrons emitted at angle θ with energies between E and $E+dE$ is $f(E)dE$, then

$$DE_0=\int_0^\infty Ef(E)dE$$

and

$$Dk^2=\int_0^\infty (E-E_0)^2f(E)dE, \quad \left[D=\int_0^\infty f(E)dE\right].$$

The function $f(E)$ was calculated on the assump-

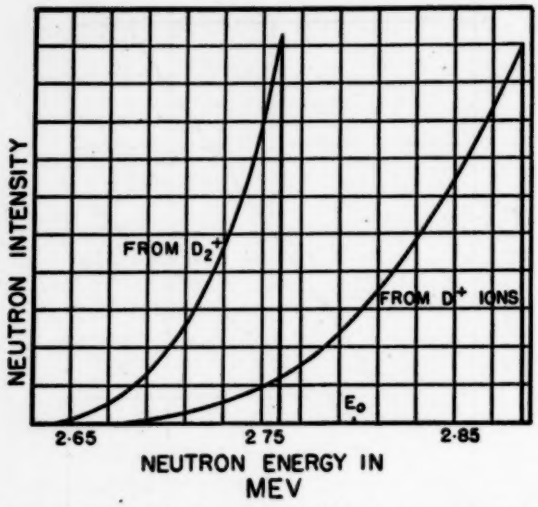

FIG. 5. Distribution in energy of the neutrons coming off the target in the forward direction calculated for 100 kv accelerating potential for the cases (*a*) pure molecular beam, (*b*) pure atomic beam.

tion that the ice target was thick (an effort was made always to fulfill this condition experimentally), and that the unanalyzed beam of deuterons was 20 percent atomic and 80 percent molecular. In addition, the 1 Mev group of neutrons reported by Bonner[12] and others was not taken into consideration because of general uncertainty regarding it. The excitation function used was that given by Baldinger, Huber, and Staub.[13] By way of an example, the neutron spectrum calculated in this way for $\theta=0°$ is given in Fig. 5. Values of E_0 and k for $\theta=0°$ and certain additional angles are listed in the following table:

θ	0°	58°	76°	92°	109°	129°
E_0 (Mev)	2.80	2.65	2.57	2.49	2.41	2.34
k (Mev)	0.065	0.035	0.020	0.009	0.010	0.025

The other quantities in square brackets in (2), namely, $h=\eta dE_0/2d\theta$, $d^2E_0/d\theta^2$, dt/dE_0, and d^2t/dE_0^2, were found graphically. As mentioned before, the correction was entirely due to the term $-\frac{1}{2}(h^2+k^2)d^2t/dE_0^2$. In absolute magnitude it was in every case between 0 and 0.008; that is, it was of the order of 1 percent or less of t.

The cross section for each material and for each chosen neutron energy was calculated from the corresponding transmission after the corrections mentioned above had been applied. This value of the transmission was the average of from five to twenty measurements made on different days. The probable error of the average transmission was calculated from the deviations of the individual values about their means. In Table I are given as functions of neutron energy the average transmission (corrected), its probable error, and the corresponding cross section in units of 10^{-24} cm^2.

The cross sections given in Table I are plotted against neutron energy in Fig. 6. The coordinates of the center of each rectangle are the most probable values of the cross section and the

[13] Baldinger, Huber, and Staub, Helv. Phys. Acta **11**, 245 (1938).

TABLE I. *Average corrected transmission coefficients, their probable error (P.E.) and cross section in units of 10^{-24} cm^2 as functions of neutron energy.*

E (Mev)	2.80	2.65	2.57	2.49	2.41	2.34
			Aluminum (thickness 10.6 g cm^{-2})			
Trans.	0.556	0.496	0.496	0.598	0.596	0.556
P.E.	0.004	0.005	0.004	0.003	0.006	0.006
σ_{Al}	2.48	2.94	2.94	2.18	2.19	2.49
			Magnesium (thickness 8.75 g cm^{-2})			
Trans.	0.602	0.576	0.630	0.684	0.657	0.623
P.E.	0.007	0.006	0.007	0.004	0.006	0.010
σ_{Mg}	2.34	2.54	2.14	1.76	1.94	2.19
			Carbon (thickness 7.80 g cm^{-2})			
Trans.	0.543	0.566	0.585	0.585	0.580	0.579
P.E.	0.006	0.007	0.005	0.005	0.003	0.010
σ_C	1.57	1.45	1.38	1.38	1.39	1.41
			Sodium (thickness 5.73 g cm^{-2})			
Trans.	0.700	0.686	0.668	0.668	0.668	0.663
P.E.	0.004	0.007	0.007	0.005	0.006	0.006
σ_{Na}	2.38	2.50	2.69	2.69	2.69	2.74
			Sodium azide (NaN_3) (thickness 6.78 g cm^{-2})			
Trans.	0.680	0.671	0.650	0.665	0.671	0.656
P.E.	0.004	0.007	0.006	0.006	0.002	0.013
σ_{NaN_3}	6.13	6.35	6.86	6.50	6.35	6.72
σ_N	1.25	1.28	1.39	1.27	1.22	1.33

corresponding energy. The height of the rectangles for a given element is the experimental probable error in σ. This was calculated from the average observed probable error of the corresponding transmissions. Widths of the rectangles indicate the amounts by which the neutron energy would change due to a change in proportion of atomic deuterons in the beam from 10 to 30 percent about a mean of 20 percent. The side of the rectangle corresponding to 10 percent atoms is the one nearer the energy of 2.50 Mev.

There are two additional possible sources of error in the neutron energies:

1. An error dQ in the Q value for the D−D reaction would cause the cross-section curves to be shifted horizontally by approximately $3dQ/4$. Bonner's estimate for dQ is ± 0.04 Mev.[12]

2. Fluctuations of the accelerating voltage. This voltage was measured frequently and believed to be 100 ± 5 kv. The effect on the neutron energy would be similar to but smaller than that produced by fluctuations in the proportion of atoms in the deuteron beam.

The results of Aoki[5] and of Zinn and others[6] for the elements reported here have been added to Fig. 6 after they were recalculated with $Q=3.32$ Mev and allowances made for the widths of the neutron spectra. Each of their values is represented by the chemical symbol of the element, the former's surrounded by a circle and the latters' by a triangle.

A Theory of Anomalous Scattering of Fast Neutrons

We shall now attempt to discuss on the basis of present theory the anomalous behavior of the magnesium cross section around 2.5 Mev and later make a few remarks about the case of aluminum.

What happens when magnesium is bombarded by fast neutrons is complicated by the presence of three isotopes of masses 24, 25, and 26 and respective proportions 0.78, 0.11, and 0.11; but because of the greater abundance of Mg^{24}, we shall attribute the anomaly in cross section to an excited level in the intermediate Mg^{25} nucleus formed from Mg^{24}. The possible reactions to be considered are elastic and inelastic scattering and the following disintegrations and capture:

1. $Mg^{24}+n^1\rightarrow Na^{24}+H^1-4.0$ Mev,
2. $Mg^{24}+n^1\rightarrow Ne^{21}+He^4-2.3$ Mev,
3. $Mg^{24}+n^1\rightarrow Mg^{25}+h\nu$ (7.0 Mev).

With 2.5-Mev neutrons, the first disintegration is energetically impossible, and the second highly improbable because of the small amount of surplus energy for the α-particle. The third can be

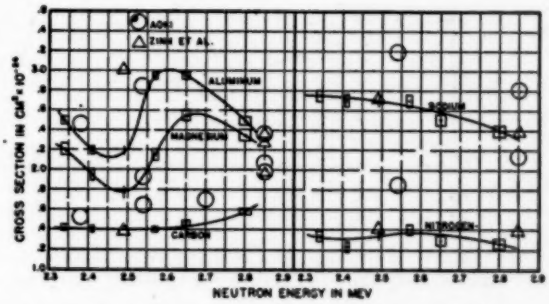

FIG. 6. Observed scattering cross sections as a function of neutron energy. The rectangles represent the present observations, their heights and widths corresponding to the range of error in cross section and energy determinations. The circles give the results of Aoki, the triangles those of Zinn, Seely, and Cohen (both recalculated; see text).

neglected too, being about 10^{-4} times as probable as scattering.[14]

Inelastic scattering also is apparently small. The cross section for this process has been given by Kikuchi and others[15] as 0.08×10^{-24} cm² or only about 3 percent of the total cross section. We therefore conclude that the only important process to be considered is elastic scattering by the nucleus Mg^{24}.

The cross section for elastic scattering of particles of zero spin by nuclei also of zero spin is[16]

$$\sigma=4\pi\lambda^2\sum_n(2n+1)\sin^2\delta_n, \qquad (3)$$

where $\lambda=\hbar/(2ME)^{\frac{1}{2}}$. M is the reduced mass of the incident particle, E its kinetic energy, and n its orbital quantum number in the field of the nucleus. The δ's are phase shifts of the outgoing or scattered waves with respect to an incident wave unaffected by the scattering nucleus. If,

[14] H. A. Bethe, Rev. Mod. Phys. 9, 160 (1937). Table XXVIII.

[15] Kikuchi, Aoki, and Husimi, Proc. Phys. Math. Soc. Japan 18, 115 (1936).

[16] N. E. Mott and H. S. W. Massey, *The Theory of Atomic Collisions*, p. 24.

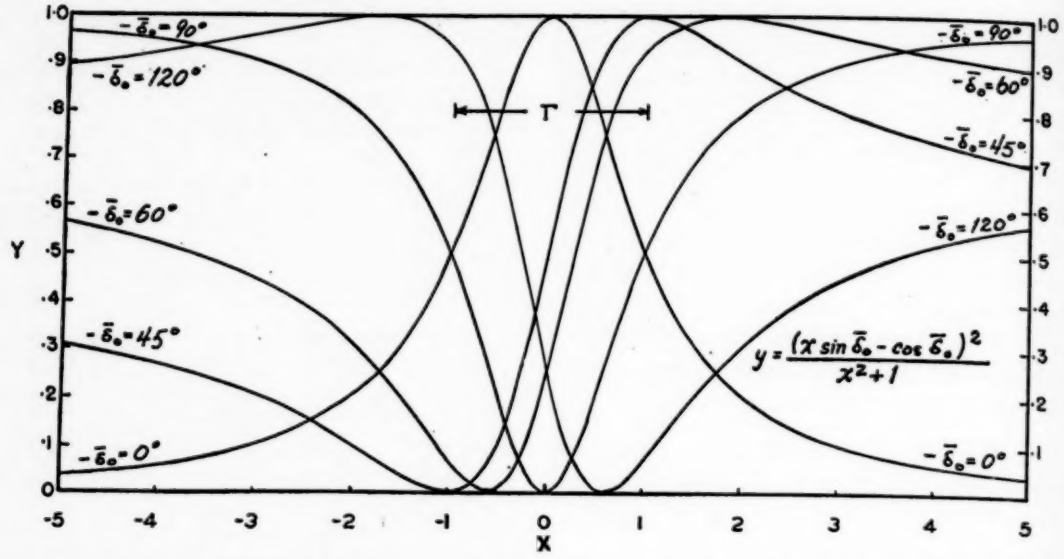

FIG. 7. If the elastic scattering cross section is multiplied by neutron energy, theory predicts in certain simple cases that the result is a function of energy which is composed of a constant part and a part which varies with energy as $y=\sin^2\delta$, where $\delta=\bar{\delta}-\text{arc cot}\ (E-E_0)/\frac{1}{2}\Gamma_0=\bar{\delta}-\text{arc cot}\ x$. The theoretical curves given here for y as a function of x are compared with the observations to find the value of $\bar{\delta}$ which gives the best agreement.

however, the incident particles have spin $\frac{1}{2}$, the nuclei still having spin 0, the cross section will be

$$\sigma=4\pi\lambda^2\sum_{s=\pm\frac{1}{2},\ n=0,\ 1,\ \cdots}(n+\tfrac{1}{2})\sin^2\delta_{ns}. \qquad (4)$$

For orbital quantum number $n=0$ there is only one phase shift to consider, $\delta_0=\delta_{0,\frac{1}{2}}=\delta_{0,-\frac{1}{2}}$.

The phase shifts occurring in (4) are in principle determinable by solving the wave equation for the compound nucleus temporarily formed in the scattering process. We are interested in the case when this compound nucleus possesses a certain semi-stable level which is narrow in comparison both with the kinetic energy of the neutron and with the distance between levels. We denote by n, s the orbital and spin quantum numbers of the neutron which is required to form this state from the original nucleus, by E_{ns} the energy which the incident neutron should have to be in resonance with this state, and by Γ_{ns} the width of the resonance level. The mean lifetime, T, of the compound state is connected with Γ_{ns} by the relation $T=\hbar/\Gamma_{ns}$. According to the theory of nuclear scattering,[17, 18] the neutron wave corresponding to the given orbital and spin quantum numbers will be shifted in phase with respect to an unperturbed wave by an amount which depends on the neutron energy E and which is given by

$$\delta_{ns}=\bar{\delta}_{ns}-\text{arc cot}\ (E-E_{ns})/\tfrac{1}{2}\Gamma_{ns} \qquad (5)$$

provided the neutron energy does not come into the neighborhood of another resonance level. The constant $\bar{\delta}_{ns}$ expresses the influence of all other levels of the compound nucleus which belong to the given spin and orbital quantum numbers.

It is evident from (5) what will happen as the neutron energy is increased. Considerably below the resonance energy we shall have a phase shift $\delta_{ns}=\bar{\delta}_{ns}$. As E increases, the phase shift rises more and more rapidly until we reach the center of the resonance level, where $E=E_{ns}$ and $\delta_{ns}=\bar{\delta}_{ns}+\pi/2$; the phase shift then continues to increase, but more and more slowly, reaching finally the value $\bar{\delta}_{ns}+\pi$. This is true of course only of the phase shift corresponding to the given orbital and spin quantum numbers; the variation with energy of the other phase shifts may be neglected if we are dealing with the scattering in the neighborhood of a single isolated resonance level. The actual scattering cross section, according to (4), is the product of the slowly varying factor $4\pi\lambda^2$ (in-

[17] G. Breit and F. L. Yost, Phys. Rev. **48**, 203 (1935).
[18] P. L. Kapur and R. Peierls, Proc. Roy. Soc. **166**, 277 (1938).

versely proportional to neutron energy) and a sum of terms due to neutrons of various orbital and spin quantum numbers. Of these terms only one will change appreciably through the resonance region and be responsible for the variation of cross section with energy. This term is (except for the constant factor $n+\frac{1}{2}$)

$$y=\sin^2\bar{\delta}_{ns}.$$

It may either increase or decrease as we approach the resonance level, according as the constant $\bar{\delta}_{ns}$ happens for the particular nucleus to be less than or greater than $\pi/2$. In fact, from the manner in which the cross section varies near resonance we can even estimate the actual value of $\bar{\delta}_{ns}$ with some accuracy. Curves are drawn in Fig. 7 showing the variation with energy of the term $y=\sin^2\bar{\delta}_{ns}$ for a number of values of $\bar{\delta}_{ns}$. The independent variable in these curves is $x=(E-E_{ns})/\frac{1}{2}\Gamma_{ns}$; since it varies linearly with energy, the theoretical curves can be compared as regards *shape* (quite without any reference to the *absolute magnitude* of the scale of independent and dependent variables) with a plot of the observed cross section as a function of energy. It was found in this way that $\bar{\delta}_{ns}=-60°$ gave a theoretical variation of cross section with energy in closest accord with the observations on magnesium reported here.

By comparing on an *absolute* scale the theoretical and observed scattering, we can determine in addition to $\bar{\delta}_{ns}$ (i) the value of the quantum number n (ii) which appears in the statistical factor $n+\frac{1}{2}$, the energy E_{ns} (iii) and width Γ_{ns} (iv) of the resonance level, and the essentially constant contribution (v) to the scattering due to deflection of neutrons with other spin and orbital quantum numbers. Conversely, we may say that we have four adjustable constants and our choice of a certain integer n with the help of which to fit the theoretical formula to the observations. To determine n, we note that the factor y varies as we go through resonance between a minimum value of 0 and a maximum value of 1, so that the scattering cross section changes by the amount

$$\begin{aligned} &4\pi\lambda^2 && \text{if} && n=0, \\ &4\pi\lambda^2(n+\tfrac{1}{2}) && \text{if} && n=1, 2, \cdots \end{aligned} \qquad (6)$$

(provided we neglect the slight variation of λ^2 itself with energy) its minimum value being determined by the contribution (v).

We shall apply (6) to the experimental results for magnesium, but must first multiply $4\pi\lambda^2$ by the relative abundance 0.78 of the isotope Mg^{24}. With a neutron energy of 2.55 Mev we have $0.78\times4\pi\lambda^2=0.84\times10^{-24}$ cm^2. Therefore the total variation in cross section through resonance will be

$$0.84\times10^{-24}\text{ cm}^2 \quad \text{if} \quad n=0. \qquad (7)$$

$$0.84\times10^{-24}(2n+1)/2 \quad \text{if} \quad n=1, 2, \cdots, \qquad (8)$$

according to theory. The observed value taken from Fig. 6 is 0.80×10^{-24} cm^2. Thus all values of n other than $n=0$ seem to be entirely excluded. On the other hand, with $n=0$, we obtain a real check between theory and observation.

The constant $\bar{\delta}_{ns}$ is to be designated as $\bar{\delta}_0$ in the present case and has already been estimated to be $-60°$. The resonance energy E_0 and level width Γ_0 are conveniently found from the energies E_1 and E_2 at which the observed cross section reaches, respectively, its maximum and minimum values by the help of the relations

$$E_0=\tfrac{1}{2}(E_1+E_2)+\tfrac{1}{2}(E_1-E_2)\cos 2\bar{\delta}_0, \qquad (9)$$

$$\Gamma_0=(E_2-E_1)\sin 2\bar{\delta}_0, \qquad (10)$$

which follow directly from Eqs. (4) and (5). Observing that $E_1=2.67$ Mev and $E_2=2.50$ Mev (see Fig. 6) we complete our determination of the

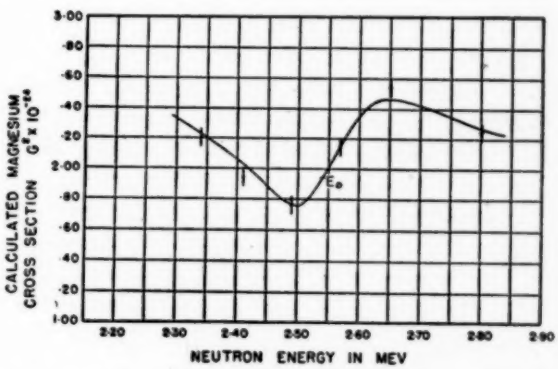

FIG. 8. The vertical lines represent the present observations on magnesium for six different energies and are compared with the smooth theoretical curve calculated with the best values of the four adjustable parameters discussed in the text. These parameters allow no freedom as to the vertical scale of the theoretical curve; for the increment in cross section between minimum and maximum theory gives 0.84×10^{-24} cm^2, observation gives 0.80×10^{-24} cm^2.

TABLE II. *The complexity of the states of the compound nucleus* Al^{28}. *A few of the lowest states are classified according to parity, total angular momentum, orbital angular momentum and multiplicity.*

Parity	Total angular momentum 0	1	2	
Even	^5D	$^5D\ ^7D\ ^7G$	$^5S\ ^5D\ ^7D\ ^5G\ ^7G$	etc.
Odd	^7F	$^5P\ ^5F\ ^7F$	$^5P\ ^7P\ ^5F\ ^7F\ ^7H$	

parameters which enter the theoretical formula for the cross section near resonance. They are four in number (since $n=0$ is not really an adjustable constant):

(i) $\bar{\delta}_0=-60°$,
(iii) $E_0=2.54$ Mev,
(iv) $\Gamma_0=0.15$ Mev,
(v) Cross section's minimum value
$$=1.76\times10^{-24}\ \text{cm}^2. \quad (11)$$

The value found for Γ corresponds to a mean life of the given level of the compound nucleus of 4.5×10^{-21} sec. On the other hand, the time for a 2.5-Mev neutron to travel a nuclear diameter (say 10^{-12} cm) is 4.5×10^{-22} sec. That is, the neutron spends about 10 times as long inside the nucleus as it would take to travel straight across it with no interaction.

With the constants given in (11), the cross section was calculated as a function of energy. In this calculation the variation with energy of the factor $4\pi\lambda^2$ in Eq. (4) was taken into account. The results are plotted in Fig. 8. The six experimental values indicated by the vertical strokes are added for reference and show satisfactory agreement with the theoretical formula containing the four adjustable parameters.

The conclusion, based on the foregoing interpretation, is that the anomalous scattering found in magnesium is due to an S level in Mg^{25} at a height of 9.5 Mev above ground. This height was calculated from the masses of the neutron, of Mg^{24}, and of Mg^{25} as well as from the neutron energy at resonance.

Because there is but one aluminum isotope, Al^{27}, the situation is much better in this respect than for magnesium. The problem is however greatly complicated by the large nuclear spin, 5/2,[19] of Al^{27}. The simplification in the case of magnesium was due to the fact that only one orbital quantum number n could be assigned to a state of given parity and given total angular momentum. On the other hand, the complexity of the states of the compound nucleus, Al^{28}, is indicated in Table II in which a few of the lowest ones are classified according to parity, total angular momentum, orbital angular momentum, and multiplicity (given by the superscript). The scattering cross section for a particular state is now not only determined by the corresponding values of n but also by the transition probabilities between the different components of that state. These are unfortunately unknown.

This method of treating elastic neutron scattering is accordingly limited in its applicability to nuclei of spin zero. It would however be possible to extend it to light nuclei of spin $\frac{1}{2}$ for which S states might be expected to be most probable. If $n=0$, the variation of cross section near resonance would then be given by $3\pi\lambda^2\sin^2\delta_{03}$ or by $\pi\lambda^2\sin^2\delta_{01}$ according as the state was a triplet or singlet. The δ's would of course still be determined by Eq. (5). This is a case which it will be useful to test as more experimental results are obtained.

It is a pleasure to express my thanks to Professor Ladenburg, Professor Wheeler, and Dr. Giarratana for suggestions and help with this problem.

[19] S. Millman and P. Kusch, Phys. Rev. **56**, 303 (1939).

An Electrical Quadrupole Moment of the Deuteron

The Radiofrequency Spectra of HD and D_2 Molecules in a Magnetic Field*

J. M. B. KELLOGG, I. I. RABI, N. F. RAMSEY, JR.
Columbia University, New York, New York,

AND

J. R. ZACHARIAS
Columbia University and Hunter College, New York, New York

(Received February 17, 1940)

The molecular-beam magnetic-resonance method has been applied to study the radiofrequency spectra of the molecules D_2 and HD, in the state $J=1$. All the measurements were made in applied magnetic fields large enough to decouple the angular momentum vectors concerned. The spectrum of D_2 for the transitions $m_I=\pm 1$ consists of six lines as in H_2. The HD spectrum consists of two sets, one of nine lines in the region of the Larmor frequency of the proton, and another of twelve lines in the region of the Larmor frequency of the deuteron. The analyses of these spectra into sets of energy levels and a consistent theory are presented. As a consequence of the analysis one has to assume the existence in the deuteron of an electrical quadrupole moment, Q. The other quantities which are evaluated from these measurements are the spin-orbit interaction constants for the molecules concerned and the magnetic moments of the proton and deuteron, through the magnetic dipole-dipole interactions. The values of the constants are $Q=2.73\times10^{-27}$ cm², $H'(D_2)=14.0$ gauss, $H'_D(HD)=20.1$ gauss, and $H'_P(HD)=20.48$ gauss. These spin-orbit interaction constants represent the magnetic field produced by the molecular rotation at the position of a nucleus. The values of the magnetic moments of the proton and deuteron agree with the direct measurements previously reported.

IN a previous note[1] we described experiments which indicated the existence of an electrical quadrupole moment of the deuteron. In this paper we shall present a more complete report of these and further experiments and of their interpretation.

It is hardly necessary to emphasize the particular importance for nuclear physics of the presence of an electrical quadrupole moment in the deuteron. Indeed, when these experiments were started there was no question of investigating such a quadrupole moment, because current theory predicted, under the assumption of central forces between the proton and neutron, that the deuteron is in a $^3S_1$ state which possesses no electrical dipole, quadrupole nor higher moment. The implication of the quadrupole moment is that the forces between proton and neutron in the deuteron are not "central."

Since the publication of the first note on the deuteron quadrupole moment the question has received theoretical discussion by a number of writers[2] who have examined the problem chiefly from the point of view of the meson theory of nuclear forces.

The possibility that a nuclear charge may depart from spherical symmetry was suggested by Racah[3] and by Pauli.[4] Schuler and Schmidt[5] were the first to present clear experimental evidence for such an effect, which they found in the departure from the interval rule of some lines in the hyperfine structure spectrum of europium.

The way in which a nuclear quadrupole moment manifests itself is through the fact that its energy in an external electric field depends not only on its position but also on its orientation with respect to the gradient of the field. In an atom the electric field is that of the electronic

* Publication assisted by the Ernest Kempton Adams Fund for Physical Research of Columbia University.

[1] J. M. B. Kellogg, I. I. Rabi, N. F. Ramsey, Jr. and J. R. Zacharias, Phys. Rev. **55**, 318 (1939).

[2] H. Bethe, Phys. Rev. **55**, 1261 (1939). R. F. Christy and S. Kusaka, Phys. Rev. **55**, 665L (1939). D. Inglis, Phys. Rev. **55**, 988L (1939); Phys. Rev. **55**, 329 (1939); Phys. Rev. **56**, 1175 (1939). E. Wigner and L. Eisenbud, Phys. Rev. **56**, 214 (1939). S. M. Dancoff, Phys. Rev. **56**, 385L (1939). P. Critchfield, Phys. Rev. **56**, 540 (1939). M. E. Rose, Phys. Rev. **56**, 1064 (1939). C. Kittel and G. Breit, Phys. Rev. **56**, 744 (1939). M. Phillips, Phys. Rev. **57**, 160 (1940).

[3] G. Racah, Zeits. f. Physik **71**, 431 (1931).

[4] W. Pauli, Zurich Conference, 1931.

[5] H. Schuler and Th. Schmidt, Zeits. f. Physik **94**, 457 (1935).

charge distribution. In a molecule the field arises from the other nuclei as well as from the electrons.

The quantum theory of the effect of a nuclear quadrupole moment on atomic energy levels was given by Casimir.[6] A similar theory for molecules can be constructed along analogous lines. The part of the energy operator which concerns the quadrupole moment of a nucleus is, according to Casimir,

$$e^2qQ\{3(\mathbf{i}\cdot\mathbf{J})^2+\tfrac{3}{2}(\mathbf{i}\cdot\mathbf{J})-i(i+1)J(J+1)\}/$$
$$2J(2J-1)i(2i-1). \quad (1)$$

Q is the magnitude of the nuclear quadrupole moment and is given by $Q=\langle 3z^2-r^2\rangle_{Av}$ and the average is taken over the nuclear charges for the state which has the largest component of the spin i in the z direction. The origin is at the centroid of the nucleus. The quantity $q=\langle\Sigma_k(3\cos^2\theta_k-1)/R_k^3\rangle_{Av}$. The sum is taken over all of the molecular charges except the nucleus under discussion. The electrons contribute negatively. This average is taken over the state of the molecule which has the greatest component of its angular momentum J along the z direction. R_k is the distance of the kth element of charge from the nucleus in question. $\mathbf{J}$ and $\mathbf{i}$ are the molecular and nuclear angular momentum operators. θ_k is the angle which R_k makes with the z axis. The factor (qe) is the average of $\partial^2V/\partial z^2$ where V is the electrostatic potential at the nucleus.

The evaluation of our experimental results will give us the value of the product qQ. Unlike the atomic case there is no empirical information like fine-structure splitting from which the molecular q can be evaluated. One must[7] fall back on theoretical calculations from molecular wave functions to obtain q. Hence the value of Q must result partly from a calculation of q.

Since the effect of artificial external electric fields on a nuclear quadrupole moment is not measurable at present because of its very small size, it is impossible to measure quadrupole electric moments as directly as nuclear magnetic moments. The existence of a nuclear quadrupole moment is therefore at present an inference from the manner in which certain energy levels are shifted with respect to one another. In our experiments these shifts are of the same nature, in their manifestation, as those due to the magnetic dipole-dipole interaction between the two nuclei, and must therefore be disentangled from this type of interaction. However, this is not difficult, as we know the magnitudes of the magnetic moment of the proton and the deuteron and the internuclear distance.

A quadrupole moment effect is relatively large in our experiments whereas in atomic hyperfine structure studies the effect is generally small. For atomic deuterium in the ground state the effect vanishes because it is an S state for which q is zero. In excited states the effect would be smaller than the natural width of the energy level due to radiation damping. In general, in the atomic case, the quadrupole effect is superposed on the large interaction between the nuclear magnetic moment and the magnetic field produced by the electrons. These fields may be of the order of 10^6 gauss. In the D_2 and HD molecules which are the subject of our study these fields are well under 50 gauss. Since our resolving power[8] is about 10^5 times as great as with optical methods we can measure the effects of even the small magnetic fields in the molecule. The quadrupole effect is therefore relatively great because the gradient, "q," of the electric field which interacts with the quadrupole moment is of the same order of magnitude in molecules as in atoms.

Method

These investigations were carried out by the molecular beam magnetic resonance method.[9] The main features of this method as applied to gases were described in a previous paper[10] to which we will refer as I.

All of the spectra in paper I were observed in the following way: The radiofrequency oscillator was set at a definite constant frequency f_0 and the molecular beam intensity was observed as a

[6] H. B. G. Casimir, "On the interaction between atomic nuclei and electrons," Prize Essay published by Teyler's Tweede Genootschap (1936).

[7] However, see E. Teller, Phys. Rev. **57**, 556(A) (1940).

[8] By resolving power we mean the smallest absolute interval in wave numbers in which two lines can be resolved, that is we mean $\Delta\nu$ rather than $\Delta\nu/\nu$.

[9] I. I. Rabi, S. Millman, P. Kusch and J. R. Zacharias, Phys. Rev. **55**, 529 (1939).

[10] J. M. B. Kellogg, I. I. Rabi, N. F. Ramsey, Jr. and J. R. Zacharias, Phys. Rev. **56**, 728 (1939).

function of the value of the homogeneous magnetic field H in which nonadiabatic transitions take place. At appropriate values of the magnetic field the beam intensity reaches a minimum and the various values of the magnetic field for which this occurs are called positions of the minima or positions of the lines. These minima occur whenever the product (hf_0) for the oscillator is equal to the difference in energy between two molecular states. The whole pattern of minima is referred to as the radiofrequency spectrum. In paper I we were chiefly concerned with the magnetic moments of the proton and of the deuteron. The measurements were made on HD and D_2 molecules in the state with rotational angular momentum $J=0$, and H_2 molecules in the state $J=1$. In the state $J=0$ the HD and the D_2 molecules each give rise to a one-line radiofrequency spectrum, for each nucleus. In the state $J=1$ the H_2 molecules give a 6-line spectrum in the frequency region in the neighborhood of the Larmor frequency of the proton, and another six-line spectrum in the region of the Larmor frequency of the rotational moment of the molecule. Only the first of these spectra was considered in I.

Resumé of H_2 Results

In this paper we shall report on the nuclear radiofrequency spectra of HD and D_2 molecules in the state $J=1$, and on our analysis of these spectra. Since the treatment of D_2 as given here is so much like that of H_2 as given in I, and since we wish to make use of certain of the H_2 results in the discussion of the analysis of the D_2 spectrum, we give here a brief resumé of the important features and results of the H_2 analysis.

The H_2 experiments were performed on a beam of molecules emerging from a liquid-nitrogen-cooled source. Parahydrogen molecules at liquid-nitrogen temperatures are practically all in the state $J=0$ and have the total nuclear spin $I=0$. They are inert as far as our experiments are concerned, so that our study of H_2 was made on orthohydrogen molecules in the state $J=1$, $I=1$. In this state there are $(2J+1)(2I+1)=9$ energy levels. Because of the selection rule $\Delta m_I=\pm 1$ for transitions with $\Delta m_J=0$, there are 6 transitions allowed between these levels giving rise to the six-line nuclear spectrum. We were able to analyze this six-line radiofrequency spectrum and thereby obtain values for two important physical quantities: 1, the value of $\langle \mu_P/r^3\rangle_{Av}$ (called H'') which appears because of the dipole-dipole magnetic interaction between the two protons; and 2, the magnetic field H' produced by the molecular rotation at the position of a nucleus. More properly H' is the constant in the expression for the spin-orbit interaction of the proton moments with the molecular rotation. In high magnetic fields with correspondingly high oscillator frequency, the six lines for H_2 are symmetrically disposed with respect to H_0 (defined by $H_0 \equiv hf_0/2\mu_P$) and with no minimum at the position H_0. Assuming complete Paschen-Back effect, the positions of the minima are given by the following simple formulae:

$$H_0 \pm (3S_P + H'); \quad H_0 \pm (3S_P - H'); \quad H_0 \pm 6S_P,$$

where S_P is related to H'' by $S_P = \frac{1}{8}H''$. The values obtained for these quantities were $H' = 27.2$ gauss and $S_P = 6.8$ gauss.

These *two* constants, H' and S_P, are sufficient to account for the positions of all *six* lines and for the variations in their position with gross changes of field. Furthermore the constant H'' can be calculated from the known value of the proton moment and the known internuclear distance of H_2. This value agrees with the experimental value of H''. The consistency and reasonableness of the analysis of the H_2 spectrum shows that we have not omitted any important features of the molecular constitution in setting down the fundamental equation on which our analysis rests.

The D_2 Spectrum

Turning now to the discussion of the D_2 molecule we take note of the following facts. The D_2 molecule is homonuclear, the nuclei have spins of one and obey the Bose statistics. The lowest rotational state of D_2 is therefore a state in which the wave function of the nuclear spins is symmetrical and the total spin angular momentum I, is either zero or two. For the next higher rotational state, $J=1$, (para-D_2) the wave function for the two nuclear spins must be antisymmetrical and the total spin angular momentum is 1. For the state $J=2$ the wave function is again sym-

metrical and I is either zero or two. At liquid-nitrogen temperatures almost all the molecules are in these states and they are therefore the only ones we need consider. (See Table I of paper I).

This may most easily be done under the classification of their total rotational angular momentum and spin:

1. $J=0$, $I=0$. 9.3 percent of the beam. These molecules are inert in our apparatus since they have no magnetic moment.

2. $J=0$, $I=2$. 46.7 percent of the beam. These molecules give rise to the deep central minimum which is so prominent on any of the D_2 nuclear curves and which was used in paper I for the determination of the deuteron magnetic moment.

3. $J=2$, $I=2$. 8.7 percent of the beam. These molecules are divided among $(2J+1)(2I+1)=25$ energy states in a strong magnetic field. Thus each state contains 0.35 percent of the molecules. The selection rule $\Delta m_I=\pm 1$, for $\Delta m_J=0$ gives, for each m_J level, 4 possible transitions. Thus there should be a total of 20 transitions possible. Since in our experiments transitions from level b to level a are counted as well as those from a to b, there would be 0.7 percent of the total beam in each of these 20 minima. However the effect of the velocity distribution operates to decrease this intensity by about 25 percent, and since, using a D_2 beam our apparatus will not detect changes of beam intensity of less than $\frac{1}{2}$ percent of the total beam, we did not expect to observe, and did not observe any minima from molecules in this state.

4. $J=2$, $I=0$. 1.7 percent of the beam. The same considerations apply here as far as intensity is concerned as to the molecules in state $J=2$, $I=2$. Furthermore the only transitions possible are those for which $\Delta m_J=\pm 1$ and this would give rise to lines in the rotational spectrum.

5. $J=1$, $I=1$. 33 percent of the beam. These are the molecules with which we are concerned in the experiments on D_2 reported in this paper. In a strong magnetic field there are $2J+1=3$ possible orientations of J and for each of these $2I+1=3$ possible orientations of I; altogether 9 states. Each energy state should therefore contain 3.7 percent of the molecules of the beam. Between these 9 levels there should be 6 possible transitions corresponding to changes of m_I of ± 1 while m_J remains unchanged. If the effect of the velocity distribution is neglected the intensity of each of these minima should therefore be 7.4 percent of the total beam intensity. If the effect of the velocity distribution is included this intensity should drop to about 5.4 percent of the total beam intensity.

Thus, excepting the intensity considerations, the situation for para-D_2 molecules in the state $J=1$, $I=1$ is exactly that which obtained for ortho-H_2 molecules as discussed in paper I. Because of our knowledge of the H_2 constants, we expected to be able to predict the positions of the six D_2 minima at least approximately. This should be made clearer by the following discussion.

Preliminary Discussion of D_2 Spectrum

In the section called theory we will derive expressions for the nine energy levels (given in Table I) of para-D_2 on the assumption that there are three types of interaction to consider, i.e., spin-orbit, with constant H'; spin-spin, with constant H''; and nuclear electric quadrupole, with constant H'''. The possible transitions between these energy levels are given in Table II. Inspection of this table shows that if the electric quadrupole interaction constant, H''', is set equal to zero, the transitions between the energy levels for D_2 will be represented by exactly the same expressions as for H_2. The values of the constants

Table I. *Energy levels correct to the third-order perturbations for the first rotational state of para-D_2 molecules in a magnetic field. The terms in H' and S_D give the first-order perturbation, the terms in C_2 and C_2' the second, and the terms in C_3 the third. The definitions of the quantities are as follows:*

$$S_D=\tfrac{1}{2}(H''+H'''); \quad \alpha=\mu_R/\mu_D=0.440/0.855=0.515;$$
$$C_2=[(H'+3S_D)^2+18S_D^2]/(1-\alpha)H;$$
$$C_2'=(H'-3S_D)^2/(1-\alpha)H;$$
$$C_3=(H'+3S_D)^2(H'-9S_D)/(1-\alpha)^2H^2;$$
$$H''=\langle\mu_D/r^3\rangle_{Av}; \quad H'''=(-5e^2qQ/4\mu_D).$$

m_J	m_I	Energy
1	1	$-\mu_D($ $H+\alpha H+H'-S_D$ $)$
1	0	$-\mu_D($ $+\alpha H$ $+2S_D$ $-C_2'$ $)$
1	−1	$-\mu_D(-H+\alpha H-H'-S_D-C_2$ $+C_3)$
0	1	$-\mu_D($ H $+2S_D$ $+C_2'$ $)$
0	0	$-\mu_D($ $-4S_D$ $-2C_3)$
0	−1	$-\mu_D(-H$ $+2S_D$ $-C_2'$ $)$
−1	1	$-\mu_D($ $H-\alpha H-H'-S_D+C_2$ $+C_3)$
−1	0	$-\mu_D($ $-\alpha H$ $+2S_D$ $+C_2'$ $)$
−1	−1	$-\mu_D(-H-\alpha H+H'-S_D$ $)$

H' and S_D will of course be different, but these should be readily calculable from the known values of the constants for H_2. The spin-orbit constant, H', can be taken to be one-half of that for hydrogen since the angular velocity of rotation of the D_2 molecule is half as great and the internuclear distances are so nearly the same for the two molecules. We can make this assumption with some confidence because it has been shown experimentally[11] that the ratio of the rotational magnetic moments of the two molecules is 2 to 1. Similarly the value of the spin-spin constant $H''=\langle\mu_D/r^3\rangle_{Av}$ can be obtained for D_2 since (μ_D/μ_P) and μ_P/r^3 are both known. These constants then become $H'=13.6$ gauss and $H''=10.5$ gauss. $S_D=H''/5=2.1$ gauss. Inserting these values into the expressions given above for H_2 we obtain the predicted spectrum with minima as indicated by vertical lines in Fig. 1.

The complete lack of correspondence between the experimental and predicted curves is somewhat startling, especially so when one recalls how well the theory fits the case of H_2. As is evident from the figure it was expected that the six-line D_2 spectrum would fall within the wings of the deep central minimum arising from the state $J=0$, since the ratio of the depths of the small to the large minima is 1 to 7.

It was suspected that the discrepancy between theory and experiment was due to a quadrupole moment of the deuteron.

The apparatus was remodeled to increase the resolving power for a more accurate study of the phenomenon. It was shown in paper I that the resolving power of our apparatus depends upon the length of time that the molecule remains under the influence of the radiofrequency field. In fact, the minimal half-width (width, ΔH, in gauss at half-depth) for a transition without any fine structure is given by $\Delta H=hI\nu/\mu L$ where L is the length of the radiofrequency field and v is the velocity of the molecule traversing the field. At the time the experimental curve of Fig. 1 was taken the path of the molecules in this field was 2.7 cm. We calculate for this length of field and for D_2 at 80°K the minimal half-width of a line as predicted by the above equation to be about 30 gauss. By increasing the length of the radiofrequency field to 13.5 cm this minimal half-width can be cut down by a factor of 5.

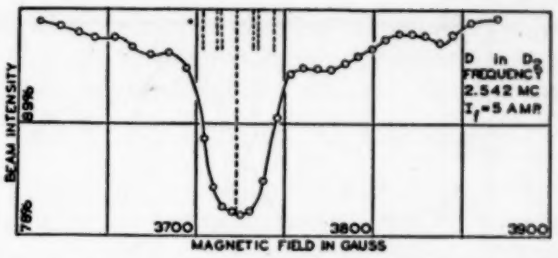

FIG. 1. Radiofrequency spectrum of D_2 at 80°K for changes of total spin magnetic quantum number m_I of ±1 with m_J unchanged. This curve was taken at a time when the length of the radiofrequency field was only 2.7 cm. The spectrum predicted on the assumption of no quadrupole moment is indicated by the dotted lines, both as to position and relative intensity. The theoretical minimal half-width for any of these minima, 30 gauss, is in good agreement with the observed curve.

The apparatus was accordingly lengthened. The deflecting magnets were separated enough to allow for a homogeneous field 15 cm long. This magnet and its radiofrequency field wires were also used in the experiments of paper I.

The curve of Fig. 2 represents data obtained with the improved conditions. The subsidiary minima are resolved from each other and from the central minimum. The positions of the secondary minima are in violent disagreement with the provisional theory outlined above. In fact the interval between the extreme lines is six times greater than was expected.

TABLE II. *Changes of energy associated with the change of orientation of the total nuclear spin by ±1 for para-D_2 molecules in the first rotational state.* $S_D=\frac{1}{5}(H''+H''')$.

m_J	m_I	$\Delta E/\mu_D$
1	0→1	$H+H'-3S_D+0+C_2'+0$
1	−1→0	$H+H'+3S_D+C_2-C_2'-C_2$
0	0→1	$H+0+6S_D+0+C_2'+2C_2$
0	−1→0	$H+0-6S_D+0+C_2'-2C_2$
−1	0→1	$H-H'-3S_D+C_2-C_2'+C_2$
−1	−1→0	$H-H'+3S_D+0+C_2'+0$

DETAILED DISCUSSION OF D_2 SPECTRUM

A set of energy levels which accounts completely for these lines will be developed in the section called "Theory of energy levels" of D_2. The only assumption in addition to those made for H_2 is that a nuclear electric quadrupole interacts with the molecular electric field. The nine energy levels for D_2 in the first rotational state

[11] N. F. Ramsey, Jr., Phys. Rev. **55**, 595 (1939).

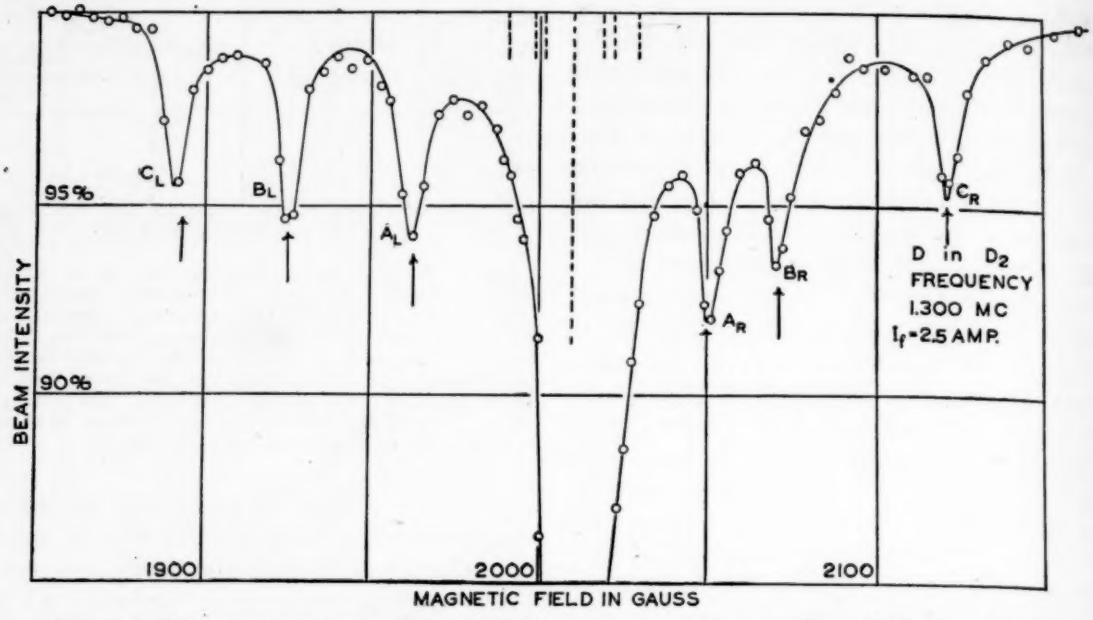

FIG. 2. Radiofrequency spectrum of D_2 at 80°K for $\Delta m_I = \pm 1$, with m_J unchanged. The length of the radiofrequency field is 13.5 cm. Dotted lines indicate spectrum predicted on the assumption of no quadrupole moment. Arrows indicate positions of lines predicted from the complete theory and the constants from the 2.419-MC data. Theoretical minimal half-width for any of these minima is about 6 gauss. The central minimum is not symmetrical about the central dotted line because of the method of producing the radiofrequency field, as discussed by S. Millman (Phys. Rev. **55**, 628 (1939)). If the directions of all of the static magnetic fields are reversed, the asymmetry is reversed. This result was used to show that the deuteron magnetic moment is positive.

are given in Table I which is complete up through the third order of the perturbation theory expanded about the strong field levels. The terms in H' and S_D to the first power are the first-order perturbations produced by the three types of interaction mentioned above. These terms are independent of field and remain even in the presence of a large applied field. The terms C_2 and C_2' are second-order terms which are inversely proportional to H and therefore vanish in high fields. They arise because of incomplete Paschen-Back effect or incomplete decoupling of the total nuclear spin and the molecular rotation. The same is true of the third-order terms C_3 except that the decrease with increasing field is even more rapid. Throughout the following discussion the terms in C_3 can and will be neglected.

Energy differences for transitions of m_I of ± 1 with m_J held constant are listed in Table II. Dividing the terms of Table II through by μ_D and setting $\mu_D H_0 = hf_0$ we obtain expressions for the positions of the lines for the frequency f_0 as given in Table III.

As in paper I we can use the asymmetry of the positions of the minima to identify the individual lines with the quantum numbers of the transitions given in Table III. This identification can be made unambiguously from the 2.419-MC data of Table IV, since, for the fields at which these transitions occur, all perturbations higher than second order have no appreciable effect, and the only terms which render the pattern unsymmetrical are C_2 and C_2'. It can be seen from Table III that four of the lines should be shifted from symmetrical positions about H_0 by amounts $-C_2'$ while two other lines are shifted by amounts $-(C_2-C_2')$. Thus the midpoint between one pair of lines should be shifted from the position H_0 by $-(C_2-C_2')$ while the midpoints of two other pairs should be shifted from H_0 by amounts $-C_2'$.

This is just the type of shift which is found experimentally as can most easily be seen from the 2.419-MC data as follows:

$$\tfrac{1}{2}(C_R+C_L)-H_0=-0.9 \text{ gauss},$$
$$\tfrac{1}{2}(B_R+B_L)-H_0=-6.0 \text{ gauss},$$
$$\tfrac{1}{2}(A_R+A_L)-H_0=-1.1 \text{ gauss}.$$

We see from this that the B minima correspond to the second and fifth rows of Table IV, and therefore that $(C_2'-C_2)$ is about 6 gauss. Similarly since the A and C minima correspond to the other rows we conclude that C_2' is approximately 1 gauss. Substituting this value and $H=3700$ gauss into the expression for C_2' we can arrive at a preliminary rough value for $(3S_D-H')$ of ± 43 gauss. Since the A minima are displaced from H_0 by very nearly that amount and the C minima by much more we can take the interval between the A minima of 90.3 gauss as $2(3S_D-H')$. Thus the A minima correspond to the third and fourth rows of Table III. This leaves the C minima to go with the first and sixth rows. We can now summarize as follows:

$$2(3S_D-H')=A_R-A_L=90.3 \text{ gauss},$$
$$2(3S_D+H')=B_R-B_L=147.0 \text{ gauss},$$
$$2(6S_D)=C_R-C_L=234.2 \text{ gauss}.$$

In the above summary we have taken S_D and H' as positive for the following reason. Since $(3S_D-H')$ is numerically less than $(3S_D+H')$ we conclude that S_D and H' must have the same sign. Now we know that H' is positive because it is the spin orbit constant for D_2 and would have the same sign as the corresponding spin-orbit constant for H_2, which was shown in paper I to be positive. From this consideration we will later derive the sign of qQ. This completes the identification and the detailed assignment of quantum numbers as given in Table III.

In order to evaluate the constants H' and $3S_D$ from the data as precisely as possible the following procedure was adopted. First a preliminary evaluation was made from the equations above. These values were used to evaluate the constants C_2, C_2' and C_3 as given in Table V. With these constants and the 2.419-MC data of Table IV a set of six equations linear in H' and $3S_D$ can be set up and solved by the method of least squares. The values obtained this way are

$$H'=14.00 \text{ gauss} \quad \text{and} \quad 3S_D=58.86 \text{ gauss}.$$

The general consistency of the experiment with the theory is best exhibited in Table V. The two experimental parameters H' and $3S_D$ are used to predict the positions of the six minima. The greatest deviation between the calculated and experimental values is 0.5 gauss. This is better than 1 gauss, the estimated probable error in the determination of a minimum. The second-order perturbations as evaluated experimentally above are 1 gauss for the A and C minima and 6 gauss for the B minima. These are to be compared with the theoretical values of 1.1 gauss, and 5.6 and 5.9 gauss given in Table V.

Further agreement of experiment with the theory is provided by the 1.300-MC data as exhibited in Table VI. The constants H' and $3S_D$ as evaluated above from the 2.419-MC data have been used for predicting the positions of the lines for the frequency of 1.300 MC. Table VI shows that for these low fields (approximately 2000 gauss) the perturbation theory used does not converge. For the minima C_R and C_L the third order is as large as the second. It was therefore necessary to calculate the energy levels directly from the secular equation and to find the positions of the minima from them. For four of the lines the agreement between predicted position and experimental position is unusually good, whereas for the other two lines the agreement is just within the sums of the limits of error for the

TABLE III. *Magnetic fields for which resonances will occur for changes of orientation of the total nuclear spin by ± 1 for para-D_2 molecules in the first rotational state. $H_0=hf_0/\mu_D$.*

m_J	m_I	MAGNETIC FIELD IN GAUSS	LINE DESIGNATION
1	$0\leftrightarrow 1$	$H_0-H'+3S_D-C_2'+0+0$	A_R
1	$-1\leftrightarrow 0$	$H_0-H'-3S_D+C_2'-C_3+C_3$	B_L
0	$0\leftrightarrow 1$	$H_0+0-6S_D-C_2'+0-2C_3$	C_L
0	$-1\leftrightarrow 0$	$H_0+0+6S_D-C_2'+0+2C_3$	C_R
-1	$0\leftrightarrow 1$	$H_0+H'+3S_D+C_2'-C_3-C_3$	B_R
-1	$-1\leftrightarrow 0$	$H_0+H'-3S_D-C_2'-0+0$	A_L

TABLE IV. *Displacements in gauss for minima of para-D_2 from H_0, the central minimum of ortho-D_2. These displacements are considered reliable to ± 1 gauss for the 2.419-MC data and to ± 1.5 gauss for the 1.300-MC data. Note that B_L and B_R are much more unsymmetrically placed than the others; that they are all more symmetrical in the higher field, $H_0=3710$ gauss.*

DESIGNATION OF MINIMUM	DISPLACEMENTS IN GAUSS FOR OSCILLATOR FREQUENCIES OF 2.419 MC	1.300 MC
C_L	-118.0	-118.0
B_L	-79.5	-84.0
A_L	-46.3	-47.6
H_0	(3710)	(1995)
A_R	44.0	40.7
B_R	67.5	61.3
C_R	116.2	112.0

TABLE V. *This table shows the magnitudes of the calculated perturbations of the lines in the D in D_2 spectrum at 2.419 MC and the comparison with the experimentally found perturbations. The "Line Designations" are those assigned to the minima of Fig. 2.*

PERTURBATIONS				LINE DESIGNATION AND EXPERIMENTAL PERTURBATION
FIRST ORDER	SECOND ORDER	THIRD ORDER	TOTAL	
$6S_D$ 117.7	$-4140/H$ −1.1	$-7.3\times10^6/H^2$ −0.4	116.2	C_R 116.2
$3S_D+H'$ 72.9	$-21{,}300/H$ −5.6	$3.6\times10^6/H^2$ 0.2	67.5	B_R 67.5
$3S_D-H'$ 44.9	$-4140/H$ −1.1	0 0	43.8	A_R 44.0
$-(3S_D-H')$ −44.9	$-4140/H$ −1.1	0 0	−46.0	A_L −46.3
$-(3S_D+H')$ −72.9	$-21{,}300/H$ −5.9	$-3.6\times10^6/H^2$ −0.2	−79.0	B_L −79.5
$-6S_D$ −117.7	$-4140/H$ −1.2	$7.3\times10^6/H^2$ 0.4	−118.5	C_L −118.0

constants and the experimental determination of the minima. This is most likely due to the fact that the 1.300-MC data were taken only once, whereas the 2.419-MC data are the result of averaging several runs.

The quantity S_D is defined as $\frac{1}{3}(H''+H''')$ so that the experiment with D_2 is incapable of providing a determination of either H'' or H''' separately. We can, however, take the value of H'' from the experiment on H_2 as discussed above. That value of H'' of 10.5 gauss subtracted from $5S_D=98.1$ gauss yields 87.6 gauss for H'''. It is to be noted that this value of H''' is positive. The significance of this quantity will be discussed later.

EXPERIMENTS ON HD

Experiments on HD were undertaken to prove that the quantity H''' is certainly a property of the deuterium nucleus and is not just a peculiarity of the D_2 molecule. This proof takes the following simple form. In HD one set of transitions can occur for changes of the magnetic quantum number for the proton and another set for the deuteron. In the first case the pattern should be completely accounted for without any necessity for considering a quadrupole moment of the deuteron because even if such a quantity does exist the changes of energy of the molecule accompanying changes of m_P would not be affected thereby. This follows, since if no reorientation of the deuteron occurs within the molecule relative to the extranuclear electrical configuration, no changes of energy would occur. On the other hand, if we consider the transitions of m_D, then such energy changes should occur, and the spectrum should show the presence of the quadrupole moment. As this turns out to be the case these experiments show that the effect is a property of the deuteron and not some molecular property.

Furthermore in HD the spin-spin and quadrupole interactions can be evaluated experimentally and therefore *the value of the deuteron quadrupole moment will not depend on subtracting a calculated quantity, H'', as in D_2.* A further check on the correctness of the theory will be afforded by a comparison of the interaction constants obtained with HD with those previously obtained with H_2 and D_2.

NUCLEAR SPECTRA OF HD

The HD molecule is heteronuclear and there is no quantum number of total spin. There are therefore three coupled angular momenta J, I_D and I_P with projections for the strong field case of m_J, m_D, and m_P. At the temperature of liquid N_2, 63 percent of the molecules are in the state $J=0$, and for this state all interactions of the type discussed in this paper average out to zero. These molecules are therefore ideally suited to the determination of the nuclear magnetic moments of the proton and the deuteron but are of no use at all in the present experiment except for the location of $H_0=hf_0/\mu$. The remaining 37 percent of the molecules are in the state $J=1$, only 0.3 percent being in the state $J=2$. Therefore any fine structure that is observed is immediately attributable to the molecules in the

TABLE VI. *Comparison of experimental D in D_2 perturbations at 1.300 MC with the perturbations as calculated with the constants obtained from the 2.419-MC data of D in D_2.*

LINE DESIGNATION	PERTURBATIONS PREDICTED FROM 2.419-MC D_2 DATA				EXPERIMENTAL VALUE
	FIRST ORDER	SECOND ORDER	THIRD ORDER	SECULAR	
C_R	117.7	−1.96	−1.63	113.0	112.0
B_R	72.9	−10.36	.86	63.7	61.3
A_R	44.9	−2.04	0.00	43.0	40.7
A_L	−44.9	−2.12	0.00	−47.4	−47.6
B_L	−72.9	−11.11	−1.00	−84.6	−84.0
C_L	−117.7	−2.20	2.07	−117.7	−118.0

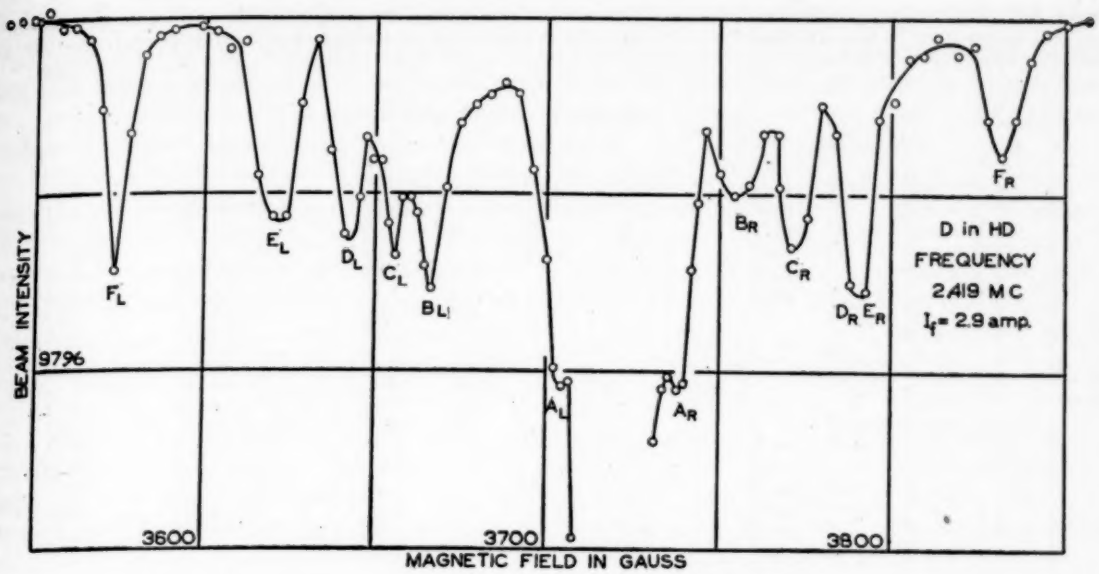

FIG. 3. Radiofrequency spectrum of HD at 80°K for $\Delta m_D = \pm 1$ with m_P and m_J unchanged.

state $J=1$. In a strong magnetic field there are three orientations of J, three orientations of the deuteron spin, and two orientations of the proton spin. This makes eighteen possible states which in strong field gives eighteen different energy levels. There are three types of transitions among these energy levels, i.e., (1) those for which m_D changes by ± 1 giving twelve different transitions; (2) those for which m_P changes by ± 1 giving rise to nine different transitions; and (3) those for which m_J changes by ± 1 giving twelve different transitions. The first group (called D in HD) clusters around $H_0 = hf_0/\mu_D$ and will be discussed first. The second group (called H in HD) clusters around $H_0 = hf_0/2\mu_P$ and will be discussed next. The third group which clusters around $H_0 = hf_0/\mu_R$ will be discussed in a separate paper devoted to the general question of rotational magnetic moments.

D IN HD

Figure 3 shows the group of minima associated with changes of m_D of ± 1 at the frequency of 2.419 MC. The deep central minimum is not completely shown in the graph so that the small minima for $J=1$ will show to better advantage. Besides the central minimum there are eleven clearly resolved minima one of which is taken to be double since twelve are expected altogether.

The experimental procedure for taking this curve is similar to that for the other data except that for this case particular attention has to be paid to the magnitude of the deflecting and refocusing fields. In the HD molecule the deflections are chiefly due to the large proton moment so that if a very large deflecting field is used to affect the motion of the molecule by action on the smaller deuteron moment the excursions produced by the proton moment are so large that the refocusing conditions are not good. Therefore a compromise is sought before the data is taken for one curve.

The column labeled "Experimental" in Table IX represents the average of two sets of data for D in HD at the one frequency.

In the section called "Theory of energy levels of HD" we will derive expressions for the eighteen energy levels of HD in the first rotational state on the assumption that there are three types of interaction to consider, i.e., spin-orbit interaction of the deuteron with the magnetic field of the molecular rotation at the position of the deuteron and the similar type for the proton, with interaction constants $\mu_D H'_D$ and $2\mu_P H'_P$; spin-spin interaction of the deuteron with the proton with interaction constant $S = \langle 2\mu_P\mu_D/5r^3\rangle_{Av}$; and the interaction of the deuteron quadrupole moment with the gradient of the electric field with inter-

TABLE VII. *Energy levels for* HD *molecules in the first rotational state. The energies are in gauss nuclear magnetons if* μ_R, μ_P, *and* μ_D *are given in nuclear magnetons. This notation is used because the second- and third-order expressions are given numerically using experimental values for the constants* H'_P, H'_D, S, *and* E. $S=\langle 2\mu_P\mu_D/5r^3\rangle_{Av}$. $E=H'''/5=e^2Q/4\mu_D$.

m_J	m_P	m_D	Energy in gauss nuclear magnetons: Zeroth order	First	Second	Third
1	½	1	$-\mu_P H-\mu_D H-\mu_R H$	$-\mu_P H'_P-\mu_D H'_D+S-\mu_D E$	$+0$	$+0$
1	½	0	$-\mu_P H-\mu_R H$	$-\mu_P H'_P+2\mu_D E$	$+10{,}160/H$	$+1.75\times10^8/H^2$
1	½	−1	$-\mu_P H+\mu_D H-\mu_R H$	$-\mu_P H'_P+\mu_D H'_D-S-\mu_D E$	$+30{,}660/H$	$+6.35\times10^8/H^2$
1	−½	1	$+\mu_P H-\mu_D H-\mu_R H$	$+\mu_P H'_P-\mu_D H'_D-S-\mu_D E$	$+621/H$	$+0$
1	−½	0	$+\mu_P H-\mu_R H$	$+\mu_P H'_P+2\mu_D E$	$+34{,}400/H$	$-4.75\times10^8/H^2$
1	−½	−1	$+\mu_P H+\mu_D H-\mu_R H$	$+\mu_P H'_P+\mu_D H'_D+S-\mu_D E$	$+23{,}600/H$	$-8.24\times10^8/H^2$
0	½	1	$-\mu_P H-\mu_D H$	$-2S+2\mu_D E$	$-10{,}780/H$	$-1.75\times10^8/H^2$
0	½	0	$-\mu_P H$	$-4\mu_D E$	$-11{,}110/H$	$+2.14\times10^8/H^2$
0	½	−1	$-\mu_P H+\mu_D H$	$+2S+2\mu_D E$	$+30{,}400/H$	$+4.72\times10^8/H^2$
0	−½	1	$+\mu_P H-\mu_D H$	$+2S+2\mu_D E$	$-30{,}400/H$	$+4.72\times10^8/H^2$
0	−½	0	$+\mu_P H$	$-4\mu_D E$	$+11{,}110/H$	$+2.14\times10^8/H^2$
0	−½	−1	$+\mu_P H+\mu_D H$	$-2S+2\mu_D E$	$+10{,}780/H$	$-1.75\times10^8/H^2$
−1	½	1	$-\mu_P H-\mu_D H+\mu_R H$	$+\mu_P H'_P+\mu_D H'_D+S-\mu_D E$	$-23{,}600/H$	$-8.24\times10^8/H^2$
−1	½	0	$-\mu_P H+\mu_R H$	$+\mu_P H'_P+2\mu_D E$	$-34{,}400/H$	$-4.75\times10^8/H^2$
−1	½	−1	$-\mu_P H+\mu_D H+\mu_R H$	$+\mu_P H'_P-\mu_D H'_D-S-\mu_D E$	$-621/H$	$+0$
−1	−½	1	$+\mu_P H-\mu_D H+\mu_R H$	$-\mu_P H'_P+\mu_D H'_D-S-\mu_D\mu$	$-30{,}660/H$	$+6.34\times10^8/H^2$
−1	−½	0	$+\mu_P H+\mu_R H$	$-\mu_P H'_P+2\mu_D E$	$-10{,}160/H$	$+1.75\times10^8/H^2$
−1	−½	−1	$+\mu_P H+\mu_D H+\mu_R H$	$-\mu_P H'_P-\mu_D H'_D+S-\mu_D E$	$+0$	$+0$

TABLE VIII. *Magnetic fields at which resonances will occur for changes of orientation of the deuteron spin in* HD *molecules in the first rotational state.* $H_0=hf_0/\mu_D$. $S'=\langle 2\mu_P/5r^3\rangle_{Av}$

m_J	m_P	Δm_D	Magnetic fields at which resonances occur: First order	Second order	Third order
1	½	$0\leftrightarrow1$	H_0	$-H'_D+S'-3E$	$-11{,}900/H$	$-2.05\times10^8/H^2$
1	½	$-1\leftrightarrow0$	H_0	$-H'_D+S'+3E$	$-24{,}000/H$	$-5.38\times10^8/H^2$
1	−½	$0\leftrightarrow1$	H_0	$-H'_D-S'-3E$	$-39{,}500/H$	$+5.56\times10^8/H^2$
1	−½	$-1\leftrightarrow0$	H_0	$-H'_D-S'+3E$	$+12{,}600/H$	$+4.09\times10^8/H^2$
0	½	$0\leftrightarrow1$	H_0	$-2S'+6E$	$+386/H$	$-4.55\times10^8/H^2$
0	½	$-1\leftrightarrow0$	H_0	$-2S'-6E$	$-48{,}500/H$	$-3.02\times10^8/H^2$
0	−½	$0\leftrightarrow1$	H_0	$+2S'+6E$	$-48{,}500/H$	$+3.02\times10^8/H^2$
0	−½	$-1\leftrightarrow0$	H_0	$+2S'-6E$	$+386/H$	$+4.55\times10^8/H^2$
−1	½	$0\leftrightarrow1$	H_0	$+H'_D+S'-3E$	$+12{,}600/H$	$-4.09\times10^8/H^2$
−1	½	$-1\leftrightarrow0$	H_0	$+H'_D+S'+3E$	$-39{,}500/H$	$-5.56\times10^8/H^2$
−1	−½	$0\leftrightarrow1$	H_0	$+H'_D-S'-3E$	$-24{,}000/H$	$+5.38\times10^8/H^2$
−1	−½	$-1\leftrightarrow0$	H_0	$+H'_D-S'+3E$	$-11{,}900/H$	$+2.05\times10^8/H^2$

TABLE IX. *Collected data on D in* HD. *Frequency 2.419 MC.*

m_J	m_P	m_D	Perturbations predicted from H_2 and D_2 constants: First order	Second order	Third order	Total	Experimental value	Line designation	Perturbations from HD constants
1	½	$0\leftrightarrow1$	−59.11	−3.26	−0.14	−62.5	−62.2	C_L	−62.6
1	½	$-1\leftrightarrow0$	+45.59	−6.39	−0.39	+38.8	+39.0	B_R	+39.0
1	−½	$0\leftrightarrow1$	−86.39	−10.89	+0.40	−96.9	−98.7	E_L	−96.3
1	−½	$-1\leftrightarrow0$	+18.31	+3.38	+0.30	+22.0	+23.2	A_R	+22.8
0	½	$0\leftrightarrow1$	+77.42	+0.1	−0.33	+77.2	75.9	D_R	+78.0
0	½	$-1\leftrightarrow0$	−131.98	−13.55	−0.22	−145.8	−145.9	F_L	145.4
0	−½	$0\leftrightarrow1$	+131.98	−12.62	+0.22	+119.6	+118.8	F_R	119.3
0	−½	$-1\leftrightarrow0$	−77.42	+0.1	+0.33	−77.0	−77.7	D_L	−77.8
−1	½	$0\leftrightarrow1$	−18.31	+3.41	−0.30	−15.2	−15.0	A_L	−16.0
−1	½	$-1\leftrightarrow0$	+86.39	−10.40	−0.40	+75.6	+75.9	E_R	+75.1
−1	−½	$0\leftrightarrow1$	−45.59	−6.55	+0.39	−51.8	−51.5	B_L	−51.9
−1	−½	$-1\leftrightarrow0$	+59.11	−3.15	+0.14	+56.1	+55.8	C_R	+56.2

action constant $\mu_D E = e^2qQ/4$. These energy levels are given in Table VII which is complete up through the third order of the perturbation theory expanded about the strong field levels. Algebraic expressions for the second- and third-order terms are not given in the tables as the expressions are too clumsy to print. Since these expressions involve the constants H'_D, H'_P, S, and E, the numerical values given in the table were calculated after the constants were known. For our purposes they are most conveniently given in the peculiar energy units gauss-nuclear-magnetons. They can be converted to ergs simply by multiplying by 5.04×10^{-24} erg/gauss/n. m. Just as in D_2, these terms vanish in very high field when the Paschen-Back effect is complete. However, for HD this field must be unusually large to make the magnetic energy of the rotational moment different from that of the deuteron moment by an amount large compared with the other interactions. This is true because the rotational moment (0.660 n. m.) is so nearly equal to the deuteron moment (0.855 n. m.)

Table VIII gives expressions for the positions of the lines accompanying changes of m_D by ±1. This table is derived from Table VII just as was done for the corresponding table (Table III) for D_2.

The simplest procedure to follow in the analysis of this spectrum is to estimate the values of the constants in the theory from the experimental values of the constants obtained with H_2 and D_2 and then to use these constants to predict the positions of the spectral lines. If this procedure proves successful in predicting the observed lines we will automatically have an identification of the lines with the quantum numbers of the transitions between energy levels. Once such an identification has been made we can reverse the process and calculate the values of the constants from the experimentally determined line positions. This direct intercomparison of the constants for the three different molecules is possible because the internuclear distances are almost identical. In fact, the values of $\langle r^{-3}\rangle_{Av}$ for H_2 and HD differ by only 1 part in 400. This enables us to make an excellent estimate of $S' = \langle 2\mu_P/5r^3\rangle_{Av} = 13.64$ gauss. Since the electron densities of these molecules depend primarily on the nuclear charge and the internuclear distance, the gradients of the electric field with which the quadrupole moment of the deuteron interacts will be equal in D_2 and HD. The interaction constant E can be taken over directly from H'''' of D_2. Similar considerations for the constants H'_D and H'_P are not as certain for two reasons. First, there is no complete quantitative theory for the corresponding constants in H_2 and D_2 which could be modified for HD. And second a naïve theory suffers because of the asymmetry of the HD molecule. For instance, it is not immediately evident that H'_D should equal H'_P and this question does not arise for H_2 or D_2. However, we know that the rotational magnetic moments of H_2, HD, and D_2 are 0.88, 0.66 and 0.44 nuclear magneton, respectively[11] and these quantities are in inverse ratio to the reduced masses of these molecules. We also know that $(H')_{H_2}$ is 27.2 gauss and $(H')_{D_2}$ is 14.0 gauss again in inverse ratio to the reduced masses. We therefore assume that $H'_D = H'_P = 20.4$ gauss.

The values indicated above have been substituted into the formulas for the first-, second-, and third-order perturbations for the D nuclear transitions of HD. The results of these calculations are shown in Table IX. The column marked "Total" is simply the sum of the entries in the three columns to the left of it. The experimental values and their designations are placed so that they correspond most nearly to the calculated values. The agreement in all but two cases is good. The two experimental values which do not agree with the calculated perturbations are necessarily poor because they are merely the center of gravity of a pair of unresolved lines. No further argument, then, is necessary in justification of the assignment of the quantum numbers of the transitions to the experimental lines.

Evaluation of the constants H'_P, S' and E from the experimental data given in Table IX was made in the following way. The second- and third-order perturbations were evaluated using the preliminary constants from H_2 and D_2. These appear in Table IX. The algebraic expressions for the first-order terms were equated to the experimentally evaluated perturbations diminished by the calculated second- and third-order perturbations. The lines A_R and A_L were omitted from the group for reasons that are immediately

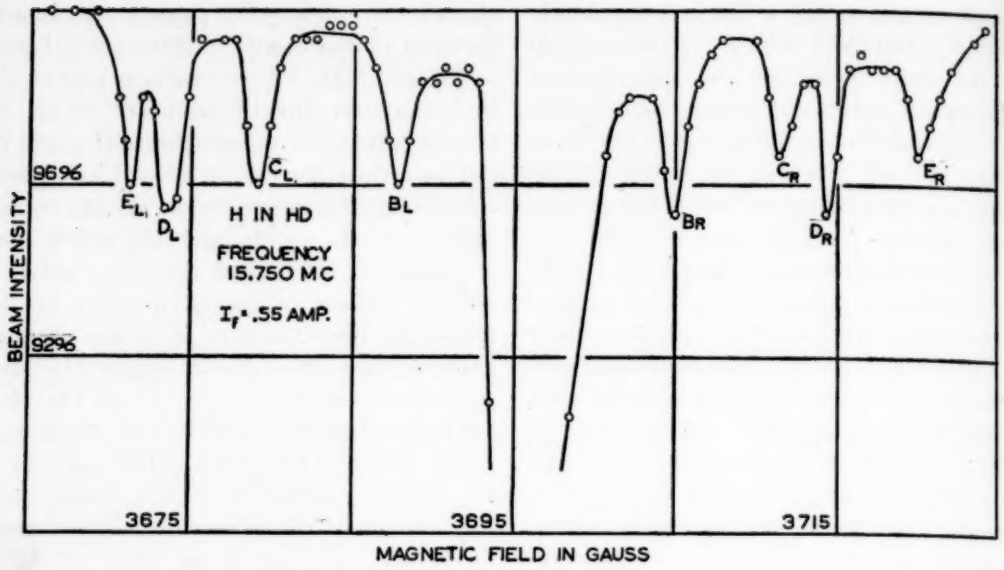

FIG. 4. Radiofrequency spectrum of HD at 80°K for $\Delta m_P = \pm 1$ with m_D and m_J unchanged.

evident in Fig. 3. The experimental lines E_R and D_R were taken together by averaging the theoretical first-order formulas and equating the resulting expression to the displacement of the one unresolved minimum which represents them both. Using this latter equation twice we get ten simultaneous equations which were solved by the method of least squares for the three constants, and we obtain:

$$H'_D = 20.07 \text{ gauss}; \qquad S' = 13.348 \text{ gauss};$$
$$E = 17.495 \text{ gauss}.$$

The perturbations calculated with these constants are given in Table IX: Agreement with the experimental values is naturally better than with the preliminary values. In fact, except for those minima (A_R, A_L, D_R, E_R) which have already been discussed, the experiment can be regarded as internally consistent to better than 0.5 gauss.

H IN HD

Figure 4 shows the group of minima for changes of m_P of ± 1 at a frequency of 15.750 MC. For these data particular attention has to be paid to the constancy of the homogeneous magnetic fields, while the intensity measurements are made. This is difficult because the intervals between the minima are a very small fraction of the total field. In fact, for the data to be of real quantitative value comparable with the other results of this set of experiments it was necessary to hold the field constant to 0.2 gauss in 3700 gauss. This implies that the field excitation current had to be adjusted and read to 0.01 amp. in 200 amp. Further the slight hysteresis in the electromagnet makes it necessary to vary the current in only one direction during a set of measurements. Because of the slowness of the action of the Pirani gauge detector (15 sec. per deflection and nine deflections per point) at least five hours is required to take one experimental curve. These requirements taxed the rheostat control and storage battery bank to their limit. It can be seen in Table X why it was not expedient to take these measurements at much lower field values where these experimental difficulties would be reduced proportionately. Control and measurement of the radiofrequency were not difficult because of the stability of the r.f. oscillator and the ease of using the General Radio No. 620A wave meter.

Reference to Fig. 4 shows that besides the deep central minimum there are eight small minima for $J=1$, whereas it is stated above that there should be nine. It will be shown presently that the theory predicts that one of the small ones should be in the position occupied by the deep central minimum, and therefore completely hidden.

The procedure followed in the analysis of the

H nuclear spectrum of HD is entirely similar to the procedure previously outlined for the analysis of the spectrum of D in HD. Table X, which is obtained from Table VII and the relationship $hf_0=2\mu_P H_0$, gives the expressions for the positions of the H in HD lines. The constants involved here are H'_P and $S''=\frac{1}{5}\langle\mu_D/r^3\rangle_{Av}$. A preliminary value of H'_P is found by taking $H'_P=H'_D=20.4$ gauss as in the case of D in HD. The value of $5S''$ may be estimated from $(\mu_D/r^3)=(\mu_D/\mu_P)(H'')_{H_2}=10.45$ gauss. These constants substituted in the expressions given in Table X yield the predicted perturbations listed in Table XI. It is there evident that the "Total" predicted perturbation is in excellent agreement with the experimental value. The assignment of the quantum numbers to the experimental lines is therefore accomplished.

The line expected at -1.98 gauss is completely hidden by the central minimum. The other eight minima are clearly resolved and can be used to form eight simultaneous equations for evaluating the two constants H'_P and S'' (see Table X). The values obtained by the method of least squares are $H'_P=20.48$ gauss and $S''=2.12$ gauss. Using these values to recalculate the positions of the minima we get the last column of Table XI. The internal consistency of this set of data is well within the limit of 0.2 gauss.

Theory of Energy Levels

D_2

The energy levels of the D_2 molecule in the state $J=1$ and situated in an external magnetic field H, taken in the direction of the z axis, are given by the characteristic values of the operator

$$\begin{aligned}\mathcal{H}=&-\mu_D(\mathbf{i}_1+\mathbf{i}_2)_z H-\mu_R J_z H-\mu_D H'(\mathbf{i}_1+\mathbf{i}_2)\cdot\mathbf{J}\\&+(\mu_D^2/r^3)[\mathbf{i}_1\cdot\mathbf{i}_2-3(\mathbf{i}_1\cdot\mathbf{r})(\mathbf{i}_2\cdot\mathbf{r})/r^2]\\&+\frac{e^2qQ}{2J(2J-1)i(2i-1)}\sum[3(\mathbf{i}\cdot\mathbf{J})^2\\&+\tfrac{3}{2}(\mathbf{i}\cdot\mathbf{J})-i(i+1)J(J+1)],\quad(2)\end{aligned}$$

where $\mathbf{i}_1$ and $\mathbf{i}_2$ are the spin operators for the two deuteron spins, r is the internuclear distance, and the other symbols have their usual meanings.

The first and second terms represent the effect

TABLE X. *Magnetic fields for which resonances will occur for changes of orientation of the proton spin in* HD *molecules in the first rotational state.* $H_0=hf_0/2\mu_P$. $S''=\langle\mu_D/5r^3\rangle_{Av}$.

m_J	m_P	m_D	Magnetic fields for which resonances occur: First order		Second order	Third order
1	$-\frac{1}{2}\leftrightarrow\frac{1}{2}$	1	H_0	$-H'_P+2S''$	$-109/H$	
1	$-\frac{1}{2}\leftrightarrow\frac{1}{2}$	0	H_0	$-H'_P$	$-4270/H$	$+1.15\times10^6/H^2$
1	$-\frac{1}{2}\leftrightarrow\frac{1}{2}$	-1	H_0	$-H'_P-2S''$	$+1250/H$	$+2.57\times10^6/H^2$
0	$-\frac{1}{2}\leftrightarrow\frac{1}{2}$	1	H_0	$-4S''$	$+3460/H$	$-1.15\times10^6/H^2$
0	$-\frac{1}{2}\leftrightarrow\frac{1}{2}$	0	H_0		$-3880/H$	
0	$-\frac{1}{2}\leftrightarrow\frac{1}{2}$	-1	H_0	$+4S''$	$+3460/H$	$+1.15\times10^6/H^2$
-1	$-\frac{1}{2}\leftrightarrow\frac{1}{2}$	1	H_0	$+H'_P+2S''$	$+1250/H$	$-2.57\times10^6/H^2$
-1	$-\frac{1}{2}\leftrightarrow\frac{1}{2}$	0	H_0	$+H'_P$	$-4270/H$	$-1.15\times10^6/H^2$
-1	$-\frac{1}{2}\leftrightarrow\frac{1}{2}$	-1	H_0	$+H'_P-2S''$	$-109/H$	

TABLE XI. *Collected data on H in* HD. *Frequency 15.750 MC.*

m_J	m_P	m_D	Perturbations predicted from H_2 and D_2 constants: First order	Second order	Third order	Total	Experimental value	Line designation	Perturbations from HD constants
1	$-\frac{1}{2}\leftrightarrow\frac{1}{2}$	1	-16.22	-0.03	0.00	-16.25	-16.09	C_L	-16.27
1	$-\frac{1}{2}\leftrightarrow\frac{1}{2}$	0	-20.40	-1.15	0.08	-21.47	-21.64	D_L	-21.55
1	$-\frac{1}{2}\leftrightarrow\frac{1}{2}$	-1	-24.58	0.34	0.18	-24.06	-24.11	E_L	-24.20
0	$-\frac{1}{2}\leftrightarrow\frac{1}{2}$	1	-8.36	0.93	-0.08	-7.51	-7.57	B_L	-7.63
0	$-\frac{1}{2}\leftrightarrow\frac{1}{2}$	0	0.00	-1.98	0.00	-1.98		A	
0	$-\frac{1}{2}\leftrightarrow\frac{1}{2}$	-1	8.36	0.93	0.08	9.37	9.55	B_R	9.49
-1	$-\frac{1}{2}\leftrightarrow\frac{1}{2}$	1	24.58	0.34	-0.18	24.74	24.95	E_R	24.88
-1	$-\frac{1}{2}\leftrightarrow\frac{1}{2}$	0	20.40	-1.15	-0.08	19.17	19.22	D_R	19.25
-1	$-\frac{1}{2}\leftrightarrow\frac{1}{2}$	-1	16.22	-0.03	0.00	16.19	16.37	C_R	16.21

of the external field on the deuteron and rotational magnetic moments, respectively. The third term is the "spin orbit" interaction of the deuteron magnetic moments with the molecular rotation, and the coupling constant H' has the significance of the magnetic field produced by the rotation at the location of the nuclei. The fourth term is the familiar dipole-dipole interaction between the two nuclear magnets.

The last term represents the effect of the nuclear quadrupole moment and is summed over both nuclei. The quantity q has a meaning similar to that of Eq. (1).

In the appendix it will be shown that for identical nuclei the fourth term may be written as

$$\left\{\frac{I(I+1)+4i_1(i_1+1)}{(2I-1)(2I+3)(2J-1)(2J+3)}\right\}$$
$$\times[3(\mathbf{I}\cdot\mathbf{J})^2+\tfrac{3}{2}(\mathbf{I}\cdot\mathbf{J})-I(I+1)J(J+1)]\frac{\mu_D{}^2}{r^3}, \quad (3)$$

where I is the total spin for both deuterons, which is 1 in our case, and i_1, the spin of the individual nucleus, is also 1. The factor in curly brackets is therefore $\frac{2}{3}$. It will also be shown that for the case of total spin $I=1$, the summation in Eq. (2) is equal to the negative of the operator in square brackets in formula 3. *Thus the total quadrupole moment effect is as if we had one nucleus with a nuclear spin of 1 and a quadrupole moment of sign opposite to that of the quadrupole moment of the actual particles.*[12a]

Putting in the values of I and J we may therefore write Eq. (2) as

$$\mathcal{H}=-\mu_D m_I H-\mu_R m_J H-\mu_D H'\mathbf{I}\cdot\mathbf{J}$$
$$+\left\{\frac{2\mu_D{}^2}{5r^3}-\frac{e^2qQ}{2}\right\}[3(\mathbf{I}\cdot\mathbf{J})^2+\tfrac{3}{2}(\mathbf{I}\cdot\mathbf{J})$$
$$-I(I+1)J(J+1)]. \quad (4)$$

From this form it appears that a quadrupole moment effect cannot be distinguished from dipole-dipole interaction between the two nuclei.

For purposes of convenience we will write $\{2\mu_D{}^2/5r^3-\frac{1}{2}e^2qQ\}$ as $(2\mu_D/5)(H''+H''')$, where $H''=\mu_D/r^3$, and $H'''=-5e^2qQ/4\mu_D$. H'' and H''' may be expressed in gauss and are a measure of the magniture of their respective interactions.

In an infinitely strong field (complete Paschen-Back) the diagonal elements of $\mathcal{H}$ give the value of the energy levels of the molecule. These diagonal elements are given by the formula (see appendix)

$$\mathcal{H}(m_I m_J)=-\mu_D m_I H-\mu_R m_J H-\mu_D H' m_I m_J$$
$$+\frac{\mu_D}{5}(H''+H''')[3m_I{}^2-I(I+1)]$$
$$\times[3m_J{}^2-J(J+1)]. \quad (5)$$

when we set $I=1$ and $J=1$.

If H is not infinitely great these formulae hold only approximately and must be corrected for the effect of the off-diagonal matrix elements. The energy levels including their perturbations are listed in Table I. The necessary calculations are indicated in the appendix.

HD

For the HD molecule the calculation is somewhat lengthier. The energy expression is

$$\mathcal{H}=-2\mu_P m_P H-\mu_D m_D H-\mu_R m_J H$$
$$-2\mu_P H'_P(\mathbf{i}_1\cdot\mathbf{J})-\mu_D H'_D(\mathbf{i}_2\cdot\mathbf{J})$$
$$+\frac{2\mu_P\mu_D}{r^3}\left[\mathbf{i}_1\cdot\mathbf{i}_2-\frac{3(\mathbf{i}_1\cdot\mathbf{r})(\mathbf{i}_2\cdot\mathbf{r})}{r^2}\right]$$
$$+\frac{e^2qQ}{2J(2J-1)i_2(2i_2-1)}[3(\mathbf{i}_2\cdot\mathbf{J})^2$$
$$+\tfrac{3}{2}(\mathbf{i}_2\cdot\mathbf{J})-i_2(i_2+1)J(J+1)], \quad (6)$$

where i_1 and i_2 are the proton and the deuteron spins, respectively, and H'_P and H'_D the spin orbit constants for the proton and deuteron which need not necessarily be the same; m_P, m_D, and m_R are the magnetic quantum numbers of the proton, deuteron, and rotation, respectively.

We may write

$$(2\mu_P\mu_D/r^3)\left[\mathbf{i}_1\cdot\mathbf{i}_2-\frac{3(\mathbf{i}_1\cdot\mathbf{r})(\mathbf{i}_2\cdot\mathbf{r})}{r^2}\right]$$
$$=\frac{\mu_P\mu_D}{r^3}\frac{2}{(2J+3)(2J-1)}[3(\mathbf{i}_1\cdot\mathbf{J})(\mathbf{i}_2\cdot\mathbf{J})$$
$$+3(\mathbf{i}_2\cdot\mathbf{J})(\mathbf{i}_1\cdot\mathbf{J})-2\mathbf{i}_1\cdot\mathbf{i}_2J(J+1)]. \quad (7)$$

[12a] We are indebted to Dr. Nordsieck for bringing this to our attention.

TABLE XII. *Summary of results. All quantities in gauss.*

	(μ_P/r^3)	(μ_D/r^3)	SPIN-ORBIT CONSTANT	$(-5e^2qQ/4\mu_D)$
m_I in H_2	34.1		27.2	
m_I in D_2		*10.6*	14.0±0.6	87.5±1
m_D in HD	33.4±1	*10.24*	20.1±1.	87.5±1
m_P in HD	*34.5*	10.60±0.2	20.48±0.2	

The diagonal elements of (6) for infinitely strong fields are therefore

$$\mathcal{H}(m_P m_D m_J) = -2\mu_P m_P H - \mu_D m_D H - \mu_R m_J H$$
$$-2\mu_P H'_P m_P m_J - \mu_D H'_D m_D m_J$$
$$+\tfrac{1}{8}\mu_P H''[3m_J^2 - J(J+1)]m_P m_D$$
$$-\tfrac{1}{8}\mu_D H'''[3m_J^2 - J(J+1)][3m_D^2 - i_2(i_2+1)]. \quad (8)$$

when we use the same definition of H'' and H''' as in Eq. (5). The values of i_2 and J are each equal to 1.

These elements together with their perturbations are listed in Table VII.

RESULTS

Table XII is a summary of the constants obtained from the experiments on H_2, D_2 and HD in the state $J=1$. The quantities have the dimensions of magnetic field and the results are given in gauss. Each row gives the final results obtained from the spectrum which arises from the indicated transition. The first row gives the results of paper I. The second row gives the results obtained from the 6-line spectrum of D_2, and the third and fourth rows the results of the two spectra in HD. The italicized quantity 10.6 in the second row is the value of μ_D/r^3 from the fourth row. This quantity is subtracted from the sum $[\mu_D/r^3-(5e^2qQ/4\mu_D)]$ which is measured experimentally to obtain the quantity in the fourth column. Similarly the italicized quantities μ_D/r^3 and μ_P/r^3 in the third and fourth rows are obtained by multiplying the directly measured values of μ_P/r^3 and μ_D/r^3 by the accurate ratios μ_D/μ_P and μ_P/μ_D, respectively, as obtained from the previous paper. These are entered in the table for the purpose of comparison.

From the quantities given in the first two columns one may calculate the nuclear magnetic moments in question. The results agree with the previously published[10] values of the proton and deuteron moments as is evident from the small variations of the numbers in the first two columns.

The quadrupole moment of the deuteron is calculated from the results of the fourth column. We precede this calculation with a discussion of the determination of the sign of the moment.

In the detailed discussion of the nuclear spectrum of D_2 the following argument was advanced to lead to a positive value of the sign of H'''. The D_2 spectrum requires that H' and S_D have the same sign, and, since H' has the value predicted from the H_2 spectrum, H' is most likely positive. Therefore S_D and H''' are positive. The only seeming weak point in this argument is the sign of H', but it is almost inconceivable that it be negative.

However, the D nuclear spectrum of HD permits us to be certain even with regard to this point. Let us make the violent assumption that H' for the D_2 molecule is negative. Consequently S_D is also negative. The internal consistency of the D_2 nuclear spectrum is not affected by this assumption. We would therefore have $S_D=-98.10$ gauss, and since H'' is positive and equals 10.5 gauss, the quantity $H'''=-108.6$ gauss. For HD we now have the quantity $6E=6H'''/5=-130.3$ gauss. This value combined with $2S'=+26.7$ gauss gives 157.0 gauss for the first-order term for the line with quantum numbers $(0, -\tfrac{1}{2}, -1\rightarrow 0)$. The second-order perturbation is positive and the other perturbations are negligible. Therefore a line is predicted *at least* as far from the center as 157 gauss. Experimentally the largest observed positive displacement is 118.8 gauss, and this line, of course, fits with the assumption that H''' is positive. Therefore we conclude that H''' is positive.

The measured value of $(-5e^2qQ/4\mu_D)$ is 87.5 gauss from Table XII. In a forthcoming paper, one of us (N.F.R., Jr.) will present data obtained from the analysis of the spectra of D_2 and HD arising from the transitions $m_J=\pm 1$. If we include these values in the average the quantity becomes 87.2±0.5 gauss.

To calculate Q the value of q must be inserted. Nordsieck[12] has calculated the quantity $q'=[1/R^3$

[12] A. Nordsieck, Phys. Rev. **57**, 556(A) (1940).

$-\frac{1}{2}\int \rho d\tau(3\cos^2\theta-1)/r^3]$ for the deuterium molecule. In this expression R is the internuclear distance and the integral is taken over the electronic wave function of the deuterium molecule; r is the distance of the electron from the nucleus and θ is the angle which r makes with the internuclear axis. Thus q' is $\frac{1}{2}\partial^2 V/\partial z^2$. Since our q is defined with respect to the rotational state of the molecule $m=J=1$, it is related to q' by $q=-2Jq'/(2J+3)=-2q'/5$. Nordsieck's value of q' is 1.193×10^{24} cm^{-3}, i.e., the effect of the positive nuclear charge is greater than the combined effect of the two electrons. Since $H'''=-5e^2qQ/4\mu_D$ has been shown to be positive and since q is negative, Q the nuclear quadrupole moment is positive. Thus

$$Q=\frac{87.2\times0.855\times5.04\times10^{-24}\times2}{4.80^2\times10^{-20}\times1.193\times10^{24}}$$

and therefore $Q=2.73\times10^{-27}$ cm^2.

This value is more precise than the value previously reported[1] because of the refinement of the experiments and the refinement of Nordsieck's calculation of q. The chief source of error is in q.

Discussion

The positive sign of the quadrupole moment of the deuteron shows that the charge distribution is that of a prolate spheroid spinning about its major axis. Most of the other known nuclear quadrupole moments also show this surprising property.

Although the quadrupole moment of the deuteron, 2.73×10^{-27} cm^2, is the smallest value yet reported for any nucleus, it does not mean that the deuteron is exceptional. It must be remembered that the optical methods which have been used to study other nuclei are not sensitive enough to detect quadrupole moments very much smaller than 10^{-25} cm^2. Furthermore, it should be noted from the definition of Q, $eQ=e\int\rho(3z^2-r^2)d\tau$, that for a given asymmetry, i.e., a given value of $3z^2/r^2$, the larger nuclei should have larger quadrupole moments. Moreover, more than one nuclear charge may contribute to the moment. In fact for the heavier nuclei some of the quadrupole moments are so large that this must necessarily be the case. It would perhaps be more revealing to consider Q/Z rather than Q itself for purposes of comparison.

It may be of interest to calculate the quantity $3z^2/r^2$ which is a rough measure of the departure of the deuteron from spherical symmetry. We write $3z^2/r^2=1+Q/r^2$. For r^2 we take the average squared distance of the proton from the centroid of the deuteron. This quantity calculated from the deuteron wave function[13] is 2.38×10^{-26}. The value of $3z^2/r^2$ is therefore 1.115.

It is of importance to consider whether the effect which we ascribe to the presence of a quadrupole moment in the deuteron can be due to some other form of interaction between the deuteron spin and the molecular rotation. The experimental result which is observed is an interaction of the dipole-dipole form. As J. H. Van Vleck has pointed out to us, such effects can arise in the second-order interaction of the nuclear spin with the electrons of the molecule. However, the excellent agreement of the values of the proton moment, as obtained directly, and from the analysis of the H_2 spectrum in which the moment is evaluated from the dipole-dipole interaction, precludes this possibility. This point of view receives further support from the results presented in this paper, which also show that the dipole-dipole interaction in HD is exactly the magnitude to be expected from the known values of the nuclear moments. To this evidence must be added the experimental proof that the electronic wave functions of H_2, D_2, and HD are not greatly changed because of the differences in their moments of inertia, as is shown by the fact that the rotational magnetic moments[11] are closely proportional to the angular velocities of rotation in the state $J=1$. This is likewise true for the spin-orbit coupling which, as has been pointed out, may be considered as the magnetic field produced by the rotation of the molecule at the positions of the nuclei.

As has been suggested by Schwinger,[14] the presence of a quadrupole moment in the deuteron indicates that the ground state of the deuteron is not a $^3S_1$ state but may be a mixture of $^3S_1$

[13] H. Bethe and R. Bacher, Rev. Mod. Phys. **8**, 112 (1936) (Eqs. (44a) and (44c)).

[14] J. Schwinger, Phys. Rev. **55**, 235 (1939).

and $^3D_1$. On this view the deuteron magnetic moment will be a resultant of the contributions not only of the spin moments of the proton and neutron but also of the orbital moment of the proton. If the moments of the proton and neutron were strictly additive, the effect of the quadrupole moment would result in a seeming departure from this additivity in that the deuteron moment would not be just the sum of the proton and neutron moments.

Fortunately it is possible to make this interesting comparison because of the recent measurement of the neutron moment by Alvarez and Bloch.[15] Within the experimental errors the sum of the moments of the proton and the neutron is equal to that of the deuteron. Whether this apparent additivity conceals a real nonadditivity will not be known until an adequate theory of the deuteron is given which accounts quantitatively for all the known facts including the magnitude of the quadrupole moment.

This investigation has been aided by grants from the Research Corporation and the Carnegie Institution of Washington.

Appendix

The magnetic dipole-dipole interaction of Eq. (2) of the text contains the operator $[(\mathbf{i}_1\cdot\mathbf{i}_2)r^2-3(\mathbf{i}_1\cdot\mathbf{r})(\mathbf{i}_2\cdot\mathbf{r})]/r^2$. If we introduce the total nuclear spin $\mathbf{I}=\mathbf{i}_1+\mathbf{i}_2$ this expression can be written as

$$\{\tfrac{1}{2}[\mathbf{I}^2r^2-3(\mathbf{I}\cdot\mathbf{r})^2]-\tfrac{1}{2}[\mathbf{i}_1^2r^2-3(\mathbf{i}_1\cdot\mathbf{r})^2]-\tfrac{1}{2}[\mathbf{i}_2^2r^2-3(\mathbf{i}_2\cdot\mathbf{r})^2]\}/r^2. \tag{9}$$

By a general theorem[16] we can write

$$\text{(a)}\quad \frac{(x+iy)^2}{r^2}=-\frac{2}{(2J-1)(2J+3)}(J_x+iJ_y)^2,$$

$$\text{(b)}\quad \frac{z(x+iy)}{r^2}=-\frac{2}{(2J-1)(2J+3)}\tfrac{1}{2}[J_z(J_x+iJ_y)+(J_x+iJ_y)J_z], \tag{10}$$

$$\text{(c)}\quad \frac{3z^2-r^2}{r^2}=-\frac{2}{(2J-1)(2J+3)}(3J_z^2-J_x^2-J_y^2-J_z^2).$$

When formula 9 is expanded and Eqs. (10) substituted it becomes

$$-\frac{1}{(2J-1)(2J+3)}\{[\mathbf{I}^2\mathbf{J}^2-\tfrac{3}{2}(\mathbf{I}\cdot\mathbf{J})-3(\mathbf{I}\cdot\mathbf{J})^2]-[\mathbf{i}_1^2\mathbf{J}^2-\tfrac{3}{2}(\mathbf{i}_1\cdot\mathbf{J})-3(\mathbf{i}_1\cdot\mathbf{J})^2]$$
$$-[\mathbf{i}_2^2\mathbf{J}^2-\tfrac{3}{2}(\mathbf{i}_2\cdot\mathbf{J})-3(\mathbf{i}_2\cdot\mathbf{J})^2]\}. \tag{11}$$

If i_1 and i_2 are equal, then for all matrix elements, m_I, m_J, I, $J\rightarrow m_I'$, m_J', I, J, this operator is equivalent to the operator

$$-\frac{I(I+1)+4i_1(i_1+1)}{(2I-1)(2I+3)(2J-1)(2J+3)}[\mathbf{J}^2\mathbf{I}^2-\tfrac{3}{2}(\mathbf{J}\cdot\mathbf{I})-3(\mathbf{J}\cdot\mathbf{I})^2] \tag{12}$$

for any value of the total spin I. There are matrix elements where $\Delta I=2$ which can be obtained from formula 11 but not from formula (12). For D_2 in the state $I=1$ these additional terms do not exist.

The coefficient multiplying the operator is obtained by using the expressions for the matrix elements of the spins i_1 and i_2 when combined to give a total spin I.[17]

[15] L. Alvarez and F. Bloch, Phys. Rev. **57**, 111 (1940).
[16] H. A. Bethe, *Handbuch der Physik*, Vol. 24, No. 1, Eq. (65.36).
[17] E. U. Condon and G. H. Shortley, *Theory of Atomic Spectra* (Cambridge University Press, 1935), Chapter III.

To show the total effect of the two deuteron quadrupole moments in Eq. (2) of the text we simply add the two operators in the sum. From Eqs. (11) and (12) this operator becomes

$$\left[1-\frac{I(I+1)+4i_1(i_1+1)}{(2I-1)(2I+3)}\right][\mathbf{J}^2\mathbf{I}^2-\tfrac{3}{2}(\mathbf{J}\cdot\mathbf{I})-3(\mathbf{J}\cdot\mathbf{I})^2]. \tag{13}$$

For the special case of D_2, $i_1=i_2=1$, $I=1$, the first parenthesis of 13 is equal to -1. Thus it is seen that the combined effect of the two deuterons is equivalent to that of a single spin of unity with a quadrupole moment of opposite sign.

The matrix elements of

$$F=3(\mathbf{I}\cdot\mathbf{J})^2+\tfrac{3}{2}(\mathbf{I}\cdot\mathbf{J})-I(I+1)J(J+1) \tag{14}$$

are easily written down from the expansion

$$\begin{aligned}F=&\tfrac{1}{2}[3J_z^2-J(J+1)][3I_z^2-I(I+1)]+\tfrac{3}{4}[J_z(J_z+iJ_y)+(J_z+iJ_y)J_z][I_z(I_z-iI_y)+(I_z-iI_y)I_z]\\&+\tfrac{3}{4}[J_z(J_z-iJ_y)+(J_z-iJ_y)J_z][I_z(I_z+iI_y)+(I_z+iI_y)I_z]\\&+\tfrac{3}{4}[(I_z+iI_y)^2(J_z-iJ_y)^2+(I_z-iI_y)^2(J_z+iJ_y)^2].\end{aligned} \tag{15}$$

Utilizing the rules of matrix multiplication and the matrix elements of angular momentum,

$$\begin{aligned}(m|L_z|m)&=m,\\(m|L_z+iL_y|m-1)&=[(L+m)(L-m+1)]^{\frac{1}{2}},\\(m|L_z-iL_y|m+1)&=[(L-m)(L+m+1)]^{\frac{1}{2}},\end{aligned} \tag{16}$$

we obtain all the matrix elements of F. The first term on the right-hand side of 15 gives all the diagonal elements; the second and third all the elements where m_J, $m_I\rightarrow m_J\pm1$, $m_I\mp1$; and the last two terms the elements m_J, $m_I\rightarrow m_J+2$, m_I-2 and m_J-2, m_I+2, respectively. These elements are

$$\begin{aligned}(m_Jm_I|F|m_Jm_I)&=\tfrac{1}{2}[3m_I^2-I(I+1)][3m_J^2-J(J+1)],\\(m_Jm_I|F|m_J-1m_I+1)&=\tfrac{3}{4}(2m_J-1)(2m_I+1)[(J+m_J)(J-m_J+1)(I-m_I)(I+m_I+1)]^{\frac{1}{2}},\\(m_Jm_I|F|m_J+1m_I-1)&=\tfrac{3}{4}(2m_J+1)(2m_I-1)[(J-m_J)(J+m_J+1)(I+m_I)(I-m_I+1)]^{\frac{1}{2}},\\(m_Jm_I|F|m_J-2m_I+2)&=\tfrac{3}{4}[(J+m_J)(J+m_J-1)(J-m_J+1)(J-m_J+2)(I-m_I)\\&\qquad\times(I-m_I-1)(I+m_I+1)(I+m_I+2)]^{\frac{1}{2}},\\(m_Jm_I|F|m_J+2m_I-2)&=\tfrac{3}{4}[(J-m_J)(J-m_J-1)(J+m_J+1)(J+m_J+2)\\&\qquad\times(I+m_I)(I+m_I-1)(I-m_I+1)(I-m_I+2)]^{\frac{1}{2}},\end{aligned} \tag{17}$$

These elements are evaluated for D_2 by setting $I=J=1$.

In the case of HD there is no total spin angular momentum. We multiply up the expression in the bracket of the right-hand side of Eq. (7) and write

$$\begin{aligned}G=&3(\mathbf{i}_1\cdot\mathbf{J})(\mathbf{i}_2\cdot\mathbf{J})+3(\mathbf{i}_2\cdot\mathbf{J})(\mathbf{i}_1\cdot\mathbf{J})-2\mathbf{i}_1\cdot\mathbf{i}_2J(J+1)\\=&2i_z^1i_z^2[3J_z^2-J(J+1)]-\tfrac{1}{2}[(i_x^1+ii_y^1)(i_x^2-ii_y^2)+(i_x^1-ii_y^1)(i_x^2+ii_y^2)][3J_z^2-J(J+1)]\\&+\tfrac{3}{2}[i_z^1(i_x^2-ii_y^2)+i_z^2(i_x^1-ii_y^1)][J_z(J_x+iJ_y)+(J_x+iJ_y)J_z]\\&+\tfrac{3}{2}[i_z^1(i_x^2+ii_y^2)+i_z^2(i_x^1+ii_y^1)][J_z(J_x-iJ_y)+(J_x-iJ_y)J_z]\\&+\tfrac{3}{2}(i_x^1+ii_y^1)(i_x^2+ii_y^2)(J_x-iJ_y)^2+\tfrac{3}{2}(i_x^1-ii_y^1)(i_x^2-ii_y^2)(J_x+iJ_y)^2.\end{aligned} \tag{18}$$

The matrix elements are obtained with the use of the relations of Eqs. (16). The letter i without subscripts is $\sqrt{-1}$. For the particular case of HD we set $i_1=\frac{1}{2}$, $i_2=1$, and $J=1$. The spin orbit interactions of the form $I\cdot J$ are obtained in the usual manner by setting

$$I\cdot J=I_zJ_z+\tfrac{1}{2}(I_z+iI_y)(J_x-iJ_y)+\tfrac{1}{2}(I_z-iI_y)(J_x+iJ_y)$$

together with Eqs. (16).

The perturbations of the energy levels of Eqs. (5) and (8) are obtained from the matrix elements by the usual second-order perturbation theory.

APRIL 15, 1940 PHYSICAL REVIEW VOLUME 57

Secondary Emission from Films of Silver on Platinum*

A. E. HASTINGS†
Brown University, Providence, Rhode Island
(Received February 1, 1940)

Total secondary emission and energy distribution of secondary electrons have been measured for films of known thickness of silver on platinum. The depth of origin of the total secondary emission in silver as a function of primary energy, and the depth of origin of secondaries having a given energy were determined. Practically all the secondaries from primaries of 20 ev energy originate at a depth of less than 15 atomic layers, and those from primaries of 50 ev energy originate at a depth of less than 30 atomic layers. For higher primary energies, it was found that an appreciable amount of emission comes from a depth greater than 150 atomic layers. Secondaries with energies close to that of the primaries originate at a depth small compared to that of the low energy secondaries.

INTRODUCTION

WHILE the general characteristics of secondary emission from pure metals have been well established, there is lack of agreement among investigations as to the depth at which the secondary electrons originate and as to the relative effects of the work function and the characteristic production of secondaries within the metal. Secondary emission is generally assumed to be dependent on the surface work function through which the electrons must escape and on the production and absorption of electrons within the metal, these two effects being independent and characteristic of the particular metal.

Treloar[1] concludes that a sufficiently thin film of a foreign material on a metal acts chiefly to alter the work function, the emission from the film itself being important only at greater film thickness. Plotting secondary emission against thickness of barium deposited on tungsten, he found an increase in the secondary emission as the work function was lowered to that of barium, the production of secondaries still occurring mostly in the tungsten. At greater thickness of barium film more of the secondaries originated in the film, which has a smaller production than that of tungsten, and the emission decreased, resulting in a maximum in the curve. The thickness at which half the emission came from the film and half from the base metal he estimated as 1.4 atomic layers, the mean depth of origin of secondaries from 300-volt primaries.

Coomes[2] has not observed this maximum for thorium on tungsten, but Bruining[3] has observed it for barium on molybdenum. He found that the photoelectric emission also reached a maximum for the same thickness of barium, indicating that these changes were due in part to the decreasing work function. From experimental work with rough surfaces and from an experimental value of the absorption coefficient,

* Part of the dissertation presented for the Degree of Doctor of Philosophy at Brown University.
† Now at Naval Research Laboratory, Washington, D. C.
[1] L. R. G. Treloar, Proc. Phys. Soc. **49**, 392 (1937).
[2] E. A. Coomes, Phys. Rev. **55**, 519 (1939).
[3] H. Bruining and J. H. DeBoer, Physica **6**, 941 (1939).

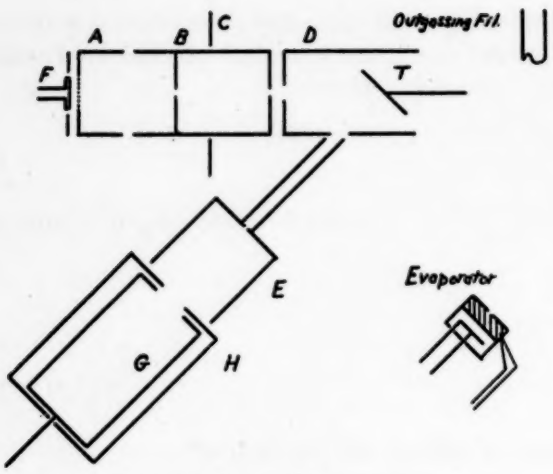

FIG. 1. Diagram of apparatus.

Bruining[4] has calculated the mean depth of origin for secondaries from primaries of 500 ev energy to be about 14 atomic layers. He has also[5–8] investigated the mechanism of secondary emission in detail.

In the present work, measurements were carried out to determine the depth of origin of the total secondary emission in silver as a function of primary energy, and the depth of origin of secondaries having a given energy. Total emission and energy distribution of secondary electrons were measured for films of silver on platinum. Energy distributions were obtained by the retarding potential method. Silver films were obtained from a calibrated source, so that the film thickness was determined absolutely from the time of evaporation. While the measurements were affected by changes in work function, resulting in the maximum in the curves described, no means for measuring the work function directly were included in the apparatus.

APPARATUS AND PROCEDURE

The electron gun is based on the one described by Farnsworth,[9] and is shown in Fig. 1. F is an oxide-coated filament, surrounded by a guard ring. Electrons from F are accelerated through a circular disk and cylinder A, and again to B, where the beam is defined by the 1.5-mm holes. C is a disk connected at filament potential to repel any electrons leaking around the gun. The beam is so defined that all the electrons pass through the hole in the disk D and strike the platinum target T. The secondaries coming from T are collected by D, and the current to D is measured by a galvanometer. The current to T and D is the primary current, and the ratio of secondary to primary current is called R.

The energy analyzer is shown below the gun. Part of the secondary emission from T passes through a hole in D and through a small shielding tube through the hole in E. The beam of secondaries is defined by the target and the hole in E, and can pass through the disk H, without striking the sides of the hole, and into the shielded collector G. A retarding field is applied between the cylinder E, and H and G. The current to G is measured with a d.c. amplifier, using an FP-54 in a DuBridge and Brown circuit and a sensitivity of about 5×10^{-14} ampere per mm. Only those secondaries from T will reach the collector whose energy in electron volts is numerically greater than the retarding potential applied between the collector and target. Curve 1, Fig. 2, shows a typical curve of secondary emission obtained with this analyzer. The retarding potential must be corrected for the contact potential of the collector. This analyzer does not give a true distribution curve in energy, but actually gives the integral of the distribution curve between the energy at the point in question and the maximum energy which is the primary energy. The slope of this curve gives the true energy distribution curve, the number of electrons dn having energy between E and $E+dE$. Instead of plotting the complete distribution curves and taking slopes at certain energies, these slopes were determined directly by measuring the collector current at two retarding potentials, one either side of the point in question, and by dividing the difference in currents by the difference in potentials. In this manner, a quantity called R_e, which is proportional to the true number of secondaries having a given energy, was determined. The primary current was of course held constant throughout these readings.

The analyzer was tested by placing it in front

[4] H. Bruining, Physica **3**, 1046 (1936).
[5] H. Bruining and J. H. DeBoer, Physica **4**, 473 (1937).
[6] H. Bruining, Physica **5**, 17 (1938).
[7] H. Bruining, Physica **5**, 901, 913 (1938).
[8] H. Bruining and J. H. DeBoer, Physica **6**, 823, 834 (1939).
[9] H. E. Farnsworth, Rev. Sci. Inst. **15**, 290 (1927).

of the electron gun, so that their axes coincided. Then electrons from the gun could enter the analyzer and their energy distribution could be determined. Curve 2, Fig. 2, shows this distribution. The lack of a very sharp drop at the right is due to the inhomogeneity in energy in the beam from the gun and to scattering in the analyzer. Curve 3 was taken with a small magnetic field along the axis of the analyzer, and the resulting sharper drop indicates that there is a slight amount of scattering in the analyzer.

The evaporator is built similar to one used by Farnsworth.[10] A block of silver is completely enclosed in a molybdenum container except for a 1-mm hole in the upper face through which silver can evaporate. The silver is heated by radiation from a flat spiral filament beneath it and enclosed in a molybdenum radiation shield. A Chromel-Alumel thermocouple imbedded in the side of the silver, in conjunction with a type K potentiometer, indicates the temperature, which is held so that the evaporation rate is constant within one percent.

The silver source was calibrated in a separate tube by depositing on clean microscope cover glasses, which could be moved into the path of the vapor stream for known lengths of time with the source at 900 degrees centigrade. The source was thoroughly outgassed in a high vacuum until the pressure was about 2×10^{-7} mm of mercury with the evaporator running, so that the rate of deposition would become constant before calibrating. In weighing on a microbalance, sensitive to about 10^{-6} g, the glass with the deposit was counterbalanced by a glass similarly treated but not exposed to silver. The film was removed either by rubbing the glass with lens paper, or by washing in 50 percent HNO_3, or both, all methods giving substantially the same result. The glass counterpoise was similarly treated. A maximum error of 5 percent was estimated for this determination. It was found that 4.65×10^{-6} gram of silver was deposited on a square cm in one hour, with the source 12.2 cm from the plates. For a (100) face, this corresponds to 21.6 atomic layers per hour, and for a (111) face, 30.6 atomic layers per hour. All data here are expressed in (100) units.

[10] H. E. Farnsworth, Phys. Rev. **49**, 605 (1936).

The electron gun is placed in the main tube, and the analyzer in a side tube sealed at 45 degrees from the axis of the main tube. The evaporator is built in a small side tube and sealed to the experimental tube. The vacuum system consists of two Apiezon vapor pumps backed by a Cenco Hyvac pump. No grease or wax seals were used in the high vacuum side. The condensing traps between the experimental tube and pumps and between the fore pump and the vapor pumps were cooled with CO_2 snow in acetone. The experimental tube was kept sealed to the pumps throughout the experiments and the vapor pumps were run continuously. Helmholtz coils were used to compensate the earth's magnetic field. Pressure in the experimental tube was measured by an ionization gauge.

Curves of R *vs.* film thickness were plotted for several primary energies, and curves of R_e *vs.* film thickness were plotted for secondary energies with primary energy held at 300 ev. These curves show the effects of the film of varying thickness on the emission characteristics.

Results and Discussion

Thin films

The curves of Figs. 3 and 4 are typical of the results obtained. All the curves of R *vs.* film thickness, except that for 20-volt primaries, show a maximum. This is the behavior observed

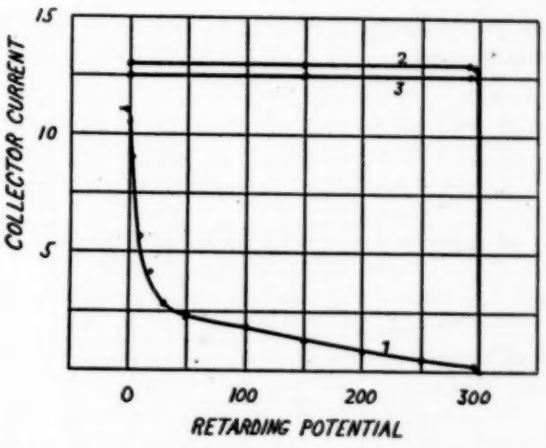

Fig. 2. Curve 1, for secondary electrons from platinum, shows the variation of collector current with retarding potential on the analyzer. Curve 2 shows the same variation for electrons coming directly from the gun. Curve 3 is similar to Curve 2, but was taken with a small axial magnetic field around the analyzer.

by Treloar for barium on tungsten, and is assumed to be due to the decrease in work function caused by a thin film of silver, since silver has a work function about two volts lower than that of platinum. The maxinum occurs at about one atomic layer, which is close to the optimum thermionic layer observed by Treloar for barium on tungsten. The maximum in R is smaller for curves taken at lower primary energies, which requires some explanation. During deposition of the first few atomic layers, two things are happening,—R is increasing because of the falling work function, and R is decreasing from the value characteristic of platinum to that characteristic of silver because of the emission from the silver film. The latter effect is more marked in the case of low primary energies, since there is smaller penetration of the low energy primaries. The former effect is more marked in the case of high primary energies, since there are many more secondaries with energy near that corresponding to the work function, and these secondaries are free to escape when the work function decreases. These effects tend to produce a greater initial increase in the curves of R at high than at low primary energies, and for 20-volt primaries, there is no maximum at all, but R decreases continually with film thickness.

The maximum does not appear in the curves of R_e *vs.* film thickness, since a change in work function of the order of two volts affects only electrons with very low energies in the metal, which are always excluded at the retarding potentials used.

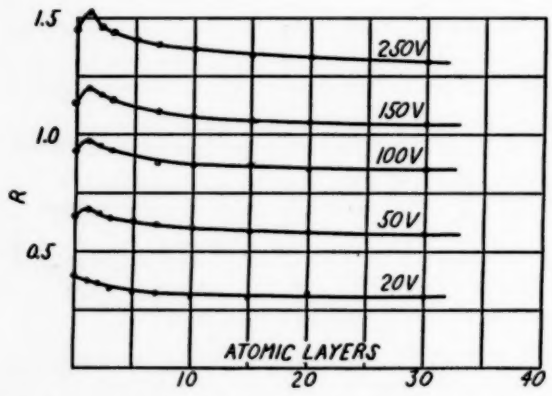

FIG. 3. Secondary emission R (ratio of secondary to primary current) is shown as a function of atomic layers of silver on platinum for several primary energies.

R_e increases with film thickness for secondaries with energy near that of the primaries, and decreases for secondaries with low energies, because of the change in the secondary energy distribution from that characteristic of platinum to that characteristic of silver. However, the increase at high secondary energies is much more sudden than the decrease at low secondary energies, which would mean that most of the secondaries of high energy originate at a smaller depth than those of low energy, and that most of the high-energy secondaries come from only a few atomic layers. This agrees with the results of Farnsworth[10] for electron diffraction. He used secondary electrons with energy very close to that of the primaries, and found that when the conditions for diffraction were established, the diffracted beam was entirely eliminated upon deposition of a few atomic layers of a foreign material. This indicates that secondaries with energy near that of the primaries do not originate at a very great depth as compared with the depth of origin of some of the low energy secondaries. This can be explained by saying that those primaries which penetrate the target to a depth of more than a few atomic layers are, because of the greater probability of scattering with loss of energy, nearly all effective in producing secondaries of low energy, while primaries scattered very near the surface have a greater probability of being returned with small loss of energy.

Thick films

The curves of R in Fig. 3 for thick films give the maximum depth of origin of secondaries as a function of primary energy, since at the film thickness where the curve becomes flat all the secondaries are coming from the film. The curves indicate that practically all the secondaries from primaries of 20 ev energy originate at a depth of less than 15 atomic layers, and those from 50-volt primaries originate at a depth of less than 30 atomic layers. For higher primary energies, the curves do not flatten sufficiently to indicate the maximum depth from which secondaries come. Some data obtained out to 150 atomic layers show that the emission is still changing.

The curves of R_e (Fig. 4) at thick films all tend to flatten out at about the same rate with film thickness regardless of secondary energy.

For a primary energy of 300 ev the curves become very nearly flat at less than 20 atomic layers. The following explanation may account for the fact that secondaries with high energies appear to come from depths no greater than those at which secondaries with low energies originate. The number of high energy secondaries, coming partly from the base metal even at large film thicknesses, is still changing at these thicknesses. These secondaries are effective in producing some low energy secondaries in the film, and thus the low energy secondaries continue to change as long as do the high energy ones.

Since the total emission R is the integral of R_ϵ over the whole range of secondary energies, R should be affected by changes in R_ϵ, and R should change with film thickness as long as any curve of R_ϵ does. Actually R for primary energies above 20 ev changes much longer than does any of the curves of R_ϵ for energies measured, for which there is no explanation.

The slope of the R *vs.* film thickness curve would give the number of secondaries originating in a layer of thickness dx at depth x. However, because the slope changes so little beyond the first few atomic layers, and because of the experimental errors, it was not possible to determine this slope graphically with sufficient accuracy to be of any value.

Effects of gas

While the pressure in the experimental tube was about 5×10^{-8} mm of mercury during readings, it rose to about 1.5×10^{-7} mm of mercury when the evaporator was running. At this pressure the values of R for the outgassed target dropped as much as 10 percent in a few minutes, as determined by running the evaporator without exposing the target to the silver vapor. This rapid change did not occur with the gun filament, but not the evaporator, running, and was not due to contamination of the target by evaporation

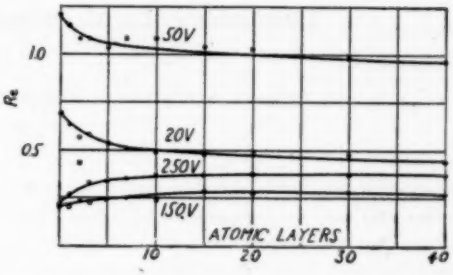

FIG. 4. Secondary emission R_ϵ of electrons having several energies ϵ is shown as a function of atomic layers of silver on platinum. The primary energy is 300 ev.

from the filament. The initial maximum in the curves of R, Fig. 3, was not observed when silver was deposited directly on the outgassed target, without first exposing it to gases from the heated evaporator. The gas condensed on the target lowered R sufficiently to overcome the rise due to the silver film. Since it was not possible to outgas thoroughly the large block of silver in the evaporator, the procedure was to expose the clean target to gas coming from the evaporator until the emission no longer changed with exposure, and to take the value of R so obtained as characteristic of platinum for this work. The fact that with this procedure the maximum in R occurred seems to indicate that the surface layer of gas remains or is constantly formed during deposition, has a constant effect on the work function, and does not affect the interpretation of the results. Moreover, readings could be checked closely over long periods after the initial contamination of the target with gas had occurred. Several sets of curves similar to those in Figs. 3 and 4 showed essentially the same behavior.

The author is greatly indebted to Professor H. E. Farnsworth for his valuable criticism and guidance, and to Dr. John C. Turnbull for certain suggestions, during the progress of the experimental work.

Luminescence of Pure Radium and Barium Compounds

D. H. KABAKJIAN
Department of Physics, University of Pennsylvania, Philadelphia, Pennsylvania
(Received December 1, 1939)

Luminescence, excited in some carefully purified crystalline barium and radium compounds by alpha-, beta-, and gamma-rays has been examined. It is found that these compounds show a faint luminescence at ordinary room temperatures. When the compounds are heated to various temperatures and then cooled, they show a continuous increase in luminescence with increase of temperature of heat treatment until a maximum is reached. Heat treating at higher temperatures diminishes the brightness. The temperature of maximum brightness is not directly related to the melting point of the individual compounds. The maximum brightness in some cases was several hundred times the initial brightness of unheated crystals. No abrupt changes in intensity of luminescence, such as might be due to changes in crystalline form, were detected. The bearing of these experiments on the modern theories of luminescence in crystalline solids is discussed.

IN a previous paper,[1] the writer described some experiments to prove that certain zinc borate compounds can be made luminescent in a state of purity. The compounds were obtained in a vitreous form by fusion in an electric furnace at about 1100°C. The clear zinc borate glass so obtained does not show any appreciable luminescence. If, however, it is devitrified by heating for a few minutes at 600°C, a strong luminescence of a purple color is developed. The structural change from the vitreous to crystalline state was verified by Debye-Scherrer photographs of the samples, which were kindly obtained for me by Professor B. E. Warren of the Massachusetts Institute of Technology.

The close relationship between crystalline structure and luminescence in inorganic solids, indicated by the above experiment, is already well established. A general theory of luminescence based on the existence of electronic energy states in a crystal lattice, has been found quite successful in explaining a large number of experimental observations.[2] Most of the investigations are carried on, however, on activated crystals, i.e., on crystals containing an impurity atom.

The possibility of luminescence in very pure crystals was doubted by most investigators until very recent times. Since the luminescence of some pure crystals is now generally admitted,[3] the nature of the luminescent centers has become a problem of theoretical interest. The writer has found that, with rays from a radioactive source, luminescence can be excited in a number of pure crystals. The initial brightness in most of these is rather faint, but in some cases it can be increased several hundred times by a proper heat treatment.

Most impurity-activated phosphors also require heat treatment in their preparation, but in these cases the object is either to insure a diffusion of the impurity into the crystal lattice of the base material (solid solution) or to develop a crystalline structure in the mixtures when these are obtained in the form of fine precipitates. In the experiments described below, these considerations do not exist, since the compounds are obtained initially in crystalline form and no impurity is added. Raising the pure compound to a given temperature and then cooling produces a modification in its crystalline state which makes luminescence possible. It was considered desirable, therefore, to investigate the relation between the temperature of heat treatment and intensity of luminescence.

Materials and Mode of Procedure

The luminescence of the following compounds has been investigated: $RaBr_2$, $RaCl_2$, $RaSO_4$, $BaBr_2$, $BaCl_2$, $BaSO_4$. Pure $RaBr_2$ was obtained from a mixture of radium bromide and barium bromide by a large number of successive crystallizations with distilled water and pure HBr. Its weight and radium-element content corresponded to pure anhydrous $RaBr_2$. Radium sulphate was

[1] D. H. Kabakjian, Phys. Rev. **51**, 365 (1937).
[2] F. Seitz, Trans. Faraday Soc. **35**, 74 (1939).
[3] N. Riehl, Ann. d. Physik (5) **29**, 637 (1937); S. Rothschild, Zeits. f. Physik **108**, 24 (1937); W. H. Byler, J. Am. Chem. Soc. **60**, 1247 (1938).

obtained from pure radium bromide by precipitation with C.P. sulphuric acid. The precipitate then was dissolved in hot concentrated sulphuric acid and was recrystallized by evaporation. The crystals were well formed and fairly large. Barium compounds were similarly purified by repeated recrystallizations.

The pure compounds were placed in hard glass or silica tubes of 1.5–2.5 mm outside diameter and 0.2 mm wall thickness. They were heated to various temperatures in an electric furnace until equilibrium was established and their brightness was measured after cooling to room temperature. On account of their small size, the samples reach room temperature in a few minutes. Tests showed that the luminescence was not affected by the rate of cooling. In radium compounds the excitation is produced chiefly by alpha-rays. In the case of barium compounds, a small quantity of radium bromide or radium sulphate was added to the corresponding barium salts for an alpha-ray excitation. Since there is a possibility that the added radium might act as an impurity activator, these were investigated by a different process which eliminates this uncertainty. The barium salt was placed between the walls of two coaxial glass or silica tubes closed at the bottom. The thickness of the barium salt was about 0.6 mm. A thin-walled monel metal tube containing 6 mg of radium element in sulphate form was fitted into the inner tube, having a wall thickness of 0.1 mm. The radium tube could be removed during the process of heating the salt. The excitation in this case is produced by beta- and gamma-rays of constant intensity since the radium is in equilibrium with its decay products.

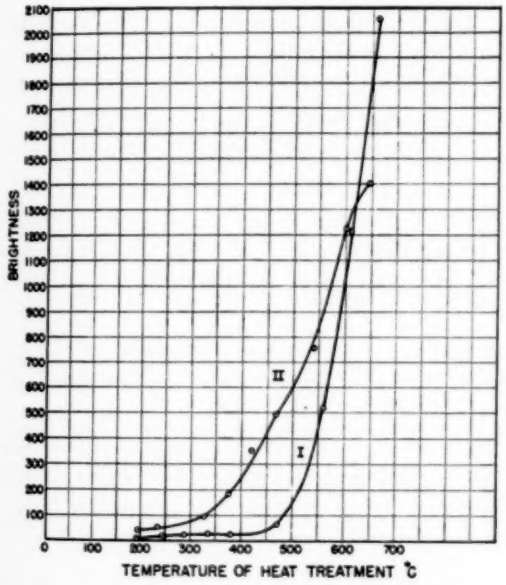

FIG. 1. Growth of brightness, in arbitrary units, of pure radium compounds with the temperature of heat treatment. Curve I, anhydrous radium bromide. Curve II, radium sulphate.

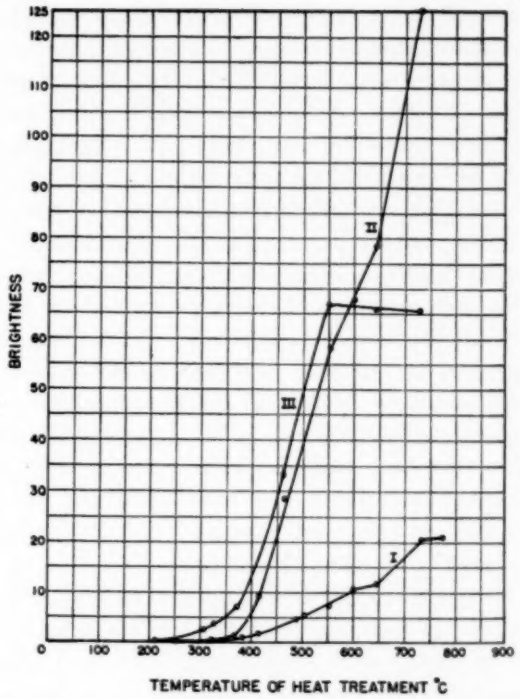

FIG. 2. Growth of brightness of pure barium bromide with the temperature of heat treatment. (I) Barium bromide mixed with 0.24 percent radium bromide, (alpha-ray excitation). (II) barium bromide mixed with 1.2 percent radium bromide. (III) barium bromide excited with beta- and gamma-rays from a sealed radium tube.

The results obtained by this method, which were in general similar to those obtained from mixtures of radium and barium compounds, showed that the production of luminescent centers is independent of the presence of radium atoms.

The brightness measurements were made on a modified Lummer-Brodhun photometer, which has been described in a previous paper.[4]

RESULTS

A large number of determinations made on the temperature-brightness relationship of these

[4] D. H. Kabakjian, Phys. Rev. **44**, 618 (1933).

compounds gave similar results. Some typical curves are indicated below. Fig. 1 gives the variation of brightness for pure radium bromide and radium sulphate with the temperature of heat treatment from 200° to 650°C. It is seen that the brightness rises as a continuous function of this temperature, reaching a maximum at about 650°C for both compounds. This maximum activation temperature apparently is not related to the melting points of the two compounds. The ratio of maximum brightness to the initial brightness for radium bromide is 182 and for radium sulphate 35.4. This ratio refers to visible luminescence only. Since a large portion of the radium sulphate emission lies in the ultraviolet region, the emission energy of the two compounds might approach equality. No attempt was made to determine this point.

Figure 2 gives the activation-temperature relationship for barium bromide. Curves I and II refer to compounds containing 0.24 percent and 1.2 percent of radium bromide, respectively. Excitation in these was produced chiefly by alpha-rays.

Curve III was obtained by beta- and gamma-ray excitation from a sealed radium tube. The curves show the same activation-temperature relationship, although there are some differences in the two types of excitation. The ratio of maximum brightness in samples I and II is roughly proportional to their radium content and therefore to the intensity of excitation. In Fig. 3 the temperature effect is shown for barium chloride also excited by beta- and gamma-rays.

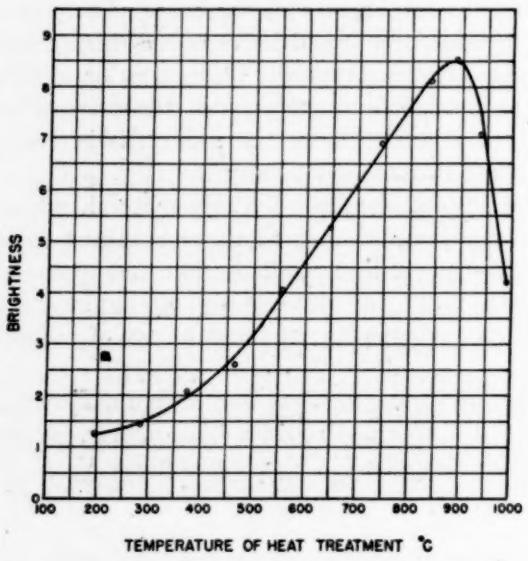

FIG. 3. Growth of brightness of pure barium chloride with the temperature of heat treatment. Beta- and gamma-ray excitation.

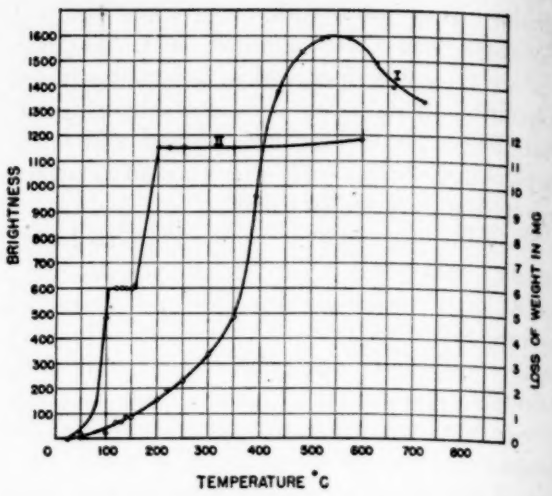

FIG. 4. Curve I. Growth of brightness of pure $BaBr_2 \cdot 2H_2O$ with the temperature of heat treatment (beta- and gamma-ray excitation). Curve II. Loss of water of crystallization during heating. Ordinates to the right.

CRYSTALLIZATION AT LOWER TEMPERATURES

The crystals in the above experiment were produced by boiling the respective solutions to saturation. The bromides contain two molecules of water of crystallization. Complete dehydration of this compound required, under the conditions of these experiments, prolonged heating at 200°C. The boiling point of the sulphate solution in concentrated sulphuric acid is about 190°C, therefore the initial brightness readings had to be started with a heat treatment temperature of 200°C. In the case of bromides, it is possible to extend this part of the curve to a much lower temperature. A saturated solution of barium bromide was prepared at room temperature and placed in a desiccator. A few large clear crystals were produced in the solution by slow evaporation extending over several days. It is assumed that these crystals approximated a perfect lattice better than those produced from hot solutions. The crystals were dried in a desiccator in the same way without heating. This compound, having a formula $BaBr_2 \cdot 2H_2O$ was ground, and its activation-temperature relationship was ex-

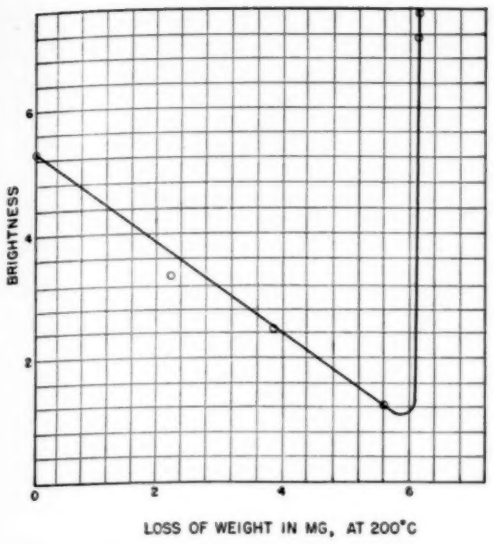

FIG. 5. Variation of brightness with gradual removal of water of crystallization at 200°C.

amined in the same way by beta- and gamma-ray excitation. The loss in weight due to dehydration was determined at the same time.

In Fig. 4, Curve I gives the rise of brightness with the heat treatment temperature. Curve II shows loss of weight due to dehydration. The initial brightness in this case was very low and difficult to measure. The ratio of maximum brightness to the initial brightness was approximately 300.

EFFECT OF WATER OF CRYSTALLIZATION

The removal of the second molecule of water of crystallization had a very marked effect on the intensity of luminescence. As the temperature was raised from 150° to 200°C, the luminescence began to decrease and continued to do so until all of the moisture was removed, when it suddenly rose again. This relation is shown in Fig. 5. A similar effect might have been produced during the removal of the first molecule of water but was not detected because of the faintness of luminescence at the lower temperature. The points on the smooth curve in Fig. 4 represent equilibrium values of brightness.

THE NATURE OF EMISSION BANDS

The compounds were sealed in clear silica tubes and their luminescence was examined by means of a quartz spectrograph. The emission of the sulphates consists of a diffuse band extending from 5800–3000A with a maximum at about 4050A. The bromides give a somewhat overlapping double band with maxima at 4700 and 3000A. The luminescence bands of the same compounds, after a small percentage of Mn or Sa was added to them were also obtained under similar conditions. The added activator in these cases produced its own band, quite distinct both in structure and wave-length, somewhat at the expense of the luminescence of the pure compound, but did not completely supersede it as in the case of zinc borate.[1] These are shown in Fig. 6.

Although absolute purity cannot be claimed for any of these compounds, from the examination of the emission bands of the "pure" and "activated" samples, it seems reasonable to assume that the wide diffuse bands are those due to the compounds themselves and not due to an undetected impurity. A more careful

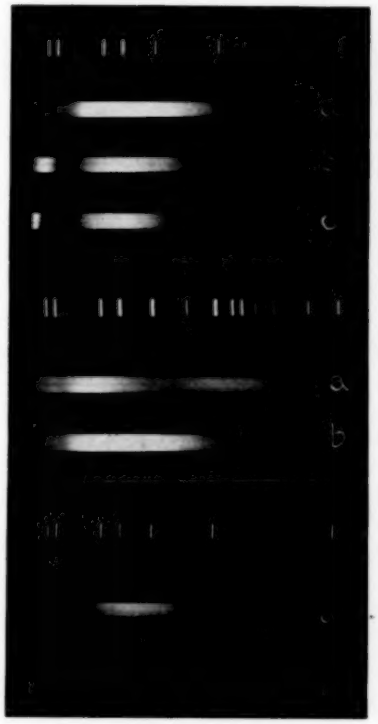

FIG. 6. Luminescence spectra of radium and barium compounds with comparison spectra of Hg arc. Upper panel: (*a*) pure $RaSO_4$; (*b*) $RaSO_4$+Mn; (*c*) $RaSO_4$+Sa. Middle panel: (*a*) $RaBr_2$; (*b*) $RaSO_4$. Lower panel: (*a*) pure $BaSO_4$; (*b*) $BaSO_4$+Sa.

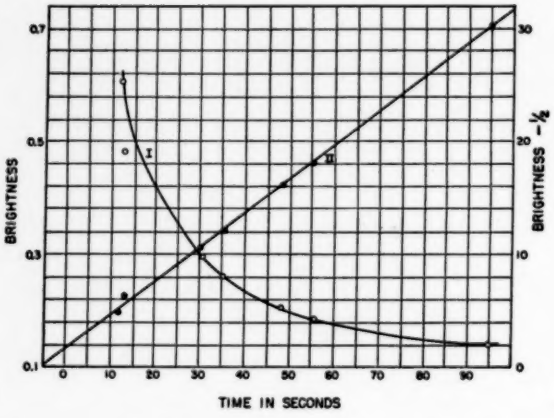

FIG. 7. Decay of phosphorescence of pure barium bromide.

examination of these bands and their dependence on the temperature of heat treatment seems desirable.

RATIO OF PHOSPHORESCENCE TO FLUORESCENCE

This ratio was determined for pure $BaBr_2$ by quickly removing the exciting source (the radium tube) and determining the decay rate of the residual brightness. This is shown in Fig. 7. Plotting the reciprocal of the square root of brightness against time gives a straight line indicating that the phosphorescence is a bimolecular reaction. From the intercept of this curve, the ratio of phosphorescence to fluorescence was found to be approximately equal to 5 percent.

DECAY OF LUMINESCENCE UNDER CONTINUOUS EXCITATION

The decay of luminescence of pure radium sulphate was investigated. The decay was very rapid at the start, but soon became asymptotic with the time axis reaching a constant value and remaining so indefinitely. The decay curve is shown in Fig. 8. The curve is similar to those obtained for pure radium bromide by Rodman[5] and pure barium bromide obtained by Smith.[6] It is very complex. Factors such as decomposition of the compound, change in the absorption coefficient of the material due to discoloration as well as the destruction of the luminescent centers probably enter into it. It has not been possible to find a simple explanation for this decay. The compounds will invariably recover their full luminescence on being heated to the temperatures of maximum activation.

DISCUSSION

When a crystal is irradiated by alpha-, beta- and gamma-rays from radium, as in the above experiments, the electrons can absorb sufficient energy to raise them to any unoccupied energy bands that may exist in the crystal, including the conduction bands (ionization). If these electrons could directly return to their normal levels, luminescence would result. The fact that only very faint luminescence can be obtained in unheated, pure crystals may mean one of two things: (*a*) that permissible and unoccupied energy bands do not exist in pure unheated crystals, (*b*) that such bands may exist but the conditions necessary for the direct return of the electrons to their normal levels, with emission of luminous energy, do not exist. The heating of the crystals to higher temperatures, and then cooling, apparently produces the structural changes necessary for luminescence. It is difficult to determine from these experiments the nature of this change. It cannot be due to a

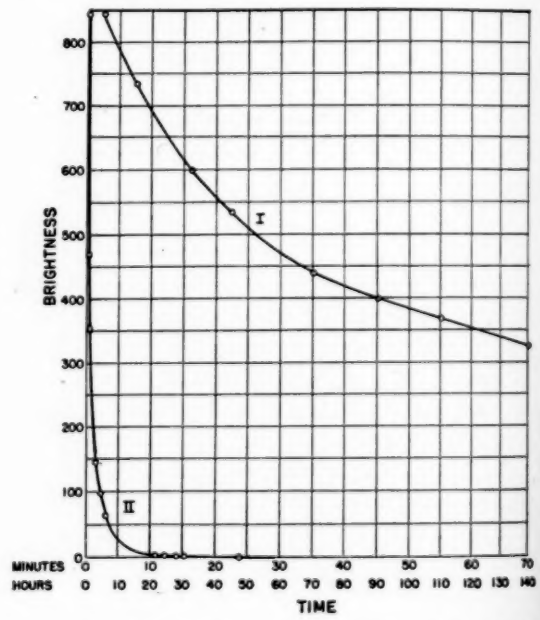

FIG. 8. Decay of luminescence of pure radium sulphate, Curve I time in minutes, Curve II time in hours.

[5] J. Rodman, Phys. Rev. **23**, 478 (1924).
[6] L. E. Smith, Phys. Rev. **28**, 431 (1926).

chemical decomposition, as the compounds remain perfectly white after heating. However, there is distinct evidence of instability, indicated by the fact that heated radium bromide becomes almost black in time, while the unheated specimens show only a slight change in color.

Seitz[7] explains the luminescence of heat-treated pure ZnS as due to Zn atoms diffusing into the interstices of the crystal lattice and acting in the same way as impurity atoms. A similar displacement may be taking place in the case of barium compounds. This would explain the brightness-temperature curves if it be assumed that the number of displaced atoms depends on the temperature of heat treatment. It is still necessary, however, to explain why these give a much broader emission band than other impurity activators as shown in Fig. 6. A more thorough examination of the emission bands and their dependence on the temperature of heat treatment seems desirable.

The author wishes to acknowledge his indebtedness to Dr. G. P. Harnwell and Dr. F. Seitz for many valuable suggestions and criticisms. This research was aided by a grant from the Faculty Research Committee of the University of Pennsylvania and also by a grant from the American Philosophical Society which are hereby gratefully acknowledged.

[7] F. Seitz, J. App. Phys. **10**, 479 (1939).

APRIL 15, 1940 PHYSICAL REVIEW VOLUME 57

The Band Spectrum of Antimony Chloride

W. F. C. FERGUSON AND ISIDORE HUDES
New York University, Washington Square, New York, New York

(Received February 9, 1940)

A band spectrum attributed to the molecule SbCl, in the region λλ4200–5600, has been excited by introducing $SbCl_3$ into active nitrogen. No other bands appeared in the range λ2000 to λ7000. The spectrum consists of bands showing pronounced progressions and degraded towards the red. They can be placed in two sub-systems of bands, designated as A_1 and A_2. Vibrational analysis shows that within experimental error the wave numbers of the heads of forty-one bands of $SbCl^{35}$ are represented by the formulas:

$$A_1 : \nu_1 = 22395 + 244.4u' - 2.28u'^2 - 368.0u'' + 0.84u''^2,$$
$$A_2 : \nu_2 = 25855 + 240.2u' - 2.19u'^2 - 370.0u'' + 1.00u''^2.$$

The chlorine isotope effect appears in 13 bands and is used to confirm the v', v'' designations. The analysis of the spectrum given here is somewhat different from that originally presented two years ago. Many more bands are here accounted for and identified. An attempt failed to produce a spectrum of AsCl by introducing $AsCl_3$ vapor into active nitrogen.

THE electron configurations of the lighter diatomic molecules have already been determined with a fair degree of certainty. Comparatively few measurements have thus far been made of the spectra of the heavy diatomic molecules. Spectra have been produced, however, for many of the diatomic halides of the elements in group IVb of the periodic table. For group Vb there are only the spectra due to SbF [1] and the four bismuth halides.[2] This experiment was undertaken to find out whether the same regularities exist for the halides of group Vb as have been shown to exist for group IVb.[3]

The arrangement of the apparatus and the methods employed for the excitation of the bands of antimony chloride are essentially the same as those originated by Strutt and Fowler[4] in their work with active nitrogen, and as further de-

[1] G. D. Rochester, Phys. Rev. **51**, 486 (1937).
[2] F. Morgan, Phys. Rev. **49**, 41 (1936).

[3] W. Jevons, L. A. Bashford and H. V. A. Briscoe, Proc. Phys. Soc. **49**, 532 and 537 (1937); W. Jevons and L. A. Bashford, Proc. Phys. Soc. **49**, 554 (1937).
[4] R. J. Strutt and A. Fowler, Proc. Roy. Soc. **A86**, 105 (1911).

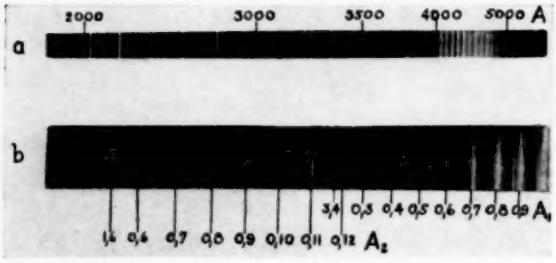

FIG. 1. The spectrum of SbCl; (a) low dispersion, (b) higher dispersion, λ4200−λ5600, with vibrational quantum numbers for systems A_1 and A_2.

veloped by Mulliken[5] in his early work on the band spectra of the copper halides. By introducing the vapor of pure antimony trichloride into a stream of active nitrogen, the spectrum attributed to the molecule SbCl was excited. The wave-length region λ2000 to λ7000 was photographed and examined.

A Hilger quartz spectrograph of low dispersion (200 A/mm at λ5000) was used in the preliminary stages with Eastman 40 plates. With exposures varying up to 70 minutes only one group of bands, between the wave-lengths λ4200–λ5600, was disclosed. Using a glass spectrograph with lenses of 492-mm focal length, dispersion 42 A/mm at λ5000, this system of bands was photographed on Ilford S. G. panchromatic backed plates in ten hours. Intensities were visually assigned. The iron arc was used for wave-length standards.

The bands shade towards the red. Enlargements of the photographs, Fig. 1, illustrate their main features. Fig. 1a was taken with the small quartz spectrograph and shows clearly the existence of the group of bands in the region λλ4200–5600. Taken with the glass instrument of greater dispersion, the general characteristics of the bands are more easily recognized from Fig. 1b. This figure contains the assignments of some of the vibrational quantum numbers in the two systems, A_1 and A_2 (see below).

The heads of forty-one bands which have been observed can be arranged in two sub-systems, designated A_1 and A_2, where A_1 identifies the less refrangible system (smaller value of ν_e). The wave numbers of the band heads are shown in a $v'-v''$ array in Table I, in which are indicated the intensities in parentheses. A_1 bands are placed above A_2 bands with $\delta\nu_e$ between. Several band heads which were impossible of identification, with their estimated intensities, follow: 23970(2); 20141(3); 19789(3); 19490(3); 18838(3); 18114(4); 18088(3); 17726(5) cm^{-1}.

Within experimental error the heads of these two sub-systems of bands of $SbCl^{35}$ are represented by the formulas:

$$\nu_1 = 22395 + 244.4u' - 2.28u'^2 - 368.0u'' + 0.84u''^2,$$
$$\nu_2 = 25855 + 240.2u' - 2.19u'^2 - 370.0u'' + 1.00u''^2,$$

where $u = v + \frac{1}{2}$.

The average of the differences between observed values of the band heads of $SbCl^{35}$ and values calculated by the formulas is ±3.1 cm^{-1}. The constants are different from those originally

[5] R. S. Mulliken, Phys. Rev. **26**, 1 (1925).

TABLE I. *Wave numbers of* $SbCl^{35}$ *band heads, in cm*$^{-1}$*;* A_1 *above* A_2.

v'	$v''=3$	4	5	6	7	8	9	10	11	12	13	14	Means $\Delta G'$ A_1 / A_2
0	21248(1)	20880(2)	20516(3)	20157(4)	19802(4)	19446(4)	19093(4)	18743(5)					
				3460	3456	3455	3454	3455					
				23617(3)	23258(4)	22901(4)	22547(4)	22198(4)	21852(4)	21503(2)	21161(2)	20823(0)	
													236.5 / 236.3
1	21485(2)	21119(2)	20758(3)	20394(4)	20038(1)	19694(0)		18980(2)					
				3457	3458	3447		3454					
				23851(2)	23496(0)	23141(0)		22434(0)	22087(2)	21743(2)	21397(1)	21054(2)	
													235.5 / 232.3
2	21717(1)	21358(3)											
						23375(0)	23021(0)	22664(0)	22319(1)			21287(0)	
													234.3 / —
3	21943(0)	21591(2)											
Means $\Delta G''$ A_1		361.0	362.5	361.0	355.5	353.0	350.0	350.0	—	—	—	—	
A_2		—	—	—	357.0	356.0	354.0	353.0	346.0	346.5	344.0	340.5	

given in a note on the spectrum of SbCl.[6] Whereas only 28 band heads were identified in the earlier note, 54 band heads (including isotope heads) are taken into account here and identified.

It was to be expected that the band heads due to the individual antimony isotopes would not be resolved with the instrument here employed. Weaker heads of $SbCl^{37}$ are displaced toward the system origin from stronger $SbCl^{35}$ heads; the displacement coefficient, $\rho-1$, is -0.0210. The origins of the A_1 and A_2 systems are found by extrapolation to zero displacement. The displacements of 13 bands due to the $SbCl^{37}$ isotope shift are given in Table II.

The agreement of observed and calculated values of the isotope displacements confirms the locations of the system origins (A_1 and A_2). Also, the relative intensities of the isotope bands appear satisfactory for chlorine isotopes.

Evidence for the identity of the emitter of this spectrum was weighed. Vapor of $SbBr_3$ introduced into active nitrogen produced only the NBr spectrum.[7] Vapor of Sb metal produced no spectrum in active nitrogen. The presence of SbN seemed therefore to be eliminated. If, nevertheless, SbN (or SbO) were the emitter, no isotope displacement would be observed. So an alternative classification of the band heads was speculated upon, by considering the above band heads of the isotopic molecule $SbCl^{37}$ as R heads of $SbCl^{35}$ displaced from more intense Q heads of $SbCl^{35}$. This appeared reasonable but was precluded, however, because $\omega_e'-\omega_e''$ is large. Each band would then be characterized by a small interval between Q and R head.[8] This was not the case here.

From the similarity of vibrational constants of these two band systems it is probable that they comprise a doublet system. It is not possible from the present analysis to determine in which state the multiplicity occurs. The existence of a third system, making a triplet, is not impossible; because an odd multiplicity of electronic states is expected for a molecule possessing an even number of electrons. The above statements have likewise been made in reference to SbF.[1]

TABLE II. *Displacements of bands due to* $SbCl^{37}$ *isotope shift.* $\Delta\nu_{CALC.}$ *is* $[(\rho-1)(\nu-\nu_e)]$.

Band A_1	$\Delta\nu_{OBS.}$ (cm^{-1})	$\Delta\nu_{CALC.}$ (cm^{-1})	Band A_2	$\Delta\nu_{OBS.}$ (cm^{-1})	$\Delta\nu_{CALC.}$ (cm^{-1})
0,5	41.	40.	0,6	45.	47.
0,6	49.	47.	0,7	52.	54.
0,7	50.	54.	0,8	64.	62.
0,8	57.	62.	0,9	68.	69.
0,9	60.	69.	0,10	76.	76.
1,5	36.	34.	1,8	56.	57.
1,6	36.	42.			

For group Vb halides a comparison between the constants of the antimony halides and the bismuth halides was made. The constants of the bismuth halides were plotted against the number of electrons in the molecule and were then compared to similar plots for the antimony halides. The expected trends were found in both cases, namely, with increasing number of electrons and mass of a molecule there is a decrease in the values of ω_e and $X_e\omega_e$ in both the upper and lower states, a decrease in ν_e, and an increase in the value of $\delta\nu_e$. Similar trends were found also in the values of the constants of any one halide of the two metals.

The introduction of $AsCl_3$ into streaming active nitrogen produced no characteristic band spectrum in the region λλ2000–7000.

Appreciation is expressed to Thomas J. W. O'Neil for his assistance with this experiment.

[6] I. Hudes, Phys. Rev. **52**, 1256 (1937).
[7] A. Elliott, Proc. Roy. Soc. **A169**, 469 (1939).
[8] W. Jevons, *Report on Band Spectra of Diatomic Molecules*, p. 63.

Spectra of Lead Hydride and Tin Hydride in the Near Infra-Red

WILLIAM W. WATSON AND RALPH SIMON
Sloane Physics Laboratory, Yale University, New Haven, Connecticut

(Received February 2, 1940)

Revised calculations of energy constants of the PbH molecule are presented as a result of analyses of bands in the photographic infra-red. Former v' values are raised by one unit. An isolated weak PbH band is found at 3815A. Additional SnH bands in the red produced in the high pressure arc are briefly discussed.

IN previous reports[1, 2] on the spectra of PbH and SnH in the visible, the probable existence of spectra of both these molecules in the photographic infra-red was mentioned. With further development of the high pressure arc in hydrogen, together with long exposure times and wider slit widths, PbH bands have been recorded to 9105A and SnH bands to 7234A. In addition, careful search for the PbH analog of the violet $^2\Delta \rightarrow {}^2\Pi$ SnH bands reveals a single weak band centered at 3815A. This band is not well developed and is not accompanied by another at any plausible interval for a $^2\Pi$ PbH state.

The Pb and Sn arcs have been run in hydrogen at 4 to 5 atmospheres pressure. All spectrograms were obtained in the second order of a 21-foot grating, average dispersion 2.13A per mm, except those of PbH for wave-lengths longer than 7200A. For the latter the first order with 4.94A per mm was used. Because of the wide-open structure of these hydride spectra, however, this lower dispersion was quite sufficient despite the considerable line widths due to pressure broadening and to the use of a wide slit (0.1 mm).

It was thought that bands involving a new electronic state of PbH might be located in the infra-red, since strong interaction with other states is revealed[1] by the details of the red $^2\Sigma \rightarrow {}^2\Sigma$ system. We find, however, that the extensive PbH spectrum in the infra-red to 9100A belongs completely to this same system. With the inclusion of the data from the analysis of these new bands, plus additional lines in previ-

[1] W. W. Watson, Phys. Rev. **54**, 1068 (1938).
[2] W. W. Watson and R. Simon, Phys. Rev. **55**, 358 (1939).

TABLE I. *Additional bands in the* $^2\Sigma \rightarrow {}^2\Sigma$ *system of* PbH. cm^{-1} *units; d denotes fused lines.*

	(0,2)				(0,3)				(0,4)				(1,3)			
K''	P_1	R_1	P_2	R_2	P_1	R_1	P_2	R_2	P_1	R_1	P_2	R_2	P_1	R_1	P_2	R_2
3		14,543.3							11,800.3		11,808.9					
4		529.3*d*	14,504.0						778.1	11,823.4	790.4	11,831.6				
5		511.6	476.1		13,072.8	13,128.7	13,090.6		751.9	808.9	768.2	819.4	13,555.7		13,575.7	
6	14,422.2*d*	489.0	446.6	14,506.9*d*	042.9	109.6	063.2	13,124.6	723.4	790.4	742.7	803.3	527.4		551.4	
7		462.7	411.1	482.0	008.9	086.1	031.9	102.3	691.7	768.2	712.9	783.4			522.3	
8	344.9*d*	431.5*d*	373.3	453.9	12,970.9	056.9	12,997.2	076.5	656.4	742.7	679.7	759.8	460.2		489.4	
9	301.0*d*	396.7	331.9	420.5	929.2	024.5	957.4	046.3	617.5	712.9	643.1	732.5*d*	420.4*d*	13,520.4	452.7	13,547.8
10	251.7	357.0	285.1	383.6	883.4	12,988.0	913.8	012.3	574.8	679.7	602.7	701.1	376.5	486.9	412.2	517.1
11	199.5	312.6*d*	234.8	342.2	833.5	947.3	866.4	12,973.9	528.4	642.3	558.4	666.3	329.5	449.1	367.8	481.9
12		264.5	180.3	296.2	779.6	902.4	814.9	931.3	478.5	601.2	510.5	626.7	278.3	407.4	319.6	442.7
13	080.9	212.0	121.1	245.5	721.9	853.5	759.6	884.4	424.6	556.2	458.7	583.7	223.5	361.6	267.5	399.4
14	013.5	154.5	057.4	191.5	660.1	800.3	699.7	833.5	367.2	507.6	403.0	537.0	164.9	311.7	211.2	351.7
15	13,943.8	*090.8*d*	13,989.4	131.6	594.3	743.2	636.1	778.3	306.0	454.9	343.6*d*	486.0	102.4*d*	257.4	150.8	300.1
16	869.9*d*	026.5	917.2	066.8	524.4	681.7	568.3	719.0	241.2	398.6	280.6	431.3	035.7	199.2	086.1	243.6
17	790.4	13,956.2*d*	840.3	13,999.5	450.6	616.1	496.4	655.1	172.9*d*	338.2	213.9	372.6	12,964.8	136.8	018.0	183.3
18	707.0	880.5	759.2	926.2*d*	372.5	546.3	420.1*d*	587.2	100.6	274.1	143.3	309.9	890.0	068.4	12,945.2	118.0
19	619.6	800.9	673.6	848.4	290.7	472.4	340.3	515.0	024.5	206.1	069.0	243.5	811.4	12,997.2	868.3	049.8
20	527.4*d*	716.8	583.7	766.3	204.9	394.2	256.2	438.7*d*		134.3	10,990.3	172.9*d*	726.8*d*	921.8	787.2	12,973.9*d*
21	431.2*d*	628.2	489.4	679.8	114.8	312.0		358.1		058.6		098.9	640.3	841.7	702.5	896.2
22		535.1	391.0	588.5	021.1	225.6	075.8	273.4		10,979.4		020.9	548.8	757.3	611.2	813.7
23		438.2	288.6		11,923.4	135.4	11,979.7	184.6					453.2	668.2	517.9	726.8*d*
24		336.3	181.1		821.8	041.1*d*	879.6	091.7					353.4	574.7	420.1*d*	635.0*d*
25		230.3			716.4	11,942.4	775.7	11,994.8					249.4	476.9	317.6	539.0
26						840.0*d*	667.8	894.4					141.1	374.7	211.0	438.7*d*
27						733.4*d*							028.4	268.0	100.6*d*	333.7
28													11,911.9		11,985.4	224.6
29													791.2	041.1*d*	866.3	110.8*d*
30													666.3*d*	11,921.9		11,992.9
31													537.1*d*			871.2
32													404.5			745.3

* Perturbed.

TABLE II. *Corrected* PbH *band origins.* $^2\Sigma \rightarrow {}^2\Sigma$.

v'	$v''=0$		1		2		3		4
0					14,551.1	1388.5	13,162.6	1324.9	11,837.7
					479.0		478.6		
1	17,977.4	1503.1	16,474.3	1444.2	15,030.1	1388.9	13,641.2		
	448.2		448.1		448.0				
2	18,425.6	1503.2	16,922.4	1444.3	15,478.1				
	438.9		438.1						
3	18,864.5	1504.0	17,360.5						
	432.6								
4	19,297.1								
5	(19,700)								

ously analyzed bands, revision of the calculation of the energy constants[1] for PbH is necessary.

RED AND INFRA-RED PbH SPECTRUM

Assignments of the lines of four additional bands at the red end of this system are included in Table I. This analysis is based on the usual combination relations and indicates that the v' numbering of all the bands described in reference 1 should be increased one unit. The results of a recomputation of all band origins are given in Table II. Since we can find no traces of bands that would extend this array upwards, we believe that these vibrational quantum numbers are now correct. New constants of the energy terms are collected in Table III.

These data emphasize the peculiar nature of the upper $^2\Sigma$ state as discussed in reference 1.[3] The new B_0' being markedly lower than the old one, the tendency for the B_v' values to increase with v to a maximum and then to decrease is even more apparent. Since about 500 cm^{-1} are now added to the extent of the stable levels of this state, the cut-off of levels comes actually at about 0.42 volt above the bottom of the potential energy curve. These and the other peculiarities of this $^2\Sigma$ state all point to the existence of additional near-lying electronic states of PbH. The faint band at 3815A is, however, the only indication we can find of other PbH spectra. Because of competition from the continuous background always present in high pressure sources and which is particularly strong to the violet of the 4019 PbI atomic line, long exposure times do not yield better registrations of this band. For this reason and also because of its isolated character we have not attempted its analysis. We conclude that the only stable states of the PbH molecule are those involved in this red band system.

[3] Also cf. L. Gerö, Physica **7**, 155 (1940).

TABLE III. *Constants of the energy terms for* PbH *in* cm^{-1} *units.*

CONSTANT	$^2\Sigma'$	$^2\Sigma''$
B_0^*	2.478	4.899
B_1^*	2.660	4.754
B_2^*	2.766	4.609
B_3^*	2.770	4.467
B_4^*	2.646	4.324
B_e^*		4.971
α		0.144
r_0		1.848A
D_0	-2.66×10^{-4}	-2.01×10^{-4}
ω_e	~520	1564.1
$\chi_e\omega_e$		29.75
ν_e	~18018	

RED SnH SPECTRUM

SnH bands have been photographed further into the red than those already reported.[2] Prominent heads of the red-degrading branches occur at 6745, 6892 and 7030A with a pile-up of lines at 6931A. Between the latter and a long series of lines on its violet side, as well as between two other branches, we find $^2\Pi$-state combination differences.[2] We have not found differences relating these bands to the bands at 6095 and 6214A, however, and since the analysis of all these bands is far from complete we refrain from presenting it. They are definitely of a different type than those of the PbH system, probably $^2\Sigma \rightarrow {}^2\Pi$, judging from the number of branches. It is altogether probable that more SnH bands exist further into the infra-red. Their measurement should prove helpful in the analysis of the bands already photographed, but we find it impossible to obtain high dispersion spectrograms in the infra-red with the present high pressure Sn arc as a source.

Index of Refraction of Methane in the Infra-Red and the Dipole Moment of the CH Bond

R. ROLLEFSON AND R. HAVENS
University of Wisconsin, Madison, Wisconsin

(Received February 21, 1940)

The index of refraction of methane has been measured for 49 different wave-lengths in the infra-red between 1 and 15μ. These data have been interpreted in terms of the active infra-red frequencies of methane, and yield what may be considered estimates of the dipole moment of the CH bond and the rate of change of this moment with CH distance. The measurements show that the infra-red bands are only about one-sixth as strong as would be necessary to remove the discrepancy between $n_\infty - 1$ as obtained from indices of refraction measured at optical wave-lengths and extrapolated to infinite wave-length, and $\epsilon - 1$ as determined from dielectric constant measurements.

THE need for quantitative information on the intensities of infra-red bands of molecular gases has frequently been pointed out. Van Vleck[1] has called attention to the fact that such data would permit quantitative calculation of the contribution of "atomic polarization" to the dielectric constant, thus furnishing a check on dielectric constant measurements and increasing the accuracy of measurements of dipole moments. Dennison[2] and Mulliken[3] have used intensity measurements to calculate "effective charges" of the vibratng molecules (or the rate of change of the dipole moment with internuclear distance) and have pointed out the need for more quantitative data. This paper contains essentially the same information as would be obtained from accurate measurements of the intensities of the infra-red bands of methane. Since the reasons for measuring the refractive index instead of the intensity of absorption have already been pointed out by Van Vleck,[1] and have been fully explained in a previous communication,[4] they will not be repeated here.

The method consists in measuring the change in deviation produced by a change in pressure in a hollow prism containing the gas being studied. The apparatus used was essentially similar to that used for the measurements on HCl,[4] except for the thermopile. The thermopile, mounted on a comparator carriage, is used to locate the image. A new design of thermopile increased the speed of taking observations by a factor of about ten and decreased the uncertainty of measurements by a factor of six.

The new thermopile has two receivers, each 10 mm by 1 mm, mounted side by side, with the edges slightly overlapping but not in contact. Each receiver is mounted on a two-junction pile and the two piles are connected in opposition. Fig. 1 shows a typical curve of galvanometer deflection against position as this thermopile is moved across a slit image. In practice it was necessary to take only four or five points along the straight center portions of the curve, and the two zeros, in order to determine the image position. In the high energy regions of the spectrum, successive determinations of the image position would check to within 0.3 micron. For all the wave-lengths less than 11μ, variations of more than 2 microns were rare. The thermopile case was so constructed that thermal drift was eliminated, and since the thermopile was of the compensated type and the two compensating piles were almost identical, deflections due to electrical surges induced in the galvanometer-thermopile circuit by sparks in neighboring rooms were reduced to a minimum. A Kipp and Zonen type Z C galvanometer was used for all the measurements. When necessary, the deflections were magnified by a thermal relay. With this arrangement, when working at night, it was possible to reach the limit set by Brownian motion of the primary galvanometer.

[1] J. H. Van Vleck, *The Theory of Electric and Magnetic Susceptibilities* (Oxford, 1932), Chapter 3.
[2] D. M. Dennison, Phil. Mag. **1**, 216 (1926); Astrophys. J. **62**, 84 (1925).
[3] R. S. Mulliken, J. Chem. Phys. **2**, 400; **2**, 712 (1934).
[4] R. Rollefson and A. H. Rollefson, Phys. Rev. **48**, 779 (1935).

The methane for most of the measurements was obtained by heating sodium acetate and soda lime. The gas thus obtained was purified by repeated distillations in an all-glass system. The gas was generated several times and the agreement of the refraction measurements on the different samples indicated that the gas was sufficiently pure. However, since the absolute values of the indices of refraction which were obtained did not agree with the value obtained by extrapolating data available for wave-lengths in the visible region of the spectrum, several additional checks were made. Since the same apparatus had been used for measurements on HCl and CO, gases which are easily obtained in high purity and which had given results in close agreement (better than $\frac{1}{4}$ percent) with those obtained by extrapolating the data of Cuthbertson and Cuthbertson, it was decided that the most likely source of error in the measurements on methane was impurity of the gas. The vapor pressure of the methane was then measured at the boiling point of oxygen. The value obtained fitted on the vapor pressure curve as well as those tabulated in the *International Critical Tables*. This indicated that no volatile impurities, such as hydrogen, carbon monoxide, or air, could be present in sufficient quantity to cause a noticeable change of index of refraction. Then varying fractions of the methane condensed in the liquid-air trap were distilled into the hollow prism and the index of refraction measured for each fraction. No change in the index reduced to standard conditions was noted. This indicated that if any impurity were present it must have a vapor pressure curve almost identical with that of methane, or an index of refraction nearly equal to that of methane. An additional check on the less volatile impurities was furnished by the infra-red absorption spectrum of the gas used. Absorption measurements were customarily made throughout the spectrum in order to determine for which wave-lengths there was appreciable absorption, and therefore where measurements of the index of refraction could not be made by the prism method. No bands other than those belonging to methane were observed. It must be pointed out, however, that this constitutes merely corroborative evidence and not conclusive proof of purity, since the resolving power which was used was not high and some of the organic impurities which may have been present have their strongest bands in the same regions as those of methane.

When preliminary efforts at interpretation indicated that the data were not consistent with measurements in the visible, new runs were made for which the methane was generated by a slightly modified Grignard process. Both this process and the chemicals used in it were entirely different from the sodium acetate-soda lime process. The results of the new runs agreed with the old to within 0.5×10^{-6} for the absolute value of n, and so far as shape was concerned the new curves were indistinguishable from the old. Shortly thereafter new measurements[5] on the index of refraction of methane in the visible and ultraviolet appeared. These new values for n gave a dispersion curve which when extrapolated into the infra-red gave values much closer to those we obtained, although the disagreement was still 4×10^{-6}, or about 1 percent in the absolute value of $n-1$. The slope of the new extrapolated curve allowed a much more satisfactory

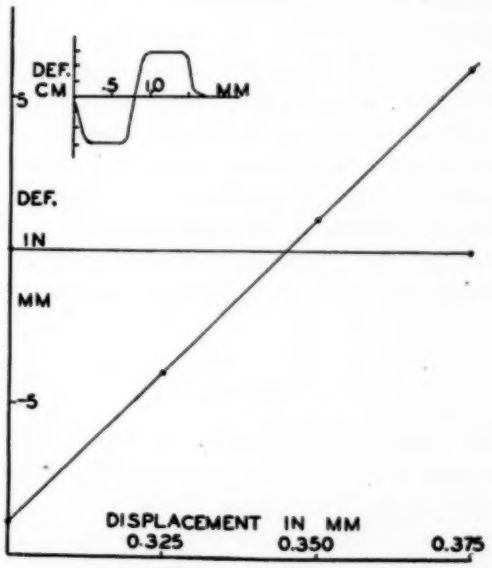

FIG. 1. Galvanometer deflection as a function of thermopile position. The upper diagram is an approximate curve for a large total displacement, while the lower curve is one actually obtained in the measurements on methane. With points as good as these, the position for zero deflection can be determined to 1μ or better if the comparator screw is reliable.

[5] S. Friberg, Diss. Lund. (1933) quoted by T. Larsen, Zeits. f. Physik **105**, 166 (1937).

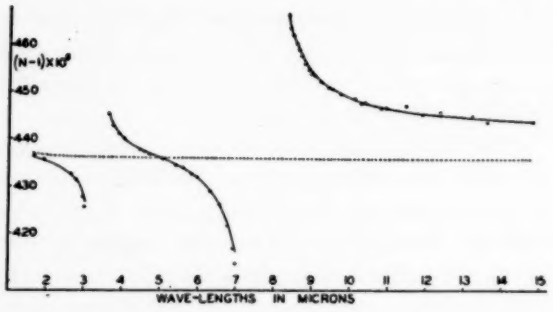

FIG. 2. Dispersion of methane. The solid curve is that given by theory; the points are averaged experimental results; the dotted curve is $(n-1)$ extrapolated.

interpretation of our results than the old. Even if the 1 percent difference which remains were due entirely to systematic error in the present experiments or impurity of the gas used, it would be of little importance in the interpretation of the results, since the changes of index which are important probably cannot be measured to within one percent. Any impurity which had active frequencies in the infra-red would of course cause trouble but would probably have been detected by its absorption.

The effect of purity of spectrum was tested by trying several different slit widths in the monochromator and gas spectrometer. The trials showed that changing slit widths over the range actually used had no effect. The values of the index of refraction which were obtained were reduced to standard conditions (0°, 760 mm) by means of coefficient of expansion and *pv* data given in the *International Critical Tables*. ($\alpha=0.003683$; the *pv* correction was at most about $\frac{1}{4}$ percent.)

RESULTS

The index of refraction of methane was measured at 49 different wave-lengths between 1.6 and 14.8μ. The values of the index for the various wave-lengths are given in Table I and plotted in Fig. 2. The values given are averages for several runs. In taking these averages, runs which did not cover the whole range of wave-lengths used were adjusted to agree in absolute value with the average of the runs which included all wave-lengths; that is, the whole curve was shifted up or down a definite amount. This was obviously necessary in order to avoid spurious kinks in the dispersion curve which would be due only to the fact that certain regions of the spectrum were more thoroughly investigated than others. The largest shift was 1.1×10^{-6} in n, and most of the curves were not shifted at all.

The contribution of the overtone bands in the neighborhood of 2.3μ is small but easily noticeable. The measurements in this region cannot, however, yield quantitative values of the intensities of the overtones. Two bands overlap in this region, and in order to get estimates of their separate contributions to the index of refraction, measurements would have to be taken in regions very near the band center where there is appreciable absorption. Such measurements would not be reliable if obtained by the prism method, since unsymmetrical absorption of the slit image causes an apparent shift of the image. Since measurements in this wave-length region are not quantitative, they are not included in Table I or Fig. 2.

The only other measurements on the dispersion of methane in the infra-red which have come to the writers' attention are those of Koch[6] who used an interferometer and residual rays of wave-lengths 6.557μ and 8.678μ; that is, wave-lengths on each side of the 7.7μ band. His values for $(n-1)\times10^6$ were 419.20 and 450.06, respectively, for the above two wave-lengths, while those obtained in the present work were 426.35 and 458.10. The quantity which is of most importance for the interpretation of the results is the difference between the values obtained for the two wave-lengths. For this difference Koch obtains 30.86 while we obtain 31.75. This must be considered satisfactory agreement, since we differ by 1.7 percent in the same direction on the absolute values.

INTERPRETATION OF RESULTS

The contribution of an infra-red band to the square of the index of refraction is given by $\Delta_i(n^2-1)=K_i/(\nu_i^2-\nu^2)$ where ν_i is the resonance frequency, ν the frequency of the light used, and the K_i are constants. $\Delta(n-1)$ due to the infra-red bands was obtained by subtracting the experimental values of n from the values obtained by extrapolating into the infra-red the measure-

[6] J. Koch, Nova Acta Soc. Upsala, 2, No. 5 (1909).

ments made by Friberg[5] in the visible and ultraviolet. The values of the K_i for the two active bands were adjusted by successive approximations until each K_i remained constant throughout the spectrum. In this adjustment the extrapolated curve was adjusted vertically to give the same value of K on both sides of a band, the assumption being that the visible and ultraviolet data gave the slope of the curve more accurately than the absolute value.

The final results are given in Table I. The average value of K_3 for the band for which $\nu_3 = 3019.6$ cm was 16.50. The average value of K_4 for the band $\nu_4 = 1304$ cm was 7.50. For the computation of these averages the various values are weighted according to the magnitude of $\Delta(n-1)$, and values beyond 11μ are not used since the energy available in this region is very small and the points consequently scatter rather badly compared with other regions of the spectrum. The values for some wave-lengths very near the absorption bands (those in parenthesis)

TABLE I. *Index of refraction of methane. Here $(n-1)_{exp}$ is the average experimental value of $n-1$ where n is the index of refraction; $(n-1)_{ext}$ is the value obtained by extrapolation of the data of Friberg; Δ_3 and Δ_4 are the contributions of ν_3 and ν_4 to the index of refraction, as determined experimentally.*

WAVE-LENGTHS IN MICRONS	$(n-1)_{EXP}\times 10^6$	$(n-1)_{EXT}\times 10^6$	$\Delta(n-1)\times 10^6$	$\Delta_3\cdot(\nu_3^2-\nu^2)$	$\Delta_4\cdot(\nu_4^2-\nu^2)$	$(n-1)_{CALC}\times 10^6$
1.680	436.50	437.07	0.57	9.21		436.22
1.940	435.70	436.74	1.04	12.91		435.49
2.670	432.70	436.40	3.70	15.16		432.43
2.790	431.50	436.35	4.85	15.58		431.25
2.960	427.80	436.30	8.50	17.72		428.34
3.000	425.85	436.30	10.45	(19.22)		427.22
3.640	445.25	436.17	9.08	16.29	8.24	445.38
3.750	442.80	436.15	6.65	16.11	8.54	442.99
3.900	441.10	436.12	4.98	16.59	7.36	441.07
4.040	440.10	436.11	3.99	17.03	6.72	439.92
4.450	437.80	436.08	1.72	16.10	7.84	437.90
4.570	437.30	436.07	1.23	15.85	7.96	437.45
4.700	436.80	436.06	0.74	15.55	8.09	437.01
5.060	435.80	436.04	0.24	16.46	7.52	435.81
5.400	434.55	436.02	1.47	16.32	7.56	434.58
5.600	434.00	436.02	2.02	17.90	7.15	433.76
5.840	432.60	436.01	3.41	16.57	7.48	432.59
5.980	432.05	436.00	3.95	18.27	7.19	431.77
6.330	429.05	435.99	6.94	16.43	7.51	429.06
6.560	426.30	435.98	9.68	16.00	7.54	426.38
6.790	421.8	435.98	14.18		(7.78)	422.40
6.940	416.8	435.97	19.17		(8.00)	418.21
7.000	413.6	435.97	22.37		(8.45)	416.39
8.36	466.5	435.9	30.6		7.67	465.9
8.42	463.6	435.9	27.7		7.40	464.0
8.48	462.0	435.9	26.1		7.44	462.2
8.57	460.3	435.9	24.4		7.54	460.2
8.63	459.0	435.9	23.1		7.50	459.0
8.70	457.7	435.9	21.8		7.48	457.7
8.80	456.0	435.9	20.1		7.36	456.3
8.89	454.7	435.9	18.8		7.25	455.3
8.95	453.8	435.9	17.9		7.14	454.6
9.05	453.4	435.9	17.5		7.38	453.7
9.20	452.2	435.9	16.3		7.36	452.5
9.41	450.9	435.9	15.0		7.35	451.2
9.52	450.6	435.9	14.7		7.52	450.6
9.73	449.6	435.9	13.7		7.52	449.6
10.11	448.6	435.9	12.7		7.72	448.3
10.28	447.6	435.9	11.7		7.30	447.9
10.38	447.7	435.9	11.8		7.56	447.6
10.80	446.5	435.9	10.6		7.24	446.8
10.94	446.7	435.9	10.8		7.60	446.6
11.46	447.1	435.9	11.2		(8.61)	445.9
11.89	445.3	435.9	9.4		(7.33)	445.5
12.36	445.8	435.9	9.9		(8.35)	445.0
13.20	445.0	435.9	9.1		(8.10)	444.5
13.60	443.7	435.9	7.8		(6.84)	444.3
14.00	448.4	435.9	12.5		(12.61)	444.1
14.8	443.8	435.9	7.9		(7.46)	443.8

are also left out in computing the weighted average, since in these regions the spread of the band due to rotation begins to have an appreciable effect. It may be noticed in Fig. 2 that near the bands the theoretical curve lies nearer to the extrapolated curve than the experimental points. Inclusion of all the points would change the averages by only about 1 percent. The agreement on the high frequency side of ν_3 is not very good, but it must be remembered that in this region the dispersion of the monochromator is at a minimum and that there are difficulties due to two overtone bands of methane and the absorption bands due to CO_2 and H_2O in the atmosphere.

In order to get a picture of what might be occurring in the methane molecule during vibration, a calculation was made to see how much charge would have to be placed on each of the hydrogen atoms (with, of course, four times as much on the carbon) in order to produce the observed effect on the index of refraction. The coordinates chosen for the calculation (shown in Fig. 3) were those given by Dennison and Johnston[7] except that the x, y, and z were reversed in direction. The expressions for the kinetic and potential energies were taken from Dennison and Johnston's paper and are

$$T=\tfrac{1}{2}\{\mu(\dot{x}^2+\dot{y}^2+\dot{z}^2)+(5m/8)(\dot{q}_1^2+\dot{q}_2^2+\dot{q}_3^2+\dot{q}_4^2+\dot{q}_5^2+\dot{q}_6^2)-2(m/8)(\dot{q}_1\dot{q}_3+\dot{q}_1\dot{q}_4+\dot{q}_1\dot{q}_5+\dot{q}_1\dot{q}_6+\dot{q}_2\dot{q}_3+\dot{q}_2\dot{q}_4+\dot{q}_2\dot{q}_5+\dot{q}_2\dot{q}_6+\dot{q}_3\dot{q}_5+\dot{q}_3\dot{q}_6+\dot{q}_4\dot{q}_5+\dot{q}_4\dot{q}_6)+2(m/8)(\dot{q}_1\dot{q}_2+\dot{q}_3\dot{q}_4+\dot{q}_5\dot{q}_6)\},$$

where $\mu=4mM/(4m+M)$ and m and M are the masses of the hydrogen and carbon particles, respectively;

$$V=\tfrac{1}{2}\{a(x^2+y^2+z^2)+b(q_1^2+q_2^2+q_3^2+q_4^2+q_5^2+q_6^2)+2c(q_1q_3+q_1q_4+q_1q_5+q_1q_6+q_2q_3+q_2q_4+q_2q_5+q_2q_6+q_3q_5+q_3q_6+q_4q_5+q_4q_6)+2d(q_1q_2+q_3q_4+q_5q_6)+2e[x(q_1-q_2)+y(q_3-q_4)+z(q_5-q_6)]\}.$$

If we let ϵ be the charge on each hydrogen atom, the potential energy due to an electric field $\mathcal{E}$ parallel to the x axis is $4\epsilon\mathcal{E}x$. The Lagrange equations which involve x are then

$$\mu\ddot{x}+ax+e(q_1-q_2)=4\epsilon\mathcal{E}, \tag{1}$$

$$(5m/8)\ddot{q}_1-(m/8)(\ddot{q}_3+\ddot{q}_4+\ddot{q}_5+\ddot{q}_6)+(m/8)\ddot{q}_2+bq_1+c(q_3+q_4+q_5+q_6)+dq_2+ex=0, \tag{2}$$

$$(5m/8)\ddot{q}_2-(m/8)(\ddot{q}_3+\ddot{q}_4+\ddot{q}_5+\ddot{q}_6)+(m/8)\ddot{q}_1+bq_2+c(q_3+q_4+q_5+q_6)+dq_1-ex=0. \tag{3}$$

The remaining equations, those involving y and z, will be of the same form as (1), (2), and (3), except that $\mathcal{E}_y=\mathcal{E}_z=0$, and will clearly be satisfied by $q_3=q_4=q_5=q_6=y=z=0$, $q_1+q_2=0$. Subtracting (3) from (2) we obtain

$$(5m/8)(\ddot{q}_1-\ddot{q}_2)-(m/8)(\ddot{q}_1-\ddot{q}_2)+b(q_1-q_2)-d(q_1-q_2)+2ex=0. \tag{4}$$

If the q_i are of the form $A\cos\omega t$, $\ddot{q}=-\omega^2q$. If the applied field is given by $\mathcal{E}=\mathcal{E}_0\cos\omega t$ the polarization per molecule due to the forced vibrations may then be obtained by solving

$$\begin{aligned}(-\mu\omega^2+a)x-e(q_1-q_2)&=4\epsilon\mathcal{E}, \\ 2\epsilon x+[(-m/2)\omega^2+b-d](q_1-q_2)&=0.\end{aligned} \tag{5}$$

This gives for the polarization per molecule p

$$p=4\epsilon x=\frac{(4\epsilon)^2\mathcal{E}(-m/2)\omega^2+b-d}{(-\mu\omega^2+a)[(-m/2)\omega^2+b-d]-2e^2}. \tag{6}$$

Since it is more convenient to have the polarization expressed in terms of the resonance frequencies, Eq. (6) can be transformed as follows: Let λ_3, λ_4 be the two values of ω^2 corresponding to the natural periods of (5). One has then

$$\begin{aligned}(m\mu/2)(\omega^2-\lambda_3)(\omega^2-\lambda_4)&\\ =(-\mu\omega^2+a)[(-m/2)\omega^2+b-d]-2e^2,&\end{aligned}$$

so that

$$\begin{aligned}\lambda_3+\lambda_4&=(2/m\mu)[\mu(b-d)+(m/2)a]\\ &=2(b-d)/m+a/\mu,\\ \lambda_3\lambda_4&=(2/m\mu)[a(b-d)-2e^2].\end{aligned}$$

From the first of these:

$$2(b-d)/m=\lambda_3+\lambda_4-a/\mu. \tag{7}$$

[7] M. Johnston and D. M. Dennison, Phys. Rev. **48**, 879 (1935).

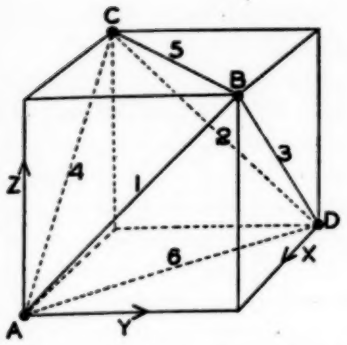

FIG. 3. Equilibrium coordinates for methane. The hydrogens are on corners a, b, c, d. The carbon is at the center of the cube and x, y, and z give the displacements of the carbon with respect to the center of gravity of the hydrogens. The $q_1 \cdots q_6$ give the increases in length of edges $1 \cdots 6$.

According to (6):

$$4\varepsilon x = \frac{16\varepsilon^2 \mathcal{E}}{\mu} \frac{-\omega^2 + (2/m)(b-d)}{(\omega^2-\lambda_3)(\omega^2-\lambda_4)}.$$

Substituting from (7) one obtains

$$4\varepsilon x = \frac{16\varepsilon^2 \mathcal{E}}{\mu} \frac{\omega^2 + \lambda_3 + \lambda_4 - a/\mu}{(\omega^2-\lambda_3)(\omega^2-\lambda_4)}$$

$$= \frac{16\varepsilon^2 \mathcal{E}}{\mu}\left[\frac{(\lambda_4 - a/\mu)/(\lambda_3-\lambda_4)}{\omega^2-\lambda_3} + \frac{(\lambda_3 - a/\mu)/(\lambda_4-\lambda_3)}{\omega^2-\lambda_4}\right]. \quad (8)$$

Then if N is the number of molecules per cc

$$\Delta(n^2-1) = \frac{4\pi N p}{\mathcal{E}} = 4\pi N \frac{16\varepsilon^2}{\mu}\left[\frac{(\lambda_4 - a/\mu)/(\lambda_3-\lambda_4)}{\omega^2-\lambda_3} + \frac{(\lambda_3 - a/\mu)/(\lambda_4-\lambda_3)}{\omega^2-\lambda_4}\right]. \quad (9)$$

where the first term gives the contribution of ν_3, the resonance frequency corresponding to λ_3, and the second term gives the contribution of ν_4. Since the oscillator is isotropic the result is unchanged when averaged over all directions of polarization of the incident light and all orientations of the molecule. The above calculation has been made according to classical theory on the assumption that the carbon and the hydrogens carry fixed "effective charges." Comparison with experiment indicates that this hypothesis is too simple, and that the two active normal modes of vibration must have different ε's. Eq. (9) may then be rewritten

$$\Delta_3(n^2-1) = \frac{(16N\varepsilon_3^2/\pi\mu)(\lambda_4 - a/\mu)/(\lambda_3-\lambda_4)}{\nu^2-\nu_3^2} = \frac{-K_3}{\nu^2-\nu_3^2}$$

and

$$\Delta_4(n^2-1) = \frac{(16N\varepsilon_4^2/\pi\mu)(\lambda_3 - a/\mu)/(\lambda_3-\lambda_4)}{\nu^2-\nu_4^2} = \frac{-K_4}{\nu^2-\nu_4^2}.$$

where $(2\pi\nu)^2$ has been substituted for ω^2, $(2\pi\nu_3)^2$ for λ_3, $(2\pi\nu_4)^2$ for λ_4, and K_3, K_4, $\Delta_3(n^2-1)$ and $\Delta_4(n^2-1)$ have the same significance as when previously introduced in the interpretation of the data. It will be noted that a is the only potential constant which appears in the above expressions. This is reasonable since it is the constant connected with the displacement of the carbon away from the center of gravity of the hydrogens, which displacement can be expected to produce electrical dissymmetry in the molecule. It will be noticed that if e, the constant giving the coupling between x and q_1 and q_2, is set equal to zero, Δ_3 will reduce to the result for a simple oscillator of mass μ and charge 4ε and force constant a, while Δ_4 will be zero.

The above expressions were used to calculate the values of ε for the two active modes of vibration. In this calculation the following numerical constants were used: $\mu = 5.03\times10^{-24}$ gram; $a = 7.670\times10^{5}$ dynes/cm (Dennison and Johnston); $m = 1.67\times10^{-24}$ gram; $\lambda_3 = 32.4\times10^{28}$; $\lambda_4 = 6.04\times10^{28}$; $\nu_3 = 9.05\times10^{13}$ vib./sec.; $\nu_4 = 3.915\times10^{13}$ vib./sec.; c = velocity of light $= 3\times10^{10}$ cm/sec.; $N = 2.69\times10^{19}$ molecules/cc under standard conditions; and $e = 4.80\times10^{-10}$ e.s.u. = electronic charge. From this calculation we obtained for ε_3, the charge required on each H atom for the vibration ν_3, 0.562×10^{-10} e.s.u. or 0.117 e where e is the electronic charge. For ε_4 we obtain 0.277×10^{-10} e.s.u. or 0.0578 e. These results should not, of course, be interpreted as meaning that the H atoms in methane actually carry a charge of 0.562×10^{-10} e.s.u. for one mode

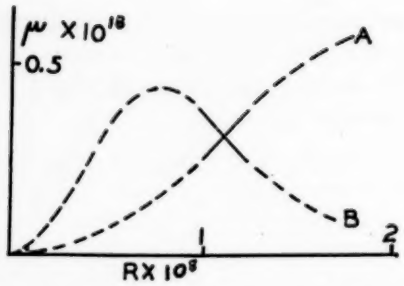

FIG. 4. Change of the dipole moment of the CH group as a function of CH distance. Curves a and b give two possibilities; the experiments yield only the value of μ and its derivative at the equilibrium position.

of vibration and 0.277×10^{-10} for the other. They merely mean that if that were the case the observed values of the index of refraction would be obtained. It is highly probable that the charge on the H atoms is not constant during a vibration. The refraction measurements which we have made cannot distinguish between the various ways in which the dipole moment of the molecule can vary during a vibration.

In order to gain further insight into what may actually be happening in the methane molecule, it is interesting to examine in closer detail the actual motions of the nuclei for each of the two active frequencies ν_3 and ν_4. For this calculation it is desirable to know the coefficients involved in the transformation to normal coordinates, and these are given in the appendix. A semi-classical calculation, which involves setting the potential energy at maximum displacement equal to $h\nu$ gives the following results: For ν_3, if only the one of the 3 equal frequency modes which involves displacement of the C in the X direction is excited, the carbon moves 0.0402×10^{-8} cm in the X direction with respect to the center of gravity of the hydrogens, q_1 decreases by 0.0906×10^{-8} cm, and q_2 increases by 0.0906A. Expressed in another way, the CH distance varies between the limits 1.045A and 1.17A while the angle between the CH bonds changes only from 109°0′ to 110°4′ or each CH bond vibrates only about ½° on each side of its equilibrium position. For ν_4 the C moves 0.751A in the $+X$ direction while q_1 increases by 0.962A and q_2 decreases by 0.962A. In more pictorial language, the CH bond vibrates between 100°14′ and 118°42′ or 9° on each side of its equilibrium position, while the CH distance changes from 1.107A to 1.118A or only about 0.005A on each side of equilibrium.

One interesting possible interpretation then presents itself. In the vibration corresponding to ν_4 the charges on the hydrogens may remain nearly constant since the CH distance remains so nearly constant and the hydrogens are so far apart. (This, of course, neglects any directional effect of the carbon on the distribution of charge.) The ε_4 above then may be interpreted as actually the charge on the hydrogen and the electric moment of the CH bond may be computed. Since the equilibrium distance between the C and the H is 1.11A, the moment of the bond is $1.11\times10^{-8}\times0.277\times10^{-10}$ or 0.307×10^{-18}. This will of course be equal to the dipole moment of the CH_3 group in methane. For ν_3, since the angles remain so nearly constant, ε_3 may be interpreted as the rate of change of the dipole moment of the CH bond with respect to the CH distance. If this interpretation is correct, the dipole moment of the CH bond may vary with CH distance somewhat as shown in Fig. 4. In this connection it is interesting to note that from measurements of the intensity of absorption in overtone bands of several halogen derivatives of hydrocarbons, Timm and Mecke[8] estimate the moment of the CH bond to be between 0.3×10^{-18} and 0.4×10^{-18} e.s.u.

One further point which must be mentioned is the extrapolation to infinite wave-length, where n_∞^2-1 should be equal to $\epsilon-1$. If we take 435.9×10^{-6} as $n_\infty-1$ from measurements in the visible and ultraviolet regions of the spectrum and add 1.81×10^{-6} and 4.41×10^{-6} as the contributions of ν_3 and ν_4, we obtain $n_\infty-1=442.1\times10^{-6}$ and $n_\infty^2-1=884.4\times10^{-6}$. Sanger ob-

TABLE A. *Coefficients for transformation to normal coordinates for methane.*

	ξ_1	ξ_2	ξ_3	ξ_4
q_1	$(2/3m)^{\frac{1}{2}}$	a	D_1	E_1
q_2	$(2/3m)^{\frac{1}{2}}$	a	$-D_1$	$-E_1$
q_3	$(2/3m)^{\frac{1}{2}}$	$b-a$	D_2	E_2
q_4	$(2/3m)^{\frac{1}{2}}$	$b-a$	$-D_2$	$-E_2$
q_5	$(2/3m)^{\frac{1}{2}}$	$-b$	D_3	E_3
q_6	$(2/3m)^{\frac{1}{2}}$	$-b$	$-D_3$	$-E_3$
x	0	0	$2D_1e/(\mu\lambda_3-a)$	$2E_1e/(\mu\lambda_4-a)$
y	0	0	$2D_2e/(\mu\lambda_3-a)$	$2E_2e/(\mu\lambda_4-a)$
z	0	0	$2D_3e/(\mu\lambda_3-a)$	$2E_3e/(\mu\lambda_4-a)$

[8] B. Timm and R. Mecke, Zeits. f. Physik **98**, 363 (1936).

tained 960×10^{-6} for $\epsilon-1$. The contribution of the infra-red bands thus reduces the discrpeancy between n_∞^2-1 optical and $\epsilon-1$ by only about 12.4×10^{-6} or 16 percent of the difference. The agreement between various determinations of $n_\infty-1$ makes it extremely improbable that changes in its value can reduce the discrepancy by more than 10 percent. The remainder must then be due to error in measurements of ϵ.

It is a pleasure to acknowledge the help received from Professor G. Breit in the interpretation of the results, and to thank the Wisconsin Alumni Research Foundation for a grant in aid.

Appendix

Table A gives the coefficients for the transformation to normal coordinates for methane. The $D_{1,2,3}$, $E_{1,2,3}$, a and b are constants which enter because of the degeneracy of the corresponding modes of vibration.

If T is to have the form

$$T=\tfrac{1}{2}(\dot{\xi}_1^2+\dot{\xi}_2^2+\dot{\xi}_3^2+\dot{\xi}_4^2)$$

there are the following restrictions on the constants:

$$a^2+b^2-ab=\tfrac{1}{4}m,$$

$$D_1^2+D_2^2+D_3^2=\left[\left(\frac{2e}{\mu\lambda_3-a}\right)^2\mu+m\right]^{-1},$$

$$E_1^2+E_2^2+E_3^2=\left[\left(\frac{2e}{\mu\lambda_4-a}\right)^2\mu+m\right]^{-1}.$$

APRIL 15, 1940 PHYSICAL REVIEW VOLUME 57

The Diffraction of Radio Ranges by Hills

William R. Haseltine
Department of Physics, University of California, Berkeley, California

(Received January 2, 1940)

The scattering of electromagnetic waves by hemispherical obstacles on a conducting plane has been investigated. The results have been applied to the problem of the splitting of radio range beacons when the range passes over hilly country. The calculations refer particularly to long wavelengths (about 1000 meters) such as used in the Oakland range. It is found that even hills of moderate size can cause wide spatial fluctuations in the received signal strength. The results of numerical calculation for one simple model of the terrain are reported. The beam is found to split into several parallel courses, giving a pattern of the same type as is observed in the field. It is concluded that this phenomenon is a typical diffraction effect.

IN the standard system of radio ranges for the guidance of aircraft the radiating antenna array sends out two separate signals on the same frequency. One signal, modulated with the code letter N (—·) is strong in two opposite quadrants; the other, modulated with A (·—) is strong in the remaining quadrants. Along four lines passing through the station, the A and N signals are of equal intensity, and blend into a continuous sound. These lines form the courses or "beams" defined by the system. The radiation fields are vertically polarized to eliminate some of the troubles that occurred when earlier types of antenna systems were used.

In level country these range courses are reasonably well behaved, but over mountainous or even moderately hilly terrain curious effects often arise. In particular, instead of a single course of equal signal strength, there may appear a complicated pattern of several parallel courses spread over an angular distance of up to twenty degrees. This effect is very troublesome and dangerous to air traffic.

Early in 1939, field investigations of these phenomena were carried out on the range at Oakland, California, by Captain E. C. Dyer, U.S.M.C., and Lieutenant D. E. Wait, U.S.N. It was found that the seaward course was badly split and that this seemed to be related to the hills of the San Francisco peninsula and especially Mt. Tamalpais in Marin County north of the Gate. They requested the author to make

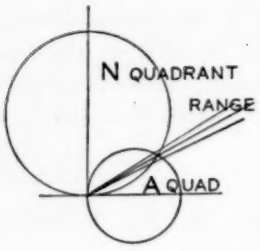

FIG. 1. Polar plot of unperturbed field strength.

a theoretical investigation of this problem to ascertain the probable cause of the multiple beams observed.

Because the great complexity of the terrain prohibits study of the actual conditions, a simplified model of one or two hills on an infinite plane is considered. For simplicity, the field strength of the A signal is taken to vary as the cosine of the azimuth measured from an arbitrary zero, and the N signal as the sine of the same angle.

The electric and magnetic field strengths radiated must satisfy Maxwell's equations. If $\boldsymbol{E}=\mathbf{E}e^{-i\omega t}$, $\boldsymbol{H}=\mathbf{H}e^{-i\omega t}$, these reduce to

$$\nabla^2\mathbf{E}+k^2\mathbf{E}=0, \quad \nabla^2\mathbf{H}+k^2\mathbf{H}=0, \quad \omega=2\pi c/\lambda \qquad (1)$$

in which c is the velocity of light, and λ the wave-length in free space. In free space (or the atmosphere),

$$k=2\pi/\lambda=\omega/c.$$

Inside matter,

$$k^2=(\omega^2/c^2)(\epsilon\mu+i4\pi\mu\sigma/\omega)=\omega^2\epsilon'\mu/c^2,$$

where ϵ is the dielectric constant, μ the permeability, and σ the conductivity in electrostatic units. This constant will be written k' to differentiate it from the value for free space. The permeability μ is supposed to be equal to one.

Consider first the solution over a plane earth with no hills present. The effect of the earth on the wave field is considerably simplified by the long wave-length involved (for the Oakland range, $\lambda=1267$ meters). Sommerfeld[1] has shown that the earth can be considered perfectly conducting so long as $(k^2/k'^2)kR\ll 1$ (R is the distance from the source). With $\sigma\backsimeq 10^8$ for average land, $\lambda=1267$ meters, and $R=15$ miles, this quantity has the value 1/10. For sea water, with its much greater conductivity, it is still smaller. Treating the earth as perfectly conducting, as is thus allowed here, is equivalent to requiring that the electric field at the surface be vertical.

Thus the solutions sought for the primary undisturbed wave are

$$\mathbf{E}_\chi=\mathbf{E}_{00}\frac{e^{ikR}}{R}\sin^2\chi\begin{Bmatrix}\cos\\ \sin\end{Bmatrix}\psi. \qquad (2)$$

χ is the polar distance; ψ the azimuth; the factor $\cos\psi$ applies to the N signal; and the $\sin\psi$ to the A signal. $\mathbf{E}_\chi$ is the electric field strength in the direction of increasing χ; the other components are zero. Fig. 1 shows a polar plot of the field in a horizontal plane.

When a hill is present, this wave will be scattered by it, and the amplitudes of the primary and the scattered waves will add with differing phase relationships at different points. An interference pattern is set up. This problem is very similar to that found in the quantum-mechanical treatment of atomic collision and scattering processes. It is almost identical with that of the scattering of electron waves by a central field of force, except that the electronic wave function is a scalar, while the wave function here is a vector. There are two general methods of attack. The first is that of small perturbations and is equivalent to the Born approximation. The second is that of partial waves. This technique was also used by Lord Rayleigh to study the scattering of sound waves. The first method can be used if the scattered field is small compared with the primary field even at the hill (as it will be when the conductivity is sufficiently small). In this case the following approximation is valid:

From the primary field strength calculate the currents set up in the hill, $\mathbf{I}=\sigma\mathbf{E}$. Then calculate the field radiated by these currents (see Hansen[2]). This is the first approximation to the scattered wave. This method was tried, but in the case of interest the conductivity was so high that the approximation broke down.

In the second method one attempts to find a rigorous solution of the wave equation having two characteristics. It must satisfy the boundary conditions at the surface of the hill (tangential components of $\mathbf{E}$ and $\mathbf{H}$ and normal components of $\mathbf{D}$ and $\mathbf{B}$ continuous across surface), and it

[1] A. Sommerfeld, Ann. d. Physik **81**, 1135 (1926).

[2] W. W. Hansen, Physics **7**, 460 (1936).

must represent the sum of the primary signal and an outgoing scattered wave. That is, it must have the form:

$$\mathbf{E}=\mathbf{E}_0+\mathbf{E}_s, \tag{3}$$

where $\mathbf{E}_0$ is the primary wave of form (2), and $\mathbf{E}_s$ is one which behaves at large distances from the hill as e^{ikr}/r, r being the distance from the center of the hill. This will be practicable only in very simple cases. Here we will investigate the case of a hemispherical boss of radius r_0. A solution of the desired type can then be found in series form.

It has been shown[3, 4] that the functions $A_{s,l,n}(r,\theta,\varphi)$ and $A'_{s,l,n}(r,\theta,\varphi)$, $(s=2,3;\ l=0,1,2,\cdots)$ defined by Hansen form a complete set for the description of any radiative solution of Eq. (1). These functions are defined as follows: let

$$\xi_{l,n}(r,\theta,\varphi)=h_{l,n}[1/(kr)^{\frac{1}{2}}]J_{l+\frac{1}{2}}(kr)P_l^{|n|}(\cos\theta)e^{in\varphi}, \tag{4}$$

$$h_{l,n}=\left[\frac{(2l+1)(l-|n|)!}{8l(l+1)(l+|n|)!}\right]^{\frac{1}{2}},$$

$$\mathbf{A}_{2,l,n}=k\nabla\times(\mathbf{r}\xi),$$

$$\mathbf{A}_{3,l,n}=-(1/k)\nabla\times\mathbf{A}_{2,l,n},$$

These $\mathbf{A}$ and $\mathbf{A}'$ functions are the convenient vector solutions of the wave equation for cases of spherical symmetry. The $\mathbf{A}'$ functions are generated in the same way as $\mathbf{A}$ except that the Bessel function $J_{l+\frac{1}{2}}$ in $\xi_{l,n}$ is replaced by $H^{1}{}_{l+\frac{1}{2}}$, the Hankel function of the first kind.

Any solution can then be written as

$$E=\sum_{s,l,n}a_{s,l,n}\mathbf{A}_{s,l,n}+b_{s,l,n}\mathbf{A}'_{s,l,n}. \tag{5}$$

Now the $\mathbf{A}'$ functions have a singularity at the origin and behave at large distances like e^{ikr}/r; they represent outgoing waves. The $\mathbf{A}$ functions behave at large distances like $(\sin kr)/r$. Furthermore, any wave field not having a singularity at the origin can be expanded in terms of the $\mathbf{A}$ functions alone. Thus in (5) the $\mathbf{A}$ terms can be considered as an incident wave and the $\mathbf{A}'$ terms the corresponding scattered wave. Then if the origin is chosen at the center of the scattering hill, this is of form (3) where

$$\mathbf{E}_0=\sum a_{s,l,n}\mathbf{A}_{s,l,n};\quad \mathbf{E}_s=\sum b_{s,l,n}\mathbf{A}'_{s,l,n}. \tag{6}$$

For any form of primary wave $\mathbf{E}_0$, i.e., any given values of $a_{s,l,n}$, the boundary conditions at the surface of the hill determine the $b_{s,l,n}$. In fact, the requirement that the appropriate fields be continuous across this boundary gives a relationship between any $a_{s,l,n}$ and the $b_{s,l,n}$ with the same indices alone. This separability of the components is the reason for using this system of functions. If, then, the expansion of $\mathbf{E}_0$ is known in terms of the $\mathbf{A}$ functions, the whole field is known. The amplitude of the scattered wave made up of the $\mathbf{A}'$ functions may then be added to that of the primary signal at any desired point. The square of the absolute magnitude of this sum is then proportional to the signal intensity received. This procedure can be carried out for both A and N signals, and the relative intensities compared.

The solutions inside the hill have the form $\mathbf{G}_{s,l,n}$, where

$$\mathbf{G}_{2,l,n}=k'\nabla\times(\mathbf{r}\xi'_{l,n})=(-1/k\epsilon')\nabla\times\mathbf{G}_{3,l,n},$$

$$\mathbf{G}_{3,l,n}=(-1/k\mu)\nabla\times\mathbf{G}_{2,l,n}.$$

ξ' is the same as ξ with k replaced by $k'=k\epsilon'^{\frac{1}{2}}$.

The equations for b are found to be

$$a_{s,l,n}\left\{\frac{J_{l+\frac{1}{2}}(kr_0)}{(kr_0)^{\frac{1}{2}}}\frac{d}{dr}\left[\frac{rJ_{l+\frac{1}{2}}(k'r)}{(kr')^{\frac{1}{2}}}\right]_{r_0}-g_s\frac{J_{l+\frac{1}{2}}(k'r_0)}{(k'r_0)^{\frac{1}{2}}}\frac{d}{dr}\left[\frac{rJ_{l+\frac{1}{2}}(kr)}{(kr)^{\frac{1}{2}}}\right]_{r_0}\right\}$$

$$+b_{s,l,n}\left\{\frac{H^{(1)}{}_{l+\frac{1}{2}}(kr_0)}{(kr_0)^{\frac{1}{2}}}\frac{d}{dr}\left[\frac{rJ_{l+\frac{1}{2}}(k'r)}{(k'r)^{\frac{1}{2}}}\right]_{r_0}-g_s\frac{J_{l+\frac{1}{2}}(k'r_0)}{(k'r_0)^{\frac{1}{2}}}\frac{d}{dr}\left[\frac{rH^{(1)}{}_{l+\frac{1}{2}}(kr)}{(kr)^{\frac{1}{2}}}\right]_{r_0}\right\}=0, \tag{7}$$

$$g_s=\begin{cases}1, & s=2\\ \epsilon', & s=3\end{cases}.$$

If the hill is assumed to be perfectly conducting, the corresponding equations are

$$a_{2,l,n}J_{l+\frac{1}{2}}(kr_0)+b_{2,l,n}H^{(1)}{}_{l+\frac{1}{2}}(kr_0)=0, \tag{8}$$

$$a_{3,l,n}\frac{d}{dr}\left[\frac{rJ_{l+\frac{1}{2}}(kr)}{(kr)^{\frac{1}{2}}}\right]_{r_0}+b_{3,l,n}\frac{d}{dr}\left[\frac{rH^{(1)}{}_{l+\frac{1}{2}}(kr_0)}{(kr)^{\frac{1}{2}}}\right]_{r_0}=0$$

[3] W. W. Hansen, Phys. Rev. **47**, 129 (1935).
[4] W. W. Hansen, Proc. I. R. E. **24**, 1594 (1936).

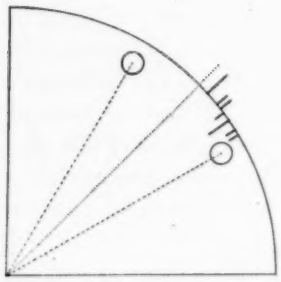

FIG. 2. Relative positions of station, scattering hills, and ranges.

Numerical calculation shows that with reasonable values for ϵ', the magnitude of the reflection coefficients b/a are not very different from those for a perfectly conducting sphere, though the phases may be different. In the following calculations, the hill was taken to be a perfect reflector.

If the radius (height) of the hill is small compared to its distance from the station, the primary wave front is only very slightly curved, and for purposes of computation can be assumed to be plane over the extent of the hill

$$\mathbf{E}_{00}\frac{e^{ikR}}{R}\sin^2\chi\begin{Bmatrix}\cos\\ \sin\end{Bmatrix}\psi \backsimeq \mathbf{E}_{00}\frac{e^{ikR_0}}{R_0}\begin{Bmatrix}\cos\\ \sin\end{Bmatrix}\psi_0 e^{ikr\cos\theta'} = \mathbf{E}_0 e^{ikr\cos\theta'}, \quad (9)$$

where R_0, $\chi_0(=\pi/2)$, ψ_0 are the coordinates of the center of the hill, and θ' is measured as polar distance from an axis through station and hill. Furthermore, the electric field is entirely vertical.

This plane wave can be expanded in a well-known form

$$e^{ikr\cos\theta'} = \sum_m (\pi/2)^{\frac{1}{2}} i^m (2m+1) \times J_{m+\frac{1}{2}}(kr)(kr)^{-\frac{1}{2}} P_m(\cos\theta'). \quad (10)$$

Each term of this series can be in turn expanded in terms of the $\mathbf{A}_{s,l,n}$ functions, bearing in mind that these are vectors and that the primary field is vertical. The result gives the $a_{s,l,n}$ quantities.

$$\begin{aligned} ka_{2,l,n} &= E_0 8ni^{l+1}(\pi/2)^{\frac{1}{2}} P^{|n|}{}_l(0) h^2{}_{l,n}, \\ ka_{3,l,n} &= -E_0 4i^{l-1}[2-\delta(0,n)](\pi/2)^{\frac{1}{2}} \times (l+|n|)P^{|n|}{}_{l-1}(0)h^2{}_{l,n}. \end{aligned} \quad (11)$$

The series expansion of the scattered wave can always be found in principle; but if the radius of the scattering body is larger than a wave-length, an inordinate number of terms must be used. Here again the long wave-length used is a help. For $kr_0 = 2\pi r_0/\lambda = 1.6$, about eight terms must be used. For $kr_0 = 4$, at least 24 must be carried. This latter figure corresponds roughly to the size of Mt. Tamalpais ($r_0 = 810$ meters).

The necessary numerical calculations are rather laborious, and have been carried out with considerable assistance from Mr. Chaim Richman working on N.Y.A. time.

The case of a small hill, $kr_0 = 1.6$, and of a single large one, $kr_0 = 4$, showed pronounced fluctuations of the signal intensity from the normal. However, there was no evidence of course splitting found. This is undoubtedly due to the simplicity and symmetry of arrangement of scattering material.

Next the scattering by two hills was investigated. The results here reported are for two hills, each of radius $kr_0 = 4$ placed on a circle distant about 12 miles ($kR_0 = 100$) from the transmitting station. One hill was at an azimuth of 30°, the other at 60°. The field was calculated for both A and N signals along a circle for which $kR = 110$. The geometrical relations are shown in Fig. 2. The work was carried out only at ground level ($\chi = \theta = \pi/2$), because at any other elevation the labor would have been multiplied at least threefold. The effect of one hill on the field of the other was neglected as a higher order perturbation.

By choosing properly the relative magnitudes of the A and N signals, the beam may be made to fall anywhere in the quadrant. When it lies at 45°, directly between the hills, there can be no splitting or parallel courses, because of symmetry, even though the fields may be violently distorted. When, on the other hand, the range

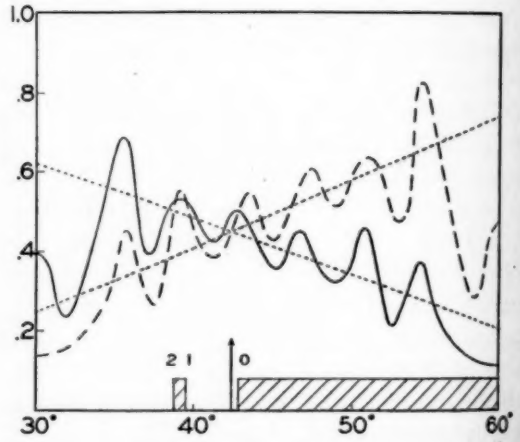

FIG. 3. Plot of signal intensities when desired range lies at 42 degrees. The multiple ranges are clearly seen.

lies only slightly off this position, the situation arises shown in Fig. 3.

The signal intensities are plotted as calculated for points along the circle of Fig. 2 from 30° to 60°. The intensities that would be observed with no scatterers present are represented by the smooth, almost straight dotted curves, the N signal decreasing to the right and the A to the left. Their crossing point defines the desired range here at about 42°. This is indicated by the tall arrow below. The magnitude of the disturbance caused by the hills can be seen from the solid and dashed curves, which represent the intensities to be expected with the hills interfering. The solid curve is for signal N and the dashed for signal A. It is seen that they cross in three places, marked below 0, 1, 2, thus giving rise to three more or less parallel courses. The cross-hatched rectangles along the lower axis indicate the regions in which the A signal is predominant.

Figure 4 is a similar plot for the case in which the desired course is about 35°. Here there are three crossing points and one point of tangency, or near-tangency, giving four courses. Again the large arrow indicates the desired course, and the actual beams are numbered 0, 1, 2, 3, the cross-hatched rectangles indicating predominance of the A signal. The small arrow at 1 indicates the course set by the point of tangency.

In Fig. 2 the pattern is represented by small solid lines attached to the large circle. These lines represent the positions along the circle at which an on-course signal would be heard. Those that extend outward refer to a beam set for 42°, and those extending inward refer to one set at 35°. In each case the longer line indicates the position of the main range. The shorter lines mark subsidiary courses.

On examination of these curves there are present all the types of beam splitting or parallel courses actually observed. The predominant signal may be the same on both sides of the course, as at 1 in Fig. 4; it may be different in either the normal order (as at 0, Fig. 3) or the reversed order (1, Fig. 4), and none of the courses need lie along that expected.

The pattern observed at a higher altitude would undoubtedly be different. But it would show the same type of phenomena.

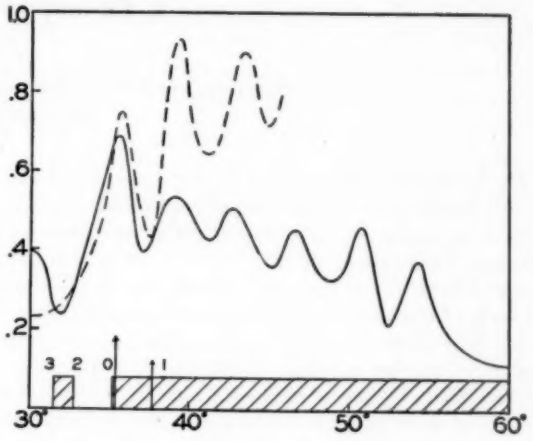

FIG. 4. Plot of signal intensities when desired range lies at 35 degrees.

The number of peaks observed in the signal strength between 30° and 60° corresponds to the fact that along this circle the wave-length represents about 4°. The relative phase with which the scattered waves add to the primary thus shifts with this period. At a greater distance from the station, the wave-length would correspond to a smaller angle, and more peaks would be found. The pattern of parallel courses would thus change entirely in going from $kR=110$ to, say, $kR=150$. These changes of pattern with both altitude and distance have been observed in the field.

In any actual geographical location where these phenomena occur, the scattering material will be present in much greater quantity, and will be distributed much more irregularly than that of the model used in this paper. It is therefore to be expected that the splitting observed will be more pronounced and more erratic. Further, the extra courses must vary with ground and weather conditions. A change in soil conductivity will introduce phase shifts of different amounts in all scattered waves and definitely affect the pattern.

The author is grateful to Captain E. C. Dyer for details on his unpublished field work, and to Professor J. R. Oppenheimer for several very helpful talks. Without the aid of Mr. Richman the work would have taken much longer, and the author expresses thanks to him and to the N.Y.A.

A Theory of Spark Discharge

J. M. MEEK
Department of Physics, University of California, Berkeley, California

(Received February 13, 1940)

The breakdown of a uniform field is considered to occur by the transition of an electron avalanche proceeding from cathode to anode into a self-propagating streamer, which develops from anode to cathode to form a conducting filament between the electrodes. A criterion is put forward for such a transition, *viz.*, a streamer will develop when the radial field about the positive space charge in an electron avalanche attains a value of the order of the external applied field. For then photoelectrons in the immediate vicinity of the avalanche will be drawn into the stem of the avalanche and will give rise to a conducting filament of plasma, and a self-propagating streamer proceeds towards the cathode. The theory thus depends on ionization by electrons and photo-ionization in the gas and dispenses with the classical assumption of ionization by positive ions in the gas or secondary actions at the cathode. On this basis an equation for breakdown is developed, and reference to $\alpha/p-X/p$ curves enables the potential required for breakdown to be determined. Satisfactory agreement between calculation and experiment is found in air for values of pressure times gap length down to $p\delta\sim100$ mm Hg×cm. The theory does not conform absolutely to Paschen's law, but the deviations are within the present day margins of experimental error. For lower values of $p\delta$ the deviation between calculation and experiment is explained by the fact that the density of photo-ionization becomes small, and the secondary mechanism, γ, is observed in this region, so that classical theory applies. The theory is indicated to be consistent with all the requirements so far established in connection with sparks for large $p\delta$ up to the lightning discharge.

INTRODUCTION

IN the early 1900's J. S. Townsend[1] evolved his now classical theory of the mechanism of spark discharge on the basis of measurements made at high values of X/p, the ratio of field strength to pressure, and low values of $p\delta$, the product of pressure times gap-length. His theory has been extrapolated to explain the mechanism of sparking under ordinary conditions for longer gap-lengths at atmospheric pressure and above. It has formed the guiding principle of all considerations of the sparking mechanism for nearly 40 years. Many researches have indicated that for values of $p\delta$ near and somewhat above the minimum sparking potential the theory was adequate and relatively accurate. The theory in this region enables calculation of the sparking potentials to be made with adequate accuracy, and recently it has been shown by Schade[2] to be consistent with time-lag studies.

In recent years, however, it has become increasingly apparent that the theory is entirely inapplicable when extrapolated to sparks for $p\delta$ greater than about 200 mm Hg×cm in air, and analogous values in other gases. The reasons for this conclusion may be stated briefly as follows:

1. The formative time lags of sparks at *atmospheric pressure*, i.e., the time required for the breakdown mechanism to materialize, have been measured by several diverse methods, and all lead to time intervals of the order of 10^{-7} sec., or even less, for a one-cm gap at small overvoltages.[2] These time intervals are far below the microseconds required by positive ion movement as shown by Schade[3] and others.[4]

2. At atmospheric pressure the sparking potential has been found to be independent of cathode material to a very high degree,[5] while the theory above, even though somewhat insensitive to the value of γ at higher pressures, requires a definite dependence of the order of 10 percent on the value of γ.[6] The values of $p\delta$ at which this de-

[1] J. S. Townsend, Nature **62**, 340 (1900); Phil. Mag. **1**, 198 (1901).

[2] P. O. Pedersen, Ann. d. Physik **71**, 371 (1923); J. W. Beams, J. Frank. Inst. **206**, 809 (1928); J. J. Torok, Trans. A. I. E. E. **47**, 177 (1928); **48**, 46 (1930); Buraway, Arch. f. Elek. **16**, 14 (1926); I. Tamm, Arch. f. Elek. **19**, 235 (1928); W. Rogowski, Arch. f. Elek. **20**, 99 (1928); F. G. Dunnington, Phys. Rev. **38**, 1535 (1931); H. J. White, Phys. Rev. **46**, 99 (1934); A. Tilles, Phys. Rev. **46**, 1015 (1934); R. R. Wilson, Phys. Rev. **49**, 1082 (1936); M. Newman, Phys. Rev. **52**, 652 (1937); R. Strigel, Wiss. Veröffentl. Siemens Werken **15**, 1 (1936).

[3] R. Schade, Zeits. f. Physik **104**, 487 (1937).

[4] I. Tamm, Arch. f. Elek. **19**, 235 (1928); W. Rogowski, Arch. f. Elek. **20**, 99 (1928); W. Rogowski and I. Tamm, Arch. f. Elek. **20**, 625 (1928); A. Tilles, Phys. Rev. **46**, 1015 (1934).

[5] L. B. Loeb, *Fundamental Processes of Electrical Discharge in Gases* (John Wiley, 1939), p. 415.

[6] Reference 5, p. 416 *et seq.*

pendence begins rapidly to vanish occur again at $p\delta \sim 200$.[5]

3. In longer sparks, in lightning discharge, and in positive point corona at atmospheric pressure, it is virtually certain that the character and action of the cathode is without any influence whatsoever on the process.

4. The observed appearance of sparks in measurements of Townsend's coefficient, α, at higher pressures and adequate x with no measurable value of γ indicates in another way that the theory based on a γ is no longer applicable at higher values of pressure and gap length.[7]

5. Observations of actual sparks in short time intervals made visible by Kerr cell-shutter studies[8] and by cloud-track pictures of spark paths after short time intervals,[9] as well as the usual visual observations of sparks, indicates that breakdown at higher pressures occurs along very narrow channels or filaments. This is incompatible with the transient rearrangement of conduction currents in a gas caused by accumulations and movements of positive ions or successive waves of electron ionization when $\gamma e^{\alpha\delta} > 1$. This discrepancy is made still more glaring by the zigzag nature of the spark filament and the frequent branching observed in longer sparks.

6. While only one electron is required to initiate a spark on the Townsend theory as interpreted by Holst and Oosterhuis[10] it is clear that the greater the number of photons incident on the cathode by external irradiation the more rapidly should the space charge accumulations occur, so that formative time lags should on that theory decrease as the illumination intensity of the cathode increases. This has been shown to be true by Schade for low values of $p\delta$. However, at high $p\delta$ observation shows no appreciable change in the *formative* time lag and of the sparking potential with illumination over a considerable range of intensity.[11] When the illumination intensity is increased by a factor of 10^5 beyond that giving the 10^7 electrons/sec./cm^2 generally used, both formative time lag and sparking potential are lowered.[12] In this case the potential is lowered at a maximum by no more than 10 percent, and the formative time lag appears to be doubled when the intensity of illumination is decreased by a factor of 500.

Theory

The above-mentioned objections to the classical theory make it imperative to formulate a new mechanism which does not so conflict with experimental observations. The importance of streamer formation in the mechanism of spark breakdown has been discussed in a recent article by Loeb and Kip[13, 13a] and more extensively by Loeb in his book *Fundamental Processes of Electrical Discharge in Gases*. The breakdown process is there pictured in qualitative fashion, but no quantitative criterion is given for streamer formation and breakdown. However, it is shown that under sparking conditions the positive space charge in an electron avalanche which is originated at the cathode produces an electric field of the same order as the external applied field when the avalanche reaches the anode. This fact was also indicated previously by Slepian,[14] who then postulated the development of thermal ionization in the avalanche. It is further stated by Loeb that the axial field distortion produced by the positive space charge inhibits the advance of the electron avalanche towards the anode, but favors the development of a positive streamer towards the cathode. An explanation of the mechanism of streamer formation and mid-gap streamers is also given, though the fundamental criterion for their appearance is lacking. However, it is indicated that breakdown will not occur until a conducting filament exists across the gap. The single electron avalanches observed by Raether[15] just below breakdown do not form such a fila-

[7] F. H. Sanders, Phys. Rev. **44**, 1020 (1933); D. Q. Posin, Phys. Rev. **50**, 650 (1936); W. E. Bowls, Phys. Rev. **53**, 293 (1938).

[8] L. von Hamos, Ann. d. Physik **7**, 857 (1930); F. G. Dunnington, Phys. Rev. **38**, 1535 (1931); H. J. White, Phys. Rev. **46**, 99 (1934).

[9] E. Flegler and H. Raether, Zeits. f. Physik **99**, 635 (1936); **103**, 315 (1936); H. Raether, Zeits. f. Physik **96**, 567 (1936); **110**, 611 (1938); **112**, 464 (1939).

[10] G. Holst and E. Oosterhuis, Phil. Mag. **46**, 1117 (1923).

[11] H. J. White, Phys. Rev. **48**, 113 (1935); R. R. Wilson, Phys. Rev. **50**, 1082 (1936).

[12] H. J. White, Phys. Rev. **48**, 113 (1935).

[13] L. B. Loeb and A. F. Kip, J. App. Phys. **10**, 142 (1939).

[13a] At the request of Professor Loeb, attention is called to page 157 of this article where a careless blunder is made in the calculation of the field strength produced by space charge. However, the order of magnitude of the calculated values is not affected by correction, and the argument given in the article is by no means invalidated thereby.

[14] J. Slepian, Electrical World **91**, 761 (1928).

[15] H. Raether, Zeits. f. Physik **107**, 91 (1937).

ment but produce a charge concentration at the anode so that positive streamer propagation to the cathode is needed.

In the above-mentioned theoretical discussions, consideration appears to have been given principally to the field distortion produced by the positive space charge in the direction of the axis of the avalanche, i.e., in the direction of the external applied field. Clearly, however, the positive space charge will also produce a field distortion in the direction radial to the axis of the avalanche, i.e., perpendicular to the external field. Consideration of this fact led the writer to the following criterion for the transition of an electron avalanche to a conducting streamer, a criterion which makes quantitative calculation possible. *A streamer will develop when the radial field about the positive space charge in an electron avalanche attains a value of the order of the external applied field.* Then photoelectrons produced in the gas in the immediate vicinity of the avalanche will not only be accelerated in the direction of the external applied field but will also be drawn into the stem of the avalanche. (It has been shown by Cravath,[16] Dechene,[17] Loeb and Kip[13] that streamer propagation depends on photo-ionization in the gas.) In this manner the positive ion space charge attracts photoelectrons from the surrounding space in sufficient numbers to originate a self-propagating streamer. For lower values of external applied field, where the multiplication of ions in the avalanche is insufficient to produce a radial field of the same order of magnitude as the external field, photoelectrons produced in the gas proceed to the anode and are not deflected to the main avalanche.

It is clear that the exact equality of the radial field and the external applied field need not be insisted upon, and it is possible that the requisite criterion could be satisfied when the radial field is only 50 percent of the applied field. However, in the calculations the two fields have been set equal, and the application of this condition at once leads to equations for field strength for spark breakdown that closely approximate experimental observations and clarifies difficulties in the qualitative picture given by Loeb. The criterion not only enables quantitative calculations of breakdown to be made, but it also assists in the interpretation of a number of other sparking phenomena. It thus seems of interest to present the results of the analysis and its applications, together with its experimental justification.

[16] A. M. Cravath, Phys. Rev. **47**, 254 (1935).
[17] C. Dechene, J. de phys. et rad. **7**, 533 (1935).

Derivation of Equation for Breakdown

Because of the cumulative character of the ionization in an electron avalanche and the relative immobility of positive ions as compared with electrons, the bulk of the positive ions left behind by the advancing electron swarm are concentrated in a region of several ionizing free paths behind the tip of the avalanche. The region is also bounded by the periphery of the avalanche, which is conditioned by electron diffusion. Since the estimation of the field produced by such a distribution is difficult it will be assumed for convenience of calculation that the positive space charge is concentrated in a spherical volume of radius, r, equal to that of the avalanche. While the volume may be more nearly in the form of an oblate or prolate spheroid, the assumption of a perfect sphere will not affect the calculated field in order of magnitude.

The field, X_1, at the surface of a spherical volume of uniformly distributed space charge is given by

$$X_1=\frac{Q}{r^2}=\frac{4}{3}\pi r N\epsilon,$$

where N is the number of ions per cm^3 and ϵ is the charge on an electron. To find N, one recalls that owing to cumulative ionization the number, n, of positive ions formed when the avalanche has progressed a distance, x, is $n=e^{\alpha x}$, where α is the Townsend coefficient for ionization by electrons. In a distance dx the number of ions created is $dn=\alpha e^{\alpha x}dx$. These ions are assumed to be contained in a cylindrical volume of radius, r, and of length, dx, so that

$$N=\alpha e^{\alpha x}/\pi r^2.$$

According to Raether[15] the radius, r, is related to the distance, x, of avalanche travel by means of the diffusion equation $r^2=2Dt=2Dx/v$, where v is the velocity of advance of the avalanche and has been measured by Raether[15] and White.[18]

[18] H. J. White, Phys. Rev. **46**, 99 (1934).

Since $v=KX$, where K is the mobility and X is the applied field, we have

$$X_1=\frac{4}{3}\frac{\alpha e^{\alpha x}\epsilon}{r}=\frac{4}{3}\frac{\alpha e^{\alpha x}\epsilon}{(2Dx/KX)^{\frac{1}{2}}}.$$

Both D and K are functions of X/p and are approximately related by the expression

$$\frac{D}{K}=\frac{P}{N\epsilon}\frac{c_1^2}{c^2},$$

where P is atmospheric pressure, $N\epsilon$ is the Faraday constant, c is the speed of thermal agitation of electrons (1.2×10^7 cm per sec. at 20°C), and c_1 is the square root of the mean-squared velocity of the electron in the applied field. Townsend[19] has shown that c_1 is considerably larger than c. According to Compton[20] the value of c_1 is given by

$$c_1^2=1.33\frac{\epsilon}{m}\frac{X\lambda}{\sqrt{f}},$$

where λ is the mean free path of the electron, X is the applied electric field, m is the mass of an electron, p is the gas pressure, and f is a factor which depends on the fractional loss of energy per collision. If λ_0 is the mean free path of an electron at a pressure of 760 mm Hg, then the value of c_1 for a pressure, p, is given by

$$c_1^2=1010\frac{\epsilon}{m}\frac{X}{p}\frac{\lambda_0}{\sqrt{f}}.$$

The values of λ_0 and f obviously depend on X/p and are not known for the high values of X/p which are necessary for spark breakdown. But inasmuch as the theory will be found insensitive to slight errors in the value of $\lambda_0/\sqrt{f}$ it is considered reasonable to calculate its value from known data based on experiments with fields close to those which produce sparking. Raether[15] found that the speed of advance of an electron avalanche was 1.25×10^7 cm per sec. in a field $X/p=41$ volts per cm per mm. Substitution of such values in the well-known Langevin equation for electron mobility, *viz.*, $v=0.815\,\epsilon\lambda X/mc_1$, enables one to calculate that $\lambda_0\sqrt{f}=5.7\times10^{-6}$. The mean free path λ_0 is taken as 3.6×10^{-5} from curves given by Brose and Saayman[21] and corresponds to an electron energy of three volts. Whence we have $f=0.025$ and $c_1=2.01\times10^7(X/p)^{\frac{1}{2}}$. Then we have

$$X_1=\frac{4}{3}\frac{\alpha e^{\alpha x}\epsilon}{(2Pc_1^2x/N\epsilon c^2X)^{\frac{1}{2}}}$$

$$=5.28\times10^{-7}\frac{\alpha e^{\alpha x}}{(x/p)^{\frac{1}{2}}}\text{ volts/cm.} \qquad (1)$$

Now for $x=\delta$, the gap length for a plane parallel gap, application of the criterion for streamer formation, that $X_1=X$, gives

$$X(\delta/p)^{\frac{1}{2}}=5.28\times10^{-7}\alpha e^{\alpha\delta}.$$

which may be written in logarithmic form as

$$\frac{\alpha}{p}p\delta+\log_e\frac{\alpha}{p}=14.46+\log_e\frac{X}{p}-\tfrac{1}{2}\log_e p\delta+\log_e\delta. \qquad (2)$$

Reference to curves of the Townsend type which relate α/p with X/p now enables the value of X/p required for sparking to be calculated for given δ and p. In the case of a one-cm gap in air at atmospheric pressure the breakdown equation is satisfied for $X/p=42.4$ ($\alpha=18.6$), i.e., $X=32.2$ kilovolts per cm,* which is in close agreement with the observed value of 31.5 kilovolts per cm.[22]

TABLE I. *Breakdown potentials corresponding to different values of p and δ.*

$p\delta$ mm×cm	Breakdown potential (kv)		
	$\delta=0.1$	$\delta=1.0$	$\delta=10.0$
7600	245	248	249
760	31.5	32.2	32.9
380	18.0	18.6	18.9

Comparison Between Calculated and Measured Values of Breakdown Potential

The form of the breakdown Eq. (2) shows that it is in agreement with Paschen's law other than

[19] J. S. Townsend, *Electricity in Gases* (Oxford University Press, 1914), p. 122ff.

[20] K. T. Compton and I. Langmuir, Rev. Mod. Phys. **2**, 220 (1930).

[21] H. L. Brose and E. H. Saayman, Ann. d. Physik **5**, 797 (1930).

* If we set the criterion for streamer formation as $X_1=0.2X$ instead of $X_1=X$, the breakdown field strength evaluted is 31.8 kilovolts per cm.

[22] W. Spath, Arch. f. Elek. **12**, 331 (1923).

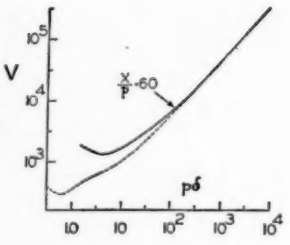

FIG. 1. Experimental and calculated curves to show relationship between breakdown voltage and $p\delta$.

for the term, $\log_e \delta$. This term has little effect, however, on the calculations, as shown by Table I for breakdown potential corresponding to different values of p and δ. The deviations, for the same value of $p\delta$, are within the present margins of experimental error in measurement, and it may be that for more accurate measurements such differences will be observed. For it should be pointed out that the derivation of Paschen's law is based on theoretical considerations analogous to those of Townsend. Such considerations make the mechanism of spark breakdown dependent on the total number of ions formed in the gap and, since the multiplicative factors in ion production depend on X/p, Paschen's law results. However, on the new theory, it is seen that the breakdown mechanism is not dependent on the total number of ions formed but depends on the ion density in an electron avalanche and the resultant space-charge field. In consequence, we would not expect that Paschen's law would be strictly obeyed. In fact, it has previously been shown[23] that with space charge distortion Paschen's law is only approximately correct, and that the deviation in breakdown potential is of the same order of magnitude as that derived here. So that unless the precision of experimental determinations of sparking potentials in the future indicates Paschen's law to hold beyond the prediction of the present theory, the deviations of the latter from Paschen's law are not thought to invalidate the theory in any way.

Both experimental and calculated curves to show the relationship between the voltage required to cause breakdown and the product, $p\delta$, of pressure times gap-length are plotted on logarithmic scale in Fig. 1. The calculated curve is based on values for the primary ionization coefficient, α, in air as given by Sanders[24] for X/p up to 100; for higher X/p the values of α are taken from Posin's observations in nitrogen.[25] The experimental curve, shown dotted, is that given by Whitehead[26] as the mean of the results given by a number of independent workers. It will be observed that the calculated curve is in agreement with that experimentally determined for values of $p\delta$ from 10,000 down to about 100 mm×cm. For values of $p\delta<100$, the calculated values are higher than those observed, and the deviation increases steadily with decreasing $p\delta$ and thus with increasing X/p. The deviation occurs in the region of $X/p=60$ which is about the minimum value of X/p for which the second Townsend coefficient is observed.[27] Thus for values of $p\delta<100$ the deviation can be accounted for by the presence of other sources of ionization in the gap. This is in agreement with calculations made in the past on a knowledge of the Townsend coefficients, and which have yielded approximately correct values of breakdown potential corresponding to low values of $p\delta$. The deviation between the two curves then indicates the region in which breakdown by streamer formation gives way to classical theory and the Townsend type of mechanism.

Preliminary calculations of the breakdown strength of other gases, such as hydrogen, have been made and give values in agreement with those observed experimentally.

CONCLUSIONS

It is seen that the above theory postulates an entirely different mechanism of breakdown for longer gaps and higher pressures than that given by classical theory.

1. The proposed mechanism depends on photo-ionization and electron multiplication in the gas (Townsend's α). This photo-ionization is justified by recent observations on the effectiveness of such ionization under the existing conditions.[16,17].

2. It requires that the density of positive ion space charge created in an electron avalanche is

[23] R. N. Varney, H. J. White, L. B. Loeb and D. Q. Posin, Phys. Rev. **48**, 818 (1935).

[24] F. H. Sanders, Phys. Rev. **44**, 1020 (1933).
[25] D. Q. Posin, Phys. Rev. **50**, 650 (1936).
[26] S. Whitehead, *Dielectric Phenomena* (D. Van Nostrand & Company, New York, 1927), p. 42.
[27] W. E. Bowls, Phys. Rev. **53**, 293 (1936).

sufficient to draw in photoelectrons and their progeny, produced by ionization by collision, in a measure which renders the positive space charge a conducting plasma, and permits the further development of the streamer. This is only possible when the field strength and gas pressure are such as to allow a sufficient density of photo-ionization in the neighborhood of the streamer head to permit self-propagation.

3. It shows that the development of long sparks is completely devoid of any dependence on cathode material, in conformity with observation.

4. It is in full accord with time-lag studies in that it involves formative time lags of $\sim 10^{-7}$ sec. or less and explains the fact that when a potential is applied to a gap in excess of the minimum required to cause breakdown midgap streamers develop and the formative time lag is reduced.[8] For in this case an electron avalanche which originates at the cathode will have developed the requisite density of positive ions to cause the initiation of a streamer before the anode is reached. The reduced distance which the avalanche has to travel before it produces a streamer makes it probable that several streamers will be initiated simultaneously. A conducting filament across the gap will be formed by the junction of such streamers, and results in a corresponding reduction in time of formation of the spark.

5. At the sparking threshold the spark is initiated by a single electron liberated from the cathode. The chance of a spark then depends on (*a*) the chance of a single electron avalanche which produces at the anode or in midgap the requisite space charge, and (*b*) the success which this space charge has in photo-ionizing the ambient gas and in attracting sufficient electrons to ensure self-propagation of a streamer. This accounts for the statistical time lags, and for the observed indefinite character of the sparking potential. That the sparking threshold is at all definite under these conditions is explained by the cumulative nature of electron ionization, i.e., $i=i_0e^{\alpha x}$, and also that $\alpha/p=f(X/p)$ where $f(X/p)$ is of the form $Ae^{BX/p}$ or $C(X/p-D)^2$.

6. The theory is completely consistent with the observations of H. Raether on the development of sparks in a cloud chamber. In fact, Raether's photographs clearly indicate the passage of an electron avalanche from cathode to anode followed by a streamer which proceeds from the anode to the cathode to form a conducting filament bridging the gap. Simultaneously and quite independently, Loeb, on the basis of corona studies, and Raether,[28] on the basis of cloud-chamber observations, postulated a qualitative picture of the sparking mechanism which is here rendered quantitative.

7. It can be shown that the field distortion produced by cumulative ionization with high densities of photoelectric current gives a lowering of sparking potential in rough quantitative agreement with the lowering observed by White,[11] Rogowski and Wallraff.[29]

8. It clearly accounts for the filamentary character of spark breakdown at longer gaps and higher pressures and explains both the zigzag character of the spark and the branching observed. This differentiates the sparks under this mechanism from those in the Townsend regime ($p\delta<100$ in air).

9. It explains the fact that in the study of the Townsend coefficients at lower X/p and higher $p\delta$ sparking occurs before values of the second coefficient, γ, can be observed.

10. The slight deviation of the theory from Paschen's law is not inconsistent with experimental data in this field of investigation.

11. While at present the inexact character of the quantitative criterion for streamer formation leaves considerable latitude owing to the exponential nature of electron multiplication by ionization by collision, the equation gives numerical results in as good agreement with experiment as those based on Townsend's theory, where a hypothetical value of γ has to be assumed, since it cannot be observed. Numerical agreement of this character between theory and experiment must not be taken too seriously as a confirmation of any particular theory in view of the latitude given by the exponential term and the lack of adequate experimental data.

12. The theory has been extended to the explanation of sparks of all lengths at higher $p\delta$

[28] H. Raether, Zeits. f. Physik **112**, 464 (1939).
[29] W. Rogowski and H. Wallraff, Zeits. f. Physik **102**, 183 (1937).

in air and the necessary conditions for sparking have been established by Loeb. A more exhaustive discussion of the application of the theory will be given in an article to appear at some future date.

13. It can be shown that the theory leads to an explanation of the breakdown of unsymmetrical gaps where the field distribution is known, and that quantitative calculations can be made. The theory may be applied to either surge-impulse or static breakdown.

14. It is found that the self-propagating streamer mechanism, as modified for longer sparks, will adequately account for the pilot streamer in Schonland's mechanism[30] for the lightning discharge, and it clarifies the theory proposed by the writer[31] for the "stepping" observed in lightning and spark discharges.

The writer wishes to express his appreciation to Professor L. B. Loeb, whose original qualitative theory stimulated this work and whose suggestions and criticisms have contributed much to the development of the present theory. He also thanks the Commonwealth Fund for the grant of a Fellowship, during the tenure of which this work was carried out.

[30] B. F. J. Schonland, Proc. Roy. Soc. **A164**, 132 (1938).
[31] J. M. Meek, Phys. Rev. **55**, 972 (1939).

APRIL 15, 1940 PHYSICAL REVIEW VOLUME 57

Ferromagnetic Anisotropy, Magnetization at Saturation, and Superstructure in Ni_3Fe and Nearby Compositions*

EUGENE M. GRABBE†
Sloane Physics Laboratory, Yale University, New Haven, Connecticut
(Received February 13, 1940)

The order-disorder transformation involving Ni_3Fe affects both the ferromagnetic anisotropy and the saturation magnetization. Iron-nickel alloys in the range 65 to 80 percent nickel have been investigated, using spheroidal specimens. With superlattice formation the anisotropy becomes more like that of pure nickel with ⟨111⟩ as the direction of easiest magnetization. The change is largest near Ni_3Fe. The saturation magnetization increases with ordering; the greatest observed increase was 5.8 percent for an alloy very near Ni_3Fe. Different rates of cooling from above the critical temperature (about 490°C) affect the saturation magnetization. These changes are attributed to changes in degree of local ordering effects. Long distance order, induced by baking for long periods, greatly influences both anisotropy and magnetization at saturation.

Introduction

IRON–NICKEL alloys in the composition range 65 to 80 percent nickel have unusual properties which are sensitive to heat treatment. They develop extremely high permeabilities when cooled rapidly from above 600°C. Baking below this temperature or cooling slowly does not produce uncommonly high permeabilities. Attempts to explain these characteristics in terms of an order-disorder transformation involving Ni_3Fe have long been hampered by the lack of conclusive evidence for the existence of this superlattice.[1]

Changes in resistance, which occur in these alloys with proper baking after quenching, are not as marked as in many order-disorder transformations. This is to be expected, however, since the differences in size and chemical properties between iron and nickel atoms are not great. Specific heat measurements have not been conclusive because the anomaly, due to the magnetic transformation, occurs near the critical ordering temperature. X-ray analyses have, until after the experiments here reported were com-

* Part of a dissertation presented to the Faculty of the Graduate School of Yale University in candidacy for the degree of Doctor of Philosophy.
† Now at the General Laboratories, United States Rubber Company, Passaic, New Jersey.

[1] O. Dahl, Zeits. f. Metallkunde **28**, 133–138 (1936); S. Kaya, J. Fac. Sci., Hokkaido Imp. Univ. **2**, 29–53 (1938); F. E. Haworth, Phys. Rev. **54**, 693–698 (1938).

pleted, given negative results. Small difference in x-ray scattering power between iron and nickel and the sluggishness of the transformation have probably been responsible for ambiguities.

The ferromagnetic anisotropy of single crystals affords an excellent means of examining this order-disorder transformation, even though the anisotropy of alloys of interesting compositions is small. Its high temperature coefficient indicates that it is sensitive to changes in lattice parameter, and lattice spacing usually decreases with ordering. Furthermore, anisotropy may be uniquely affected, since a regular arrangement of two unlike atoms having different magnetic moments may well modify the energies required to magnetize a single crystal in the principal directions. Calculations by McKeehan,[2] for purely magnetic interactions, predict such characteristic differences between ordered and disordered states.

The first reported measurements of changes with baking in the anisotropy and saturation magnetization of iron-nickel alloys near Ni_3Fe[3] have since been extended to other alloys in the range 65 to 80 percent nickel by weight. These data would be difficult to explain by other than an order-disorder transformation, since they indicate changes throughout a single crystal specimen primarily related to the crystal structure.[4] X-ray evidence presented since the experiments here reported[5,6] has proved that this superstructure occurs. Exposures as short as eight hours have now revealed superlattice lines from alloys baked for 500 hours in the temperature range 490°C to 370°C.[5] These lines were absent from similar exposures with quenched specimens.

Specimens

Large single crystals, of volume greater than 1 cm³, were grown in a vacuum furnace by the slow freezing of melts in high purity magnesia crucibles. The stock materials used were homogenized castings containing about 0.15 percent of the usual impurities: principally sulphur, silicon, and cobalt, with traces of phosphorus, manganese, aluminum, and carbon.

TABLE I. *Description of specimens.*

Ni (weight percent)	80*	74.8	70.5	69.8	68.0(a)	68.0(b)	65*
Fe (weight percent)	20*	25.2	29.5	30.2	32.0	32.0	35*
Mass, 10^{-3} g	41.2	40.2	23.8	26.2	29.1	48.7	37.4
Diameter, 10^{-4} cm	5001	5106	4076	4495	4470	5364	5082
Thickness, 10^{-4} cm	360	305	302	274	297	323	356
Volume, 10^{-8} cm³	476	470	280	309	343	578	444
Axial ratio	13.9	16.8	13.5	16.4	15.0	16.6	14.3
Demagnetizing factor							
(1) Observed	0.626	0.574	0.667	0.552	0.620	0.596	0.561
(2) Calculated	0.651	0.548	0.669	0.560	0.606	0.552	0.635

* Not analyzed.

Specimens were prepared in the form of oblate spheroids having an equatorial plane of the form {110}. This plane contains all three important magnetic axes of forms ⟨100⟩, ⟨111⟩, and ⟨110⟩, so that the anisotropy of a given alloy may be completely determined from one specimen. A slab of correct orientation is sawed out, and a disk, cut from this slab, is cemented to the shaft of a high speed motor. A highly magnified silhouette of the disk is projected on a vertical screen on which an ellipse of proper size and of the desired axial ratio has been carefully plotted. The disk, while rotating, is cut with fine files to match this contour.[7] Exceptional care was taken in preparing the samples, and their x-ray Laue patterns show that distortion by cold work was trivial. Departures of the equatorial plane from the {110} plane aimed at were not allowed to exceed a degree or two. The effect introduced by such deviations of the axes chosen for measurement from symmetry axes in the crystal should be negligible. In each spheroid, the axial ratio (diameter to thickness) was made large enough (greater than 12) to ensure a low demagnetizing factor. The volumes were calculated from densities based upon x-ray data. Table I gives the compositions, in weight percent, of the spheroids used in this investigation, their dimensions, volumes, axial ratios, and demagnetizing factors, as calculated from dimensions and as experimentally determined.

Measurements

Magnetic measurements were taken with an improved quinquefilar pendulum magnetometer. The weight was redistributed to increase the stability, and the sensitivity was greater than that of similar pendulums previously used.[7] The

[2] L. W. McKeehan, Phys. Rev. **52**, 18–30 (1937).
[3] L. W. McKeehan and E. M. Grabbe, Phys. Rev. **55**, 505 (1939); E. M. Grabbe and L. W. McKeehan, Phys. Rev. **55**, 1142(A) (1939).
[4] Order-disorder transformations in a single crystal are especially simple to analyze. Cf. W. G. Burgers and J. L. Snock, Physica **2**, 1064–1074 (1935).
[5] P. Leech and C. Sykes, Phil. Mag. **27**, 742–753 (1939).
[6] F. E. Haworth, Phys. Rev. **56**, 289 (1939).
[7] L. W. McKeehan, Rev. Sci. Inst. **5**, 265–268 (1934); L. W. McKeehan, R. G. Piety and J. D. Kleis, Rev. Sci. Inst. **7**, 494–497 (1936).

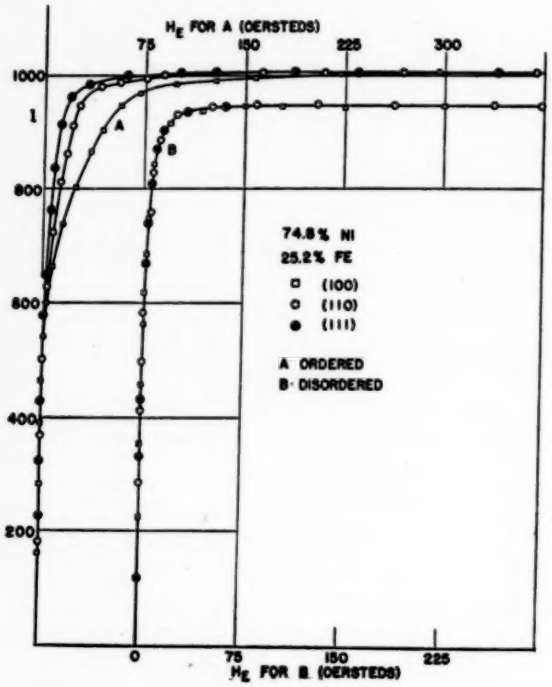

FIG. 1. *I vs. H* curves for 74.8 percent nickel.

most important modification was in the method of measuring deflections. A small square of a diffraction grating replica fastened to a thin glass plate was mounted on the pendulum beam with its rulings vertical and in the plane of permitted motion. This was intensely illuminated from behind by a platinum ribbon lamp, using circulating water in a cell to absorb heat radiation. Highly magnified images of several adjacent rulings were thrown on a translucent glass scale by means of a compound microscope. At magnifications of 1200 to 1500, the line images were quite sharp. No fixed fiducial line is used; any line image may be chosen as the zero point for the subsequent deflection. By adjustment of the field gradient the deflection can always be made an integral number of line spacings, so that the displacement of the pendulum is simply this number multiplied by the grating constant. There is then no correction for lens curvature, and the magnification need not even be known. Furthermore, the deflection range is large, and the character of the images is such that slight transverse displacements of the pendulum, vertical or horizontal, do not diminish the precision of measurements. Displacements of the order of 0.5 mm were measured to about 1 part in 1000 by this method.

The magnetizing field was supplied by a solenoid, previously described,[8] with compensating coils to level the field near the center. Two types of gradient compensating arrangements proved satisfactory; one with two series coils placed at the ends of the solenoid, the other utilized a single coil of 75 turns with reversed

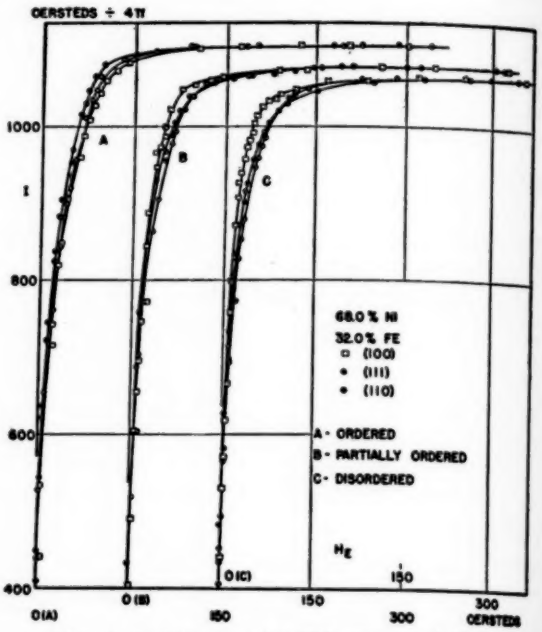

FIG. 2. *I*—*H* curves for 68.0 percent nickel.

current placed around the middle of the solenoid.[9] The field was made uniform to 1 part in 2000 for a distance of 8 mm along the solenoid axis. All the specimens saturated at low fields, and the scatter of points on the magnetization curves is small, indicating that the precision expected was attained.

HEAT TREATMENT

After shaping, the spheroids were annealed in hydrogen for 1 hour at 750°C to relieve strains. The cooling rate, attained by permitting the specimen to cool with the furnace after annealing, was about 300 degrees per hour. This cooling rate was slow enough to develop local order to a small degree. (See Results II.)

[8] L. W. McKeehan, R. G. Piety and J. D. Kleis, Rev. Sci. Inst. **7**, 494–497 (1936).
[9] L. W. McKeehan, Rev. Sci. Inst. **10**, 371–373 (1939).

In order to retain the disordered state at room temperature, a method for extremely rapid cooling was devised. The specimens were placed in the bend of a fused silica U-tube through which hydrogen at about atmospheric pressure was passed. This bend of the tube was lowered into a furnace with the ends projecting. When the temperature had reached 750°C (well above the critical temperature), the tube was quickly withdrawn and inverted. The specimens fell from the red-hot bend of the tube into a cool part of the tube. Due to its small volume and large surface, a spheroid ceased to glow while falling. The cooling rate was estimated to be 200 to 400°C per second. Maximum disorder was obtained by this drastic treatment.

The most favorable ordering temperature, in agreement with Kaya,[1] was found to be near 490°C. Specimens were baked at this temperature for at least a week in evacuated Pyrex tubes. Magnetic measurements were then made, and the spheroids were returned to the furnace and baked for another long period at a slightly lower temperature. If no changes occurred during the second baking period, it was assumed that equilibrium had been attained. It is probable that equilibrium was reached in all cases. In three instances there is additional ground for this opinion, since the same final condition was reached in consecutive programs of baking separated by a quenching process.

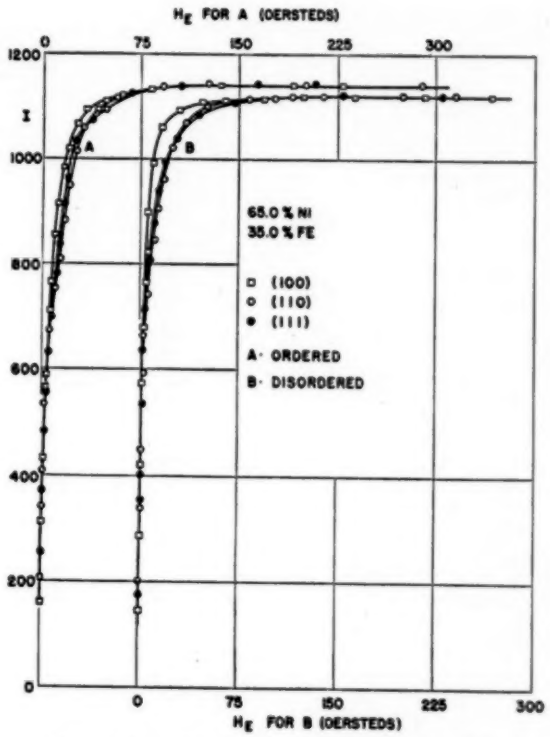

FIG. 3. I vs. H curves for 65.0 percent nickel.

RESULTS

I. Magnetic anisotropy

Baking for long periods at or below 490°C caused large changes in the ferromagnetic anisotropy of the crystals. For an alloy of 74.8 percent nickel and the remainder iron (very nearly the correct stoichiometric ratio for Ni_3Fe), the disordered state exhibited nearly zero anisotropy. In the ordered state the anisotropy observed, measured by the first anisotropy coefficient (K_1), was almost two-thirds that reported for pure nickel. The direction of easiest magnetization was [111], with [110] and [100] following in that order. Fig. 1 shows the magnetization curves for this spheroid.

For 80 percent nickel, the anisotropy after

TABLE II. *Magnetization energy differences.*

	Energies in 10^4 erg·cm^{-3} for following weight percents of Ni					
	80	74.8	70.5	69.8	68.0	65
$W_{110}-W_{100}$ Ordered	−0.31	−0.58	0.08	−0.03	−0.05	0.21
$W_{110}-W_{100}$ Disordered	−0.01	0.00	0.40	0.27	0.26	0.29
$W_{111}-W_{100}$ Ordered	−0.48	−0.83	−0.25	−0.34	−0.19	0.17
$W_{111}-W_{100}$ Disordered	−0.03	0.00	0.25	0.21	0.22	0.26
K_1 Ordered	−1.26	−2.30	0.31	−0.11	−0.18	0.83
K_1 Disordered	−0.04	0.00	1.60	1.07	1.04	1.16
K_2 Ordered	−1.75	−1.65	−9.52	−8.24	−3.55	−2.98
K_2 Disordered	−0.33	0.00	−7.76	−3.82	−3.40	−3.41

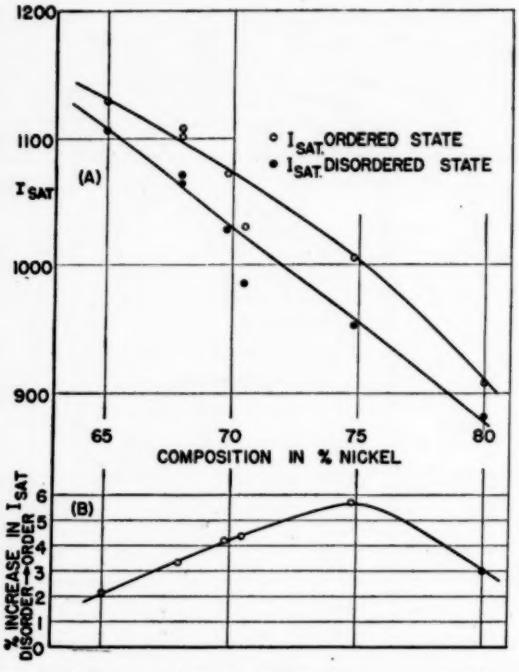

FIG. 4. (A) Saturation magnetization *vs.* composition for iron-nickel alloys. (B) Percent increase in $I_{SAT.}$ with ordering *vs.* composition.

quenching is very small, with [111] as the direction of easiest magnetization. Baking again develops a large anisotropy similar to that for the 74.8 percent alloy, but the change in K_1 is less.

For crystals containing less nickel than Ni_3Fe, the irregular order[10] of decreasing ease of magnetization [100], [111], [110] was observed at low fields for the disordered state. At higher fields, however, the [110] curve jumps to saturation, crossing the [111] curve. This crossover, which has not before been reported, was observed in the 65, 68, and 70 percent nickel alloys. In going over to the ordered state, a complete changeover occurs for the 68 and 70 percent nickel alloys. The [111] direction becomes the direction of easiest magnetization at all values of H. The [110] and [100] curves cross and recross, with [100] reaching saturation last. This crisscrossing is for almost coincident curves and may be due to errors in cutting the spheroids. That it is an inherent effect is, however, rendered more probable by the fact that it was observed to occur in three different specimens. Fig. 2 shows the upper part of the magnetization curves for a 68 percent nickel, 32 percent iron alloy for the ordered state, the disordered state, and an intermediate condition. The changes in anisotropy are small in comparison with those for the 74.8 percent alloy.

For 65 percent nickel, this complete changeover of magnetization curves does not occur. (See Fig. 3.) The irregular order [100], [111], [110] is observed for the disordered state, and the anisotropy merely decreases when the superstructure is formed. It follows that for some composition between 65 and 68 percent nickel, the anisotropy must be vanishingly small for the ordered state.

The changes in anisotropy between various degrees of disorder, induced in a specimen by the different cooling rates given above, were negligible. The large changes took place only after prolonged baking. Table II tabulates the anisotropy constants and the energy differences $W_{100}-W_{110}$ and $W_{111}-W_{100}$ for ordered and disordered crystals. The general effect of superstructure formation is to make the anisotropy more like that of pure nickel.

II. Saturation magnetization

The large changes observed in the saturation magnetization were unexpected. Considering the amount of work that has been done on the alloys in this composition range, it is surprising that such large effects have not been detected before.[11] The difference in saturation magnetization between ordered and disordered states was a maximum for the 74.8 percent nickel alloy. For

TABLE III. *Saturation magnetization values.*

Percent Nickel	Saturation Values (a) Ordered	Normal* (b) Cooling (Local Order)	Drastic** (c) Cooling (Disordered)	Percent Increase (b) to (a)	Percent Increase (c) to (a)
80.0	908	895	882	1.4	3.0
74.8	1007	963	952	4.6	5.8
70.5	1029	—	986	—	4.4
69.8	1071	1044	1028	2.6	4.2
68.0	1102	1080	1066	2.0	3.4
68.0	1108	1082	1072	2.4	3.4
65.0	1129	1117	1106	1.2	2.2

* 10°C to 100°C per minute (normally expected values).
** About 200°C per second.

[10] J. D. Kleis, Phys. Rev. **50**, 1178–1181 (1936).

[11] Confirmatory results have since been reported by P. Leech and C. Sykes, Phil. Mag. [7] **27**, 742–753 (1939) and by S. T. Pan, Phys. Rev. **56**, 933–936 (1939).

disorder attained by rapid or normal cooling, the change amounted to 4.6 percent, while for drastic cooling, the difference between ordered and disordered states was 5.8 percent of the saturation value for the disordered crystal. These values could be reproduced very accurately, regardless of previous heat treatment, and, therefore, the difference of 1.2 percent for different cooling rates is regarded as due to changes in the degree of short distance order.

For 65, 68, and 70 percent nickel, the changes with ordering, though marked, were smaller and decreased with increasing departure from Ni_3Fe. One of the specimens of composition near 70 percent nickel was difficult to magnetize to saturation and exhibited an abnormally low saturation value. The change with ordering, however, fits in with the other values. (See Fig. 4.) The increase in saturation magnetization with ordering falls off more rapidly on the nickel-rich side. At 80 percent nickel the maximum change observed was 3.0 percent, while near 70 percent nickel the shift amounted to 4.3 percent.

In line with this, it may be noted that abnormal magnetic properties extend over a wider range below 75 percent nickel than above this composition. This supports the view that the order-disorder transformation is responsible for permeability changes as well as for saturation changes.

The difference in the saturation magnetizations for different rates of cooling was of the same order of magnitude for all the alloys tested. Table III lists the saturation values obtained for different heat treatments.

The dissymmetry of the ordering forces, which is suggested by these facts, implies that the ordering forces which act below the critical temperature for order are greater if, at this temperature, the degree of ferromagnetic saturation is higher. The Curie point has its maximum near 70 percent nickel, and the magnetization at any selected temperature below the maximum Curie point has its maximum value at a still lower concentration of nickel, because the magnetic moment per atom rises with addition of iron. It is therefore suggested that ferromagnetic interaction promotes order in this series of alloys.

Curves plotted for the two ⟨111⟩ axes lying in the equatorial plane of the 74.8 percent nickel alloy proved to be identical. This test, suggested by Dr. R. M. Bozorth of the Bell Telephone Laboratories, shows that the effects are not determined by the accidental direction of a stray magnetic field present during baking, but are immediately related to the structure.

Discussion

The superstructure transformation involving Ni_3Fe is a sluggish one, with a critical ordering

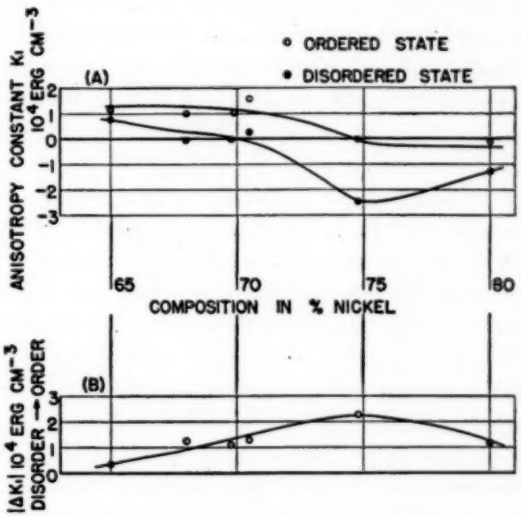

Fig. 5. (A) K_1 *vs.* composition for iron-nickel alloys. (B) Change in K_1 with ordering *vs.* composition.

temperature near 490°C. Baking just below this temperature was most effective in ordering.

Both the anisotropy and saturation magnetization are changed by baking for long periods below the critical temperature. Cooling at different rates produces appreciable changes only in the saturation magnetization. Hence, the anisotropy gives a measure of the long distance order, while the saturation magnetization change is related to local ordering, or the average magnetic moment for any one atom is determined by the nature of its nearest neighbors. Fig. 4 gives plots of magnetization at saturation *versus* composition and change in magnetization with ordering *versus* composition. The maximum is near the critical composition. Fig. 5 shows the change in the anisotropy constant K_1 by superstructure formation for different compositions. The maximum at Ni_3Fe is quite broad. The values for K_1 (disordered) are slightly lower than values

obtained by Kleis.[10] The second anisotropy constant K_2 becomes more positive with ordering except for the 65 percent nickel alloy.

The high permeability developed in these alloys by quenching is characteristic of the highly disordered state. A plausible explanation for the normal low permeability is that slow cooling forms small ordered regions which are frozen into an otherwise disordered lattice and give rise to strains. These strains increase the coercive force, and the permeability is low, while the highly disordered state is relatively strain-free and exhibits an extremely high permeability.

Cooling alloys in this composition range from above 500°C in the presence of a magnetic field also produces high permeabilities.[12] The effects of such heat treatment in a magnetic field may also be related to ordering. The critical temperature may be altered by the application of a field during cooling, if the ordering forces are in part of ferromagnetic origin. It does not appear, however, that the saturation value can be much affected by such treatment, as the following additional test indicates. Two specimens of 74.8 percent nickel and 68 percent nickel were each cooled slowly six times from 750°C with magnetic fields of 25 and 800 oersteds directed in turn along the three principal magnetic axes. The saturation magnetizations were the same as for cooling in the absence of a field, indicating, in accordance with the views expressed above, that these fields had no effect on the local order.

The addition of small amounts of the elements Mo, Mn, and Cu to these alloys increases the permeability to high values without the necessity of quenching or cooling in a magnetic field.[13] If the existence of local order is related to the permeability in these cases, the ordering forces are likely of a ferromagnetic nature, since ferromagnetic properties of pure alloys are easily disturbed by impurities in small quantities.

If the superstructure FeCo exists, indications are that it has an ordering temperature near 800°C, and it would be almost impossible to obtain the disordered state at room temperature.[14] In a preliminary test for such order, if it exists, one iron-cobalt specimen containing 56.3 percent iron (near FeCo) was repeatedly drastically quenched from temperatures ranging from 800°C and 900°C. The anisotropy and saturation value were not affected. The iron-cobalt spheroid had an axial ratio of about 20 to 1 and, consequently, saturated easily. Its magnetization at saturation was 1937.

Kaya[1] found that polycrystalline samples of compositions near Ni_3Fe were more difficult to saturate after they had been baked for long intervals. Much earlier than this, Elmen[15] had shown that such treatment greatly lowered initial permeability. This is in agreement with the results here presented, which show the appearance in the ordered state of one direction of very difficult magnetization.

As mentioned in the introduction, the reported changes in resistance with ordering are small, and so too are the possible changes in lattice parameter. It may be worth noting that the change in resistance is consistent in sign with increase in the number of free electrons and corresponding increase in the vacancies in the 3d electron group. The latter change corresponds to the observed increase in magnetic moment per atom.

McKeehan[2] has calculated the anisotropy constants K_1 and K_2 for Ni_3Fe as a disordered solid solution and as a superstructure, from magnetic multipole interaction. The quadrupole terms predict the correct sign for the change in K_1 accompanying the order-disorder transformation and are of the correct order of magnitude. For Ni_3Fe in the disordered state, K_1 (calculated) $=-0.18\times10^4$ erg·cm^{-3}, while for the ordered array, K_1 (calculated) $=-1.62\times10^4$ erg·cm^{-3}. These are to be compared with the experimentally observed values, zero and -2.30×10^4 erg·cm^{-3}, respectively. The computed sextupole part of K_1, and the computed K_2, which has no quadrupole part, do not change in the observed directions for superstructure formation.

The author wishes to express his sincere thanks to Professor L. W. McKeehan, who suggested this investigation, for his ready advice and for stimulating discussions during the course of the work.

[12] R. M. Bozorth, J. App. Phys. **8**, 575–588 (1937).
[13] S. Kaya and M. Nakayama, Zeits. f. Physik **112**, 420–429 (1939).
[14] A. Kussmann, B. Sharnow and A. Schultze, Zeits. f. tech. Physik **13**, 449–460 (1932).
[15] G. W. Elmen, J. Frank. Inst. **207**, 583–617 (1929), esp. Fig. 13.

Probable Error for Poisson Distributions

ERIC RODGERS
University of Alabama, University, Alabama
(Received February 10, 1940)

It is shown for Poisson distributions that both the probable error and the probability that a deviation not exceed the standard deviation approach as limits the corresponding values for normal distributions. Curves are given showing the manner of approach.

IF occurrences of a certain event are subject to a normal distribution, probable error is defined as that deviation from the average for which there is a half-chance that a single trial should not yield a greater deviation. For a normal distribution

$$\text{probable error} = 0.67449\sigma \qquad (1)$$

where σ is the standard deviation. For an unsymmetrical distribution, this expression does not give the probable error; or if it is taken as the defining expression of probable error, it does not have the same meaning as for normal distributions.

One type of unsymmetrical distribution is that which follows a Poisson, or Bateman, distribution formula. This formula has received considerable attention recently because of its application to counts from Geiger-Müller counters. It may be written as

$$W_n = x^n e^{-x}/n!, \qquad (2)$$

and gives the probability of occurrence of n events in a single period of observation for which the *true* average is x events. The purpose of the present paper is to discuss probable error for distributions following the Poisson formula.

We shall first take up the question as to the probability that a single observation should yield a result not differing from the average by more than the standard deviation. For a Poisson distribution, the standard deviation is simply $\sqrt{x}$. The desired probability is then

$$P_\sigma = \sum_{n=x-\sqrt{x}}^{n=x+\sqrt{x}} \frac{x^n}{n!} e^{-x}. \qquad (3)$$

This expression is easily evaluated when x is a perfect square and not too large. When x is not a perfect square, it can be evaluated only approximately. It is found that its value slowly decreases as larger and larger values of x are used. This suggests seeking its limit as x approaches infinity. To do this it simplifies things somewhat if we set $x=y^2$, and set $n=y^2+t$. We then have

$$P_\infty = \lim_{y\to\infty} \sum_{t=-y}^{t=+y} \frac{(y^2)^{y^2+t}}{(y^2+t)!} e^{-y^2}. \qquad (4)$$

It can be shown that the difference between any two consecutive terms in this sum is an infinitesimal of higher order than either of the terms as y becomes large. If for any chosen value of x in Eq. (2), the factorial be replaced by a gamma-function and n be considered to vary continuously, a smooth curve may be drawn with W as ordinate and n as abscissa. When this is done it is seen that the portion of the area under the curve bounded by the ordinates corresponding to any two consecutive integral values of n is numerically greater than one of these ordinates and less than the other. These two facts enable us to replace the sum in (4) by an integral with respect to t between the limits $-y$ and $+y$. Making the substitution $t=ky$, we get

$$P_\infty = \lim_{y\to\infty} \int_{-1}^{+1} \frac{(y^2)^{y^2+ky}}{(y^2+ky)!} e^{-y^2} y\,dk. \qquad (5)$$

If the factorial be considered as a gamma-function, the integrand is a bounded continuous function of y for $y>0$ and any chosen value of k in the range of k. Also its simultaneous limit exists as $k\to k_0$ and $y\to\infty$, where k_0 is any finite value of k. To show this it is only necessary to set $k=f(y)$, where $f(y)$ is any continuous function of y that has the limit k_0 as $y\to\infty$, and than take the limit of the result as $y\to\infty$. If this is done, it is found that the limit is independent of the form of the function $f(y)$. Thus the integrand con-

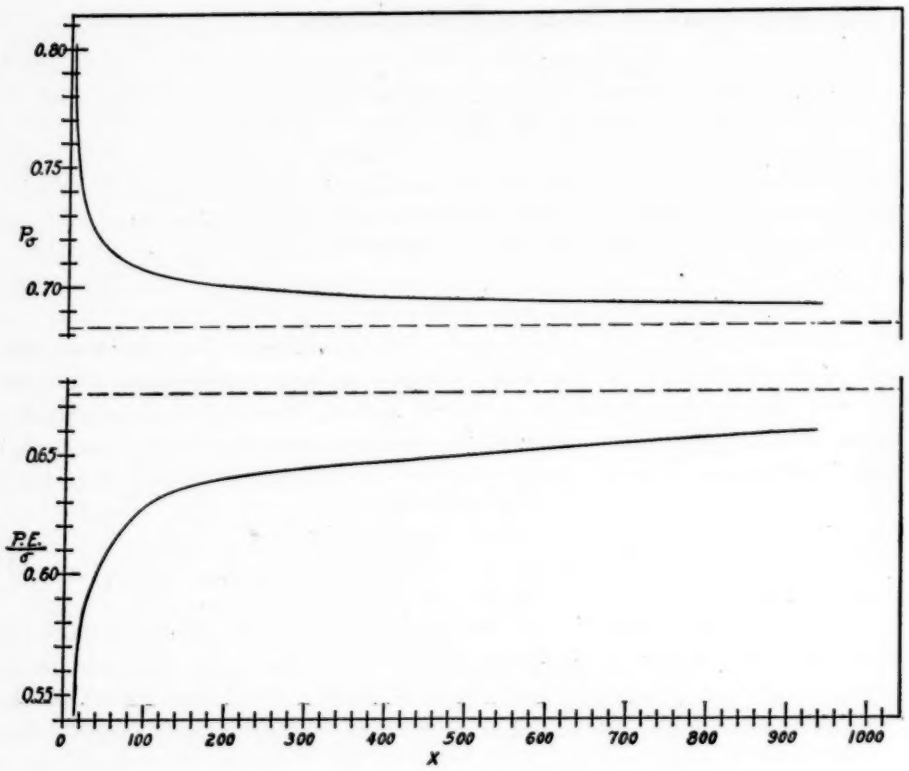

FIG. 1. The upper curve shows the manner in which the probability that a deviation not to exceed σ approaches 0.68269 as x becomes large. The lower curve shows the manner in which the ratio of probable error to σ approaches 0.67449 as x becomes large.

verges uniformly in the interval $-1 \leqslant k \leqslant +1$, and we may interchange the limit and integral sign.[1] This gives

$$P_\infty = \int_{-1}^{+1} \lim_{y\to\infty} \frac{(y^2)^{y^2+ky}}{(y^2+ky)!} e^{-y^2} y\,dk. \tag{6}$$

To evaluate the limit, we replace the factorial by the Stirling approximation and proceed as follows:

$$\lim_{y\to\infty} F(k, y) = \lim_{y\to\infty} \frac{(y^2)^{y^2+ky} e^{-y^2}}{(y^2+ky)^{y^2+ky} e^{-y^2-ky} [2\pi(y^2+ky)]^{\frac{1}{2}}},$$

$$\lim_{y\to\infty} \log F(k, y) = \lim_{y\to\infty} \left[\log \frac{1}{[2\pi(1+k/y)]^{\frac{1}{2}}} + ky + (y^2+ky) \log \frac{y}{y+k} \right]$$

$$= \lim_{y\to\infty} \left[\log \frac{1}{[2\pi(1+k/y)]^{\frac{1}{2}}} + ky + y(y+k)\left(-\frac{k}{y+k} - \frac{k^2}{2(y+k)^2} - \cdots \right) \right]$$

$$= \log \frac{1}{(2\pi)^{\frac{1}{2}}} - \frac{k^2}{2}$$

or

$$\lim_{y\to\infty} F(k, y) = \frac{1}{(2\pi)^{\frac{1}{2}}} e^{-k^2/2}.$$

Therefore

$$P_\infty = \frac{2}{(2\pi)^{\frac{1}{2}}} \int_0^1 e^{-k^2/2} dk = 0.68269, \tag{7}$$

which is just the probability that a deviation not exceed σ when the distribution is normal. This was to be expected because it is known that the Poisson distribution becomes more and more similar to the normal distribution as x becomes large.

We can now evaluate the limiting probability that a result not deviate from the average by more than $m\sigma$, where m is arbitrary. The same line of mathematical reasoning as above leads to the result

$$P_\infty = \left(\frac{2}{\pi}\right)^{\frac{1}{2}} \int_0^m e^{-k^2/2} dk, \tag{8}$$

which is just expression (7) with different limits of integration. If the integral in (8) be set equal

[1] See E. J. Townsend, *Functions of Real Variables* (Henry Holt and Co., 1928), pp. 122, 350, 360.

to 0.50, it is known that m must equal 0.67449. This means that in the limit, expression (1) gives the probable error when the distribution follows a Poisson formula.

In Fig. 1 the upper curve shows graphically how the probability that a deviation not exceed σ approaches 0.68269, and the lower curve shows how P.E./σ approaches 0.67449 as x becomes large. These curves were obtained by direct computation for small values of x, and by approximation methods for values of x greater than 1000. In both cases it is seen that the approach is rather rapid for small values of x. Also it is to be noted that, for finite values of x, P_σ is always greater than its limit while P.E./σ is always smaller than its limit. This means that the error committed in saying that P.E.$=0.67449\sigma$, or that committed in saying the probability that a single deviation not exceed σ is 0.68269 are both theoretically on the conservative side.

APRIL 15, 1940 PHYSICAL REVIEW VOLUME 57

Osmotic Diffusion in Gases

E. J. HELLUND
University of Washington, Seattle, Washington
(Received January 13, 1940)

The theory of diffusion induced in a "solvent" gas, by the pressure diffusion of two other gases, is developed on the basis of formulae derived in a previous paper by the author. The analysis is applied to the Loschmidt experiment and the pressures generated, are found analytically as a function of the time elapsed, from the onset of diffusion. All formulae are given in terms of the binary diffusion coefficients of the component gases.

INTRODUCTION

LIQUIDS and gases, because of the mobility of the molecules of each exhibit a series of closely allied phenomena. Particularly is this shown in the phenomenon of diffusion, and especially with respect to that class of diffusion associated with pressure gradients or external force fields. The latter seems intuitively to be the most understandable and has as a consequence yielded to the most elementary treatments, results which are astonishingly accurate. In other cases, however, notably in the case of thermal diffusion in gases and osmotic diffusion in liquids, elementary theories have been powerless to explain the experimental results. In the case of thermal diffusion in gases it was found necessary to develop the theory from a continuity equation, the foundations of which seem fairly secure. The kinetic theory of liquids, unfortunately, lacks any such rigorous attack and has, as a consequence, given no satisfactory interpretation of osmotic diffusion. It has therefore seemed of interest to examine the corresponding diffusion in gases even though qualitatively the phenomena in gases and liquids do possess essential differences which vitiates somewhat the attempt to establish a close correlation between the two.

Osmotic diffusion in liquids is said to occur when motion of a solvent through a semipermeable membrane takes place due to the action of a solute which cannot pass through the membrane. That is, three essential elements are present for the process to occur; a solvent, pervading the entire vessel; a substance dissolved in a portion of the solvent; and a substance which may be said to occlude the first solute from that portion of the solvent which the second solute occupies. The membrane here has been designated as a solute occupying a certain portion of the solvent, and having no effect on the solvent in which it exists. Physically this difference in point of view is immaterial, but formally it expresses more aptly the conditions to be expected for such diffusion to occur in gases.

One may then define osmotic diffusion in gases as that diffusion which would occur in a tube

pervaded by a gas of constant number density, (the solvent), due to the existence in the tube of two or more gases of varying concentration (solute), which would themselves diffuse because of their respective pressure gradients. More specifically one may expect in an experiment of the Loschmidt type, where a long tube is separated in the middle by a diaphragm, that if, initially, one gas pervades both sections with the same pressure, and if in addition two different gases are placed in the two sections, one on each side of the diaphragm, that diffusion of the first gas will occur when the diaphragm is removed. That is, a surge of the first gas will take place in a direction of the tube depending on the characteristics of the other two gases and their position in the vessel. The osmotic diffusion current may then be expressed as proportional to the number density gradient of either of the two gases of varying composition, and the constant of proportionality may be taken as the osmotic diffusion coefficient. Theoretically this coefficient was shown in a previous paper by the author,[1] to be expressible in terms of the binary diffusion coefficients, and the densities of all the gases in the mixture.

The Loschmidt experiment does not determine directly the osmotic diffusion coefficient since the results are necessarily complicated by pressure diffusion. Nevertheless, the observation of the maximum pressures generated, provides a cross check on the binary diffusion coefficients, as these pressures can be calculated in terms of these coefficients.

In the theory to follow, the results, as in the theory of the determination of the binary diffusion coefficients by the Loschmidt experiment, will be carried to that order of approximation which is deemed sufficient for the comparison with the experimental results.

The Equations of Continuity

In the following, for purposes of simplicity, only mixtures of gases containing three components will be considered. One finds for the continuity equation of the number densities, the result[2]

$$-kT\frac{\partial n_k}{\partial t}=\frac{\partial}{\partial x}\left[\frac{(\rho_i Z^k-\rho_k Z^i)}{\rho n\Delta}\left\{\frac{-1}{D_{ij}}-\frac{(\rho_k+\rho_i)}{m_k(n_k+n_i)D_{ki}}+\frac{\rho_i}{m_k(n_k+n_j)D_{kj}}\right\}\right]$$

$$+\frac{\partial}{\partial x}\left[\frac{(\rho_i Z^k-\rho_k Z^i)}{\rho n\Delta}\left\{-\frac{1}{D_{ij}}-\frac{(\rho_k+\rho_j)}{m_k(n_k+n_j)D_{kj}}+\frac{\rho_j}{m_k(n_k+n_i)D_{ki}}\right\}\right], \quad (1)$$

where $i\neq j\neq k$.

$$\Delta=\frac{1}{D_{12}D_{13}D_{32}}\cdot\frac{[n_1(n_2+n_3)D_{23}+n_2(n_3+n_1)D_{31}+n_3(n_1+n_2)D_{12}]}{(n_1+n_2)(n_1+n_3)(n_2+n_3)} \quad (2)$$

and

$$Z^j=\frac{\partial p^{(j)}}{\partial x}-\rho_j X_j;\quad n=\sum_1^3 n_i. \quad (3)$$

In the above equations, the X_j are the components of external force per unit mass acting in the x direction (only variations in the x direction are considered). The diffusion coefficients, also, are defined in terms of the particle currents, and are not to be confused with the mass coefficients employed in the paper previously cited. The coefficients appearing in (1) and (2) are thus, those which express the current moving past a stationary cross section of a constant pressure gas tube.

Let us now consider a tube of length "a" cm. A diaphragm divides the tube into two equal parts at a distance "a"/2 cm from each end. Initially gas "3" occupies both sections at the same density, and gas "1" occupies the left section and gas "2" the right section. Gas "3" thus is the solvent, and the object of the investigation is to determine the behavior of this component with time, after the diaphragm is removed. In the experiment a constant temperature will be assumed, and also the only external forces considered will be those at the walls of the tube.

[1] E. J. Hellund, Phys. Rev. **57**, 319 (1940).
[2] Reference 1, Eqs. (46) and (47).

Since the pressure is a constant throughout the tube, one has

$$n_1+n_2+n_3=n=\text{const}, \qquad (4a)$$

$$\frac{\partial n_1}{\partial x}+\frac{\partial n_2}{\partial x}+\frac{\partial n_3}{\partial x}=0, \qquad (4b)$$

which, inserted in (1), leads to the two simultaneous partial differential equations which describe the concentrations at any point of the tube, with the time.

$$-\frac{\partial n_3}{\partial t}=\frac{\partial}{\partial x}\left[\frac{\partial n_2}{\partial x}(n_3)\left\{\frac{1}{(n_3+n_1)D_{31}}-\frac{1}{(n_3+n_2)D_{32}}\right\}\frac{1}{n\Delta}\right]-\frac{\partial}{\partial x}\left[\frac{\partial n_3}{\partial x}\left\{\frac{1}{D_{12}}+\frac{n_3}{(n_3+n_2)D_{32}}\right\}\frac{1}{n\Delta}\right], \qquad (5)$$

$$-\frac{\partial n_2}{\partial t}=\frac{\partial}{\partial x}\left[\frac{\partial n_3}{\partial x}(n_2)\left\{\frac{1}{(n_1+n_2)D_{12}}-\frac{1}{(n_2+n_3)D_{32}}\right\}\frac{1}{n\Delta}\right]-\frac{\partial}{\partial x}\left[\frac{\partial n_2}{\partial x}\left\{\frac{1}{D_{31}}+\frac{n_2}{(n_2+n_3)D_{32}}\right\}\frac{1}{n\Delta}\right]. \qquad (6)$$

In (5), the coefficient of $\partial n_2/\partial x$ is thus the coefficient of osmotic diffusion and will be written,

$$D(1;3;2)=\left(\frac{n_3}{n}\right)\cdot\frac{D_{12}(n_1+n_2)\{(n_3+n_2)D_{32}-(n_3+n_1)D_{31}\}}{[n_1(n_2+n_3)D_{32}+n_2(n_3+n_1)D_{31}+n_3(n_1+n_2)D_{12}]}. \qquad (7)$$

Because of the character of the divisor, this coefficient is not necessarily constant for a constant total pressure and constant solvent density. The extent of the possible variation under the above conditions depends on the magnitudes of the various binary diffusion coefficients. Because of the positive character of all quantities appearing, and near equality of the D_{ij} the variation, however, is not large.

For times which are small one has approximately

$$-\partial n_3/\partial t=D(1;3;2)\partial^2 n_2/\partial x^2, \qquad (8)$$

$$-\partial n_2/\partial t=-D(2;1,3)\partial^2 n_2/\partial x^2, \qquad (9)$$

where

$$D(2;1,3)\equiv-\left\{\frac{1}{D_{31}}+\frac{n_2}{(n_2+n_3)D_{32}}\right\}\frac{1}{n\Delta}. \qquad (10)$$

In (9) the variability of the coefficient of $\partial n_2/\partial x$ has been ignored, and in (8) and (9) $\partial n_3/\partial x$ and $\partial^2 n_3/\partial x^2$ have been set equal to zero.

From (8) and (9) one obtains the result for n_3 that,

$$n_3(t)=n_3{}^0\exp\left[-\frac{1}{n_3}\left(\frac{D(1;3;2)}{D(2;1,3)}\right)n_2\right], \qquad 0<x<a/2; \quad t\to 0, \qquad (11)$$

where[3]

$$n_2=n_2{}^0-4\frac{n_2{}^0}{\pi}\sum_1^\infty\cos\left(\frac{n\pi x}{a}\right)\sin\left(\frac{n\pi}{2}\right)\exp\left[-D(2;1,3)t\left(\frac{n\pi}{a}\right)^2\right]. \qquad (12)$$

The superscript, 0, is used to denote the initial value of the quantity for $t=0$. Eq. (11) tells little that was not immediately apparent from elementary physical considerations. The changes in density of n_3 take place most quickly where n_2 changes most rapidly and remain constant for constant n_2 values. What is of greatest interest to the experimenter is not the variation of density throughout the tube, but the change in the total number of particles of a given kind in one section of the tube.

Because of the increasing seriousness of the approximations made in (8) and (9) one cannot use (11)

[3] Loeb, *Kinetic Theory of Gases* (McGraw-Hill, 1927), first edition, p. 233.

to obtain this information. One may, however, integrate Eqs. (5) and (6) directly as follows,

$$-\frac{\partial N_3}{\partial t}=\frac{\partial n_2}{\partial x}D(1;3;2)-\frac{\partial n_3}{\partial x}D(3;1,2), \tag{13}$$

$$-\frac{\partial N_2}{\partial t}=\frac{\partial n_3}{\partial x}D(1;2;3)-\frac{\partial n_2}{\partial x}D(2;1,3), \tag{14}$$

where large N denotes the total number of particles of a given kind in the tube between the limits $x=0$, $x=a/2$. On the right side of (12) all quantities are evaluated at the point $x=a/2$, the values at $x=0$, not appearing because of the boundary conditions that

$$\partial n_j/\partial x]_{x=0}=0. \tag{15}$$

Solution of the Continuity Equations

The relations expressed by (13) and (14) are exact and may be conveniently used to determine the functions N_3 and N_2. It is necessary however to transform, first, the partials of the densities, evaluated at $x=a/2$.

If one assumes a Fourier expansion

$$n_j=C_j^0(t)+\sum_{i=1}^{\infty}C_j^i(t)\cos\left(\frac{n\pi x}{a}\right), \tag{16}$$

satisfying the boundary conditions $\partial n_j/\partial x=0$ for $x=0$, or a, then one obtains, carrying only the first three terms of the series,

$$\frac{\partial n_j}{\partial x}\Big]_{x=a/2}=-\frac{\pi^2}{a^2}\{N_j-N_j]_{t=\infty}\}. \tag{17}$$

One has then, if variables $N_j-N_j]_{t=\infty}=N_j^*$ are introduced,

$$\frac{\partial N_3^*}{\partial t}=\frac{\pi^2}{a^2}[D(1;3;2)N_2^*-D(3;1,2)N_3^*], \tag{18a}$$

$$\frac{\partial N_2^*}{\partial t}=\frac{\pi^2}{a^2}[D(1;2;3)N_3^*-D(2;1,3)N_2^*]. \tag{18b}$$

One finds readily that the solutions, fitting the initial conditions are,

$$N_3^*=\frac{+2\Omega N_2]_{t=\infty}}{(\Phi^2-4\Omega\Psi)^{\frac{1}{2}}}\Big]_{t=0}\exp\left[\frac{-\pi^2}{2a^2}\int_0^t X\,dt\right]\sinh\left(\frac{\pi^2}{2a^2}\int_0^t(\Phi^2-4\Omega\Psi)^{\frac{1}{2}}dt+\delta\right), \tag{19}$$

$$N_2^*=-N_2\Big]_{t=\infty}\exp\left[-\frac{\pi^2}{2a^2}\int_0^t X\,dt\right]\cdot\sinh\left(\frac{\pi^2}{2a^2}\int_0^t(\Phi^2-4\Omega\Psi)^{\frac{1}{2}}dt+\delta\right), \tag{20}$$

$$\delta=\tanh^{-1}\left(\frac{(\Phi^2-4\Omega\Psi)^{\frac{1}{2}}}{\Phi}\right)\Big]_{t=0}, \tag{21}$$

where

$$\Phi=\frac{n_1}{(n)\Delta}\left(\frac{1}{(n_1+n_2)D_{12}}-\frac{1}{(n_1+n_3)D_{13}}\right)+\frac{n_2}{(n)\Delta}\left(\frac{1}{(n_1+n_2)D_{12}}-\frac{1}{(n_2+n_3)D_{23}}\right)$$
$$+\frac{n_3}{(n)\Delta}\left(\frac{1}{(n_2+n_3)D_{23}}-\frac{1}{(n_3+n_1)(D_{31})}\right), \tag{22a}$$

$$X=\left\{\frac{1}{D_{12}}+\frac{1}{D_{31}}+\frac{1}{D_{23}}\right\}\Big/(n)\Delta, \tag{22b}$$

$$\Psi=\frac{n_2}{(n)\Delta}\left\{\frac{1}{(n_1+n_2)D_{12}}-\frac{1}{(n_2+n_3)D_{32}}\right\}, \tag{22c}$$

$$\Omega=\frac{n_3}{(n)\Delta}\left\{\frac{1}{(n_3+n_2)D_{32}}-\frac{1}{(n_3+n_1)D_{31}}\right\}. \tag{22d}$$

Remembering that these functions are all evaluated at $x=a/2$ and hence are not strongly dependent on the time, one effected the integrations by multiplying the integrands (evaluated for $t=\infty$), by the elapsed time. For the binary diffusion case such an assumption is in fact exact, but in our case variations in time do occur. However even these variations are not appreciably effective, because of the character of the integrands, and the condition that $n=n_1+n_2+n_3=$constant.

Discussion of the Solutions

In view of the observations following (22), we shall use the following approximations for $N_3(t)$ and $N_2(t)$,

$$N_3(t)=N_3]_{t=\infty}+\frac{2\Omega N_2]_{t=\infty}}{(\Phi^2-4\Omega\Psi)^{\frac{1}{2}}}\exp\left[\frac{-\pi^2}{2a^2}(X)(t)\right]\cdot\sinh\left\{\frac{\pi^2}{2a^2}(\Phi^2-4\Omega\Psi)^{\frac{1}{2}}t\right\}, \tag{23}$$

$$N_2(t)=N_2]_{t=\infty}\left\{1-\exp\left[-\frac{\pi^2}{2a^2}(X)t\right]\cdot\sinh\left\{\frac{\pi^2}{2a^2}(\Phi^2-4\Omega\Psi)^{\frac{1}{2}}t+\delta\right\}\right\}, \tag{24}$$

$$\delta=\tanh^{-1}\{(\Phi^2-4\Omega\Psi)^{\frac{1}{2}}/\Phi\}, \tag{25}$$

where in the above equations Φ, Ψ, X, and Ω are all evaluated at $t=\infty$. It may be easily shown that in the case of vanishing interaction between gases "3" and "1" and "3" and "2" that the solution (24) becomes

$$N_2=N_2]_{t=\infty}(1-\exp[-(\pi^2/a^2)D_{12}t]). \tag{26}$$

This compares with the exact series, derivable from (12),

$$N_2=N_2]_{t=\infty}\left\{1-\frac{8}{\pi^2}\left(\exp\left[-D_{12}\frac{\pi^2}{a^2}t\right]+\frac{1}{9}\exp\left[-D_{12}\frac{9\pi^2}{a^2}t\right]+\cdots\right)\right\}. \tag{27}$$

In practise only three terms of the summation in (27) are employed, so that initially this expansion is unacceptable whereas (26) has been made to fit this boundary condition. On the other hand, for long elapsed times, the second term of (26) is in error by approximately 20 percent when compared to the summation in (27). The source of this discrepancy is to be found in the approximation (17) for very short times after the diaphragm has been removed. One could improve the agreement by using (11) and (12) for short intervals and then joining to the solutions of (18a) and (18b). The gain in accuracy would not seem to compensate for the increased complication in the resulting solutions.

Inasmuch as the initial high density gradients make doubtful the applicability of the diffusion equation for small elapsed times, it would seem more logical to determine N_2 and N_3 experimentally at some later time, say, τ. Then the solutions for subsequent times could be determined by evaluating the arbitrary constants for $t=\tau$. For moderate values of τ error by this method becomes negligible. In connection with the above, it is perhaps of importance to point out that physically the Loschmidt experiment

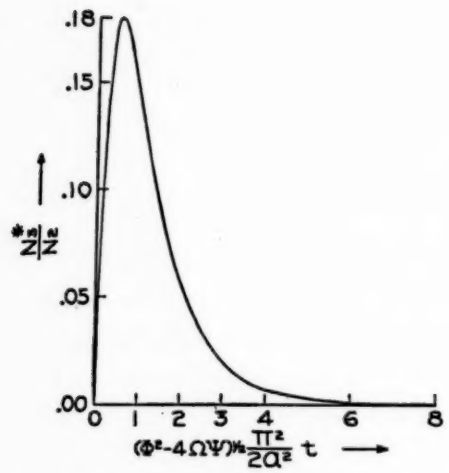

FIG. 1. Plot of the CO pressure variation, in the section from $x=0$ to $a/2$, as a function of the elapsed time.

must always introduce some uncertainty in regard to the initial conditions by virtue of the nature of the diaphragm itself and of its manner of removal.

If then one solves (18a) and (18b) in this manner the resulting expression for N_3 (and for N_2) is materially altered. The equations which correspond to the group (23), (24), and (25), together with the results derived from them may be obtained quite easily and hence will not be given here.

Returning to Eq. (23), one may evaluate the maximum pressures generated by gas "3." The result is,

$$P_{3,\max}=P_3]_{t=\infty}+\frac{2\Omega P_2]_{t=\infty}}{X+\Phi'}\left(\frac{X-\Phi'}{X+\Phi'}\right)^{(X-\Phi')/2\Phi'}, \quad (28)$$

where $\Phi'=(\Phi^2-4\Omega\psi)^{\frac{1}{2}}$. The time at which this occurs is

$$t_{\max}=\frac{a^2}{\pi^2}\Phi' \log\frac{X+\Phi'}{X-\Phi'}. \quad (29)$$

The pressures P_3 are those for a uniform distribution of n_3 from $x=0$ to $a/2$. It may be noticed that Ω is itself proportional to P_3. By the conditions assumed initially, n_2 and n_3 are equal, and thus the apparent lack of symmetry in (28) is spurious. The second term of (28) will vanish likewise if the cross section of gases "1" and "2" and their masses are equal. The osmotic pressures thus depend, as does thermal diffusion, on the differences in the properties of two gases. Such phenomena are of infrequent occurrence and of great importance in the determination of force interactions between molecules.

NUMERICAL RESULTS

The variations of the osmotic pressure with time were calculated for a mixture of H_2, CH_4, and CO_2 which were numbered in the order given to correspond to the previous theory. Thus CO_2 was taken to be the solvent gas in the above. The number densities were set equal to one another and of such a magnitude that the total pressure was 114 cm Hg. The temperature used was 0° centigrade. For the above conditions, then, experimental values of the various binary diffusion coefficients are: $D_{12}=0.625$; $D_{13}=0.538$; and $D_{23}=0.153$. For these values one finds $N_3^*/N_2]_{\max}=0.179$ which is equivalent to a pressure of 6.82 cm Hg. Also one finds in this case that: $\Phi=-0.0135$, $X=+0.521$, $\Psi\equiv D(1;2;3)=-0.129$, $\Omega\equiv D(2;3;1)=+0.122$, $(\Phi^2-4\Omega\Psi)^{\frac{1}{2}}=0.251$, and $t\Pi^2/a^2]_{\max}=4.18$.

SUMMARY

The continuity equation of a mixture of three gases has been solved by approximate methods for the case where the distribution of one of the gases of the mixture is initially uniform. It is pointed out in connection with the solutions, with respect to the space-wise distribution, that the diffusion coefficient is not a constant and that the neglect of the composition dependence over considerable time intervals is not justified. First order solutions are obtained for the pressure surges of the "solvent" gas in the Loschmidt apparatus and the results (Fig. 1) plotted for a CO_2, H_2, CH_4 mixture. In connection with the maximum pressures generated in the "solvent" gas of a ternary mixture it is possible to show from (28) that if gases "3," "2," "1" (by cyclic permutation of all three) are successively the solvent gases for the same partial pressures (i.e., $P_1=P_2=P_3=\frac{1}{3}P$), that the successive maximum pressure differences occur in the ratios, $D(2;3;1):D(3;1;2):D(1;2;3)$ and that their sum vanishes identically.

Isotope Separation by Transient Pressure Diffusion

E. J. HELLUND
University of Washington, Seattle, Washington
(Received February 9, 1940)

The separation of molecules of nearly equal masses is investigated in connection with the Loschmidt experiment. The results are obtained by a perturbation treatment of the continuity equations for a ternary mixture.

VARIOUS means have been employed in the separation of particles of nearly equal masses and effectively identical cross sections. Many of these depend on diffusion processes, which operate by virtue of the dependence of the velocity of migration on the mass of the particle in question. Most effective of these have been methods utilizing the diffusion through a porous solid. The advantage in the latter has been that the operation could be made continuous (e.g., the Hertz apparatus). Frequently, however, these methods operate discontinuously, requiring repetition after the attainment of an equilibrium state in which the separation is a maximum.

Pressure diffusion, of gases alone, has been used in the ultracentrifuge wherein the high fields produced are balanced by opposite pressure gradients. In the equilibrium state no diffusion current exists and the separation depends in no way on the cross sections of the molecules of the mixture, no matter how many components there are.

In the method to be described in the present paper the separation is dependent on the existence of a third gas and one finds a dependence on the cross sections as well as the masses. In this respect it differs from most other methods of separation. The theory is based on the solution of the continuity equations of a ternary mixture, derived in a previous paper by the author.[1]

If one denotes the particle currents of molecules of type "i" by $J_n{}^i$, the continuity equations for a ternary mixture are[2]

$$J_n{}^3=\frac{\partial n_2}{\partial x}n_2\left\{\frac{1}{\beta_{13}}-\frac{1}{\beta_{32}}\right\}\Big/n\Delta - \frac{\partial n_3}{\partial x}\left\{\frac{n-n_3}{\beta_{12}}+\frac{n_3}{\beta_{32}}\right\}\Big/n\Delta, \quad (1)$$

$$J_n{}^2=\frac{\partial n_3}{\partial x}n_2\left\{\frac{1}{\beta_{12}}-\frac{1}{\beta_{23}}\right\}\Big/n\Delta - \frac{\partial n_2}{\partial x}\left\{\frac{n-n_2}{\beta_{13}}+\frac{n_2}{\beta_{32}}\right\}\Big/n\Delta, \quad (2)$$

where

$$\beta_{ij}=(n_i+n_j)D_{ij}, \quad (3)$$

$$\Delta=\left(\frac{n_1\beta_{23}+n_2\beta_{13}+n_3\beta_{12}}{\beta_{12}\beta_{13}\beta_{23}}\right). \quad (4)$$

In (1) and (2) the condition of constant total pressure has been used to eliminate the gradients of pressure of particles of type "1." Gases "3" and "2" in the following are to be treated as the isotope mixture which tends to separate under the influence of the diffusion of gas "1."

The initial conditions of the experiment are that the mixture "23" is contained in the "left" half of a long tube of length "a" cm, and that gas "1" is contained in the right half. The diaphragm which separates the two is removed and the resulting diffusion will partially separate "2" and "3," the amount depending on the various coefficients of diffusion.

If then β_{12} and β_{13} are assumed to differ by a small fraction of their values, one may consider that the solutions of (1) and (2) approximate closely the solutions obtained by assuming the mixture to diffuse as a simple gas. The diffusion coefficient of the mixture then would lie between the values for each isotope. The exact combination to be used could be determined by requiring that the perturbation of (1) and (2) vanish if β_{23} were zero. It may be shown that this would give for the "zero-order" diffusion coefficient of the mixture the value,

$$D=\left(\frac{n_2\beta_{12}+n_3\beta_{13}}{n_2+n_3}\right)\Big/n. \quad (5)$$

Let us define further,

$$D^*=\beta_{23}/n. \quad (6)$$

[1] E. J. Hellund, Phys. Rev. **57**, 319 (1940).
[2] E. J. Hellund, "Osmotic diffusion in gases" (Phys. Rev. this issue).

Now the perturbations δn_2 and δn_3 must satisfy the same boundary conditions as n_2 and n_3 and moreover vanish for $t=0, \infty$. In view of this the following approximation[2] may be made,

$$\frac{\partial(\delta n_i)}{\partial x}\Big]_{x=a/2} = -\frac{\pi^2}{a^2}\Big[\int_0^{a/2} \delta n_i dx\Big]. \quad (7)$$

Then one obtains from (1) and (2) two simultaneous linear ordinary differential equations for

$$\epsilon_2 = \int_0^{a/2} \delta n_2 dx \quad \text{and} \quad \epsilon_1 = \int_0^{a/2} \delta n_3 dx,$$

$$d\epsilon_1/dt = a_1\epsilon_1 + b_1\epsilon_2 + c_1, \quad (8)$$

$$d\epsilon_2/dt = a_2\epsilon_1 + b_2\epsilon_2 + c_2. \quad (9)$$

The coefficients a, b in (8) and (9) are dependent on the concentrations of gases "2" and "3" and the coefficients of diffusion D and D^*. The C_1 and C_2 terms are likewise dependent on these variables and proportional in addition to the pressure gradient of gas "1" evaluated at $x=a/2$. The result of the diffusion, initially, is that the mixture "2,3" diffusing into gas "1" has its concentration changed from λ, $[\lambda = n_2/(n_2+n_3)]$, by the amount .

$$2\lambda(1-\lambda)\frac{D^*}{D^*+D}\left(\frac{\Delta D}{D}\right), \quad (10)$$

where ΔD is the difference between the coefficients of diffusion of the mixture "3,1" and the mixture "1,2."

In the time $t=a^2/\pi^2 D$ the expression (10) changes by the factor $8/(e\pi^2-8)$, or approximately $\frac{1}{2}$.

It is interesting to apply this result to the diffusion of H_2 into air, which may be taken as N_2 (80 percent), O_2 (20 percent). The change in concentration of the diffusing air, assuming a difference of one part in 200 for the diffusion of N_2 and O_2 into H_2 would be of the order of 1/2000.

Thus the air mixture diffuses in this case effectively as a simple gas. However, when the gas "1" is not light, the change may be much greater as, if the H_2 should be replaced by some gas of large molecular weight and cross section, the change in the separation may be increased by a factor of 60 or 70.

An alternative method of separation of isotopes employing the action of a third gas would be to place the isotope mixture in a tube closed at both ends by porous plugs which would be impervious to the isotope mixture, but permit the passage of some other gas which could therefore be pumped through. The separation in this case would increase with the increase in the diffusion current.

APRIL 15, 1940 PHYSICAL REVIEW VOLUME 57

Note on Grüneisen's Constant for the Incompressible Metals

J. C. SLATER
Department of Physics, Massachusetts Institute of Technology, Cambridge, Massachusetts

(Received February 19, 1940)

Grüneisen's constant γ can be determined in terms of the thermal expansion, compressibility, and specific heat, as originally shown by Grüneisen. It can also be found from the compressibility and change of compressibility with pressure. Theoretically the two methods should give approximately the same result. This has proved to be the case experimentally, except for the more incompressible metals, where the discrepancies have been very great. Bridgman has now redetermined the change of compressibility of iron with pressure, obtaining a much smaller value than before, and as iron was used as a standard, this brings about a revision of other changes of compressibility with pressure, largest in proportion for the incompressible metals, whose volume change is about the same as for iron. It is shown that this revision is just enough to bring the two methods of finding γ into agreement, for practically all the metals.

IF the frequencies of vibration of the normal modes of a crystal all vary as the inverse γ power of the volume, then it can be shown that there is a relation

$$\frac{(\text{thermal expansion})\times(\text{volume})}{(\text{compressibility})\times(C_V)} = \gamma. \quad (1)$$

This relation is due to Grüneisen,[1] and γ is often called Grüneisen's constant. By means of the relation (1), experimental values of γ can be found, and for most simple solids they lie between

[1] For discussion of this relation, see for instance J. C. Slater, *Introduction to Chemical Physics* (McGraw-Hill, 1939), Chapter XIII, Section 4.

1.5 and 2.5. In addition to (1), there is another quite different connection between γ and experiment. This arises from the fact that the natural frequencies can be computed from the elastic constants, in particular from the compressibility. The constant γ depends essentially on the change of frequency with volume, and hence on the change of compressibility with pressure. As a result of this, a value for γ can be computed from Bridgman's measurements of compressibility and its change with pressure. For many ionic crystals, and for the more compressible metals, the values computed in this way agree well with those found from Eq. (1), giving valuable verification of the theory, and a useful relation between experimental quantities, which could be used to find the thermal expansion from the change of compressibility with pressure, or vice versa. For the less compressible metals, however, the agreement is very poor, and to get better agreement, the change of compressibility with pressure should be considerably smaller (in the case of the least compressible metals several times smaller) than found by Bridgman.[2]

Bridgman[3] has now redetermined the change of compressibility of iron with pressure, obtaining a value only about a third as large as the previously measured value. This is important for all the other measurements, for iron is used as a standard, and the measurements on other elements give really the difference between the change of volume of the element in question and iron. For the compressible metals, and the ionic crystals, the change of compressibility with pressure is so much greater than that of iron that a change in the value for iron makes only a small correction in the result, but a number of the metals of the transition groups have changes of compressibility with pressure of the same order of magnitude as iron, and for these the new measurements make a very great difference. It is the purpose of this note to point out that Bridgman's new measurements for iron entirely remove the discrepancy between the two methods of determining γ for this element; and that if the old measurements of change of compressibility with pressure for other incompressible metals are corrected by using the new results for iron, they likewise fall into line, with one or two exceptions.

Bridgman's[4] experimental results are stated in the form

$$\Delta V/V_0 = -a_1P + a_2P^2, \tag{2}$$

where ΔV is the change in volume, V_0 the original volume, P the pressure, a_1 and a_2 constants at a given temperature. For iron, at 30°C, he found in 1923 $a_1 = 5.87\times10^{-7}$, $a_2 = 2.1\times10^{-12}$, where the pressure is expressed in kilograms per square centimeter. In the new paper, the change of lengths rather than that of volume is given, but when the change of volume is computed from it (taking account of the fact that in the term in P^2 we cannot simply multiply by 3, but must cube the length to find the volume), we find $a_1 = 5.83\times10^{-7}$, $a_2 = 0.80\times10^{-12}$. That is, the value of a_1 is decreased by 0.04×10^{-7}, and that of a_2 decreased by 1.30×10^{-12}. It is not hard to show that, to the accuracy with which the measurements are made, the measured values of a_1 and a_2 for other metals are to be corrected by subtracting equal amounts from them. In this way, we have obtained corrected values from the observed values of reference 4.

It is now easy to show[5] that γ can be found in terms of a_1 and a_2 by the equation

$$\gamma = a_2/a_1^2 - \tfrac{2}{3}. \tag{3}$$

In Table I we give values of a_1 and a_2 as originally found by Bridgman,[4] for most of the metals for which the most serious discrepancies existed, and the values of γ computed from them by Eq. (3); next we give revised values of a_1 and a_2, as described in the preceding paragraph, with

[2] For comments on this, see N. F. Mott and H. Jones, *Properties of Metals and Alloys* (Oxford, 1936), Chapter I, Section 4. Comparisons of the two methods of determining γ are given in Slater, reference 1, Chapter XXIII, Section 4, for the alkali halides; and Chapter XXVII, Section 2, for metals.

[3] P. W. Bridgman, Phys. Rev. **57**, 235 (1940).

[4] P. W. Bridgman, Proc. Am. Acad. Arts and Sci. **58**, 165 (1923), for most of the metals mentioned in the present note.

[5] See Slater, reference 1, Chapter XIII, Section 1; and Chapter XIV, Section 4. In Chapter XIII, Eq. (1.1), (1.4), etc., neglect a_0, which represents the thermal change of volume. Then a_1, a_2 of the present paper become identical with the quantities defined in that chapter. In Eq. (4.6), Chapter XIV, it is shown that $\gamma = -\frac{2}{3} + P_2/P_1$. In Eq. (1.10), Chapter XIII, neglecting a_0, it is shown that $P_1 = 1/a_1$, $P_2 = a_2/a_1^3$. From these the result of Eq. (3) of the present paper follows at once. This result does not agree with Eq. (42) of Mott and Jones (reference 2) which in our present notation is $\gamma = a_2/a_1^2 - \frac{1}{3}$, or $\frac{1}{3}$ unit greater than our value. We believe Mott and Jones to be wrong, for they have incorrectly defined the compressibility as $-(1/V_0)(\partial V/\partial P)_T$, rather than $-(1/V)(\partial V/\partial P)_T$, and have thus lost a term coming from the change of V with volume, leading to the difference between the formulas.

TABLE I. *Original and revised values of a_1, a_2, and γ. Data for a_1 and a_2 are from Bridgman, reference 4. Values of γ by Grüneisen's method [$\gamma(Gr)$] are from the article by Grüneisen, "Zustand des festen Körpers," in Handbuch der Physik, Vol. X (Springer, 1926).*

METAL	$a_1\times10^7$ (OLD)	$a_2\times10^{12}$ (OLD)	γ (OLD)	$a_1\times10^7$ (REV.)	$a_2\times10^{12}$ (REV.)	γ (REV.)	γ (GR)
Fe	5.87	2.1	5.4	5.83	0.80	1.68	1.60
Co	5.39	2.1	6.6	5.35	0.8	2.1	1.87
Ni	5.29	2.1	6.9	5.25	0.8	2.2	1.88
Cu	7.19	2.6	4.4	7.15	1.3	1.9	1.96
Pd	5.19	2.1	7.1	5.15	0.8	2.4	2.23
Ag	9.87	4.4	3.8	9.83	3.1	2.5	2.40
W	2.93	1.5	17.	2.89	0.2	1.7	1.62
Pt	3.60	1.8	13.	3.56	0.5	3.3	2.54

a corresponding revised γ; finally we give values of γ computed by Grüneisen's relation, Eq. (1). It is plain from the table that the revision has completely removed the discrepancies between the old computed values of γ and Grüneisen's values of that quantity. The agreement between the revised γ's and Grüneisen's is within the experimental error of the a_2's, which are only known to a very rough approximation. We must remember in connection with this that an exact agreement is not required by the theory. It would be expected only if all natural frequencies of the solid varied in the same ratio with change of volume, and if the change of frequency with volume arose only from the change of compressibility, and not from a possible change in Poisson's ratio. Neither of these conditions is likely to be exactly fulfilled, so that the two methods of calculating γ may well differ by as much as the observed amounts.

For the more compressible metals, the revised values of a_2 lead to only a small change in γ, so that the agreement is not essentially changed from the values given in Table XXVII-2.[1] There are a few incompressible metals, however, for which there are outstanding discrepancies. For manganese, Bridgman[6] finds $a_1=7.91\times10^{-7}$, $a_2=5.3\times10^{-12}$; corrected values would be $a_1=7.87\times10^{-7}$, $a_2=4.0\times10^{-12}$, from which $\gamma=5.8$. Grüneisen's value is 2.42. Since this discrepancy is so much larger than for other metals, there is good reason to suspect that Bridgman's value of a_2 is considerably too large. This is perhaps explained by the fact that he states that it is very difficult to get manganese without small cracks, on account of a polymorphic transition; a cracked specimen would show an apparently high value of a_2. For molybdenum and tantalum, there are discrepancies in the opposite direction. Bridgman finds a_2 equal, respectively, to 1.2×10^{-12} and 0.25×10^{-12} for these metals. Making our correction of subtracting 1.3×10^{-12} would give negative values of a_2. This seems most implausible on general grounds, so that the observations for these two metals are certainly to be questioned. Finally for gold he used two samples, one giving $a_2=2.1\times10^{-12}$, the other 3.1×10^{-12}. These lead to $\gamma=1.8$ and 4.8, respectively, against Grüneisen's value of 3.03. Evidently the order of magnitude is right, but the discrepancies between the two observations are so great as to throw a good deal of doubt on the accuracy of the measurements. A remeasurement of these doubtful metals, if not of all the incompressible ones, would be very desirable. Since it appears as a result of the present note that Grüneisen's relation is really rather generally satisfied, it would be justified in future measurements to question any values of change of compressibility with pressure which disagree with it violently. For convenience, we may note that for most materials $\gamma+\frac{2}{3}$ is in the neighborhood of 2.5. Thus, from Eq. (3), we may expect that approximately

$$a_2=2.5a_1^2. \tag{4}$$

This relation should be expected to give the quadratic term in the volume change, in terms of the linear term, with an error of usually not over fifteen or twenty percent.

[6] P. W. Bridgman, Proc. Am. Acad. Arts and Sci. **64**, 51 (1929).

LETTERS TO THE EDITOR

Prompt publication of brief reports of important discoveries in physics may be secured by addressing them to this department. Closing dates for this department are, for the first issue of the month, the eighteenth of the preceding month, for the second issue, the third of the month. Because of the late closing dates for the section no proof can be shown to authors. The Board of Editors does not hold itself responsible for the opinions expressed by the correspondents.

Communications should not in general exceed 600 words in length.

Cross Section of the Reaction $N^{15}(p,\alpha)C^{12}$

Of the four reactions in the "carbon cycle" which is assumed to supply the energy in ordinary stars,[1] the three $p-\gamma$ reactions have been investigated and their cross sections measured. The reaction $C^{12}(p,\gamma)N^{13}$ has been studied by Roberts and Heydenburg,[2] $C^{13}(p,\gamma)N^{14}$ by Dee, Curran and Petržílka,[3] and $N^{14}(p,\gamma)O^{15}$ by Curran and Struthers.[4]

This letter is a report of the measurement of the last reaction of the cycle;[5] *viz.*, $N^{15}(p,\alpha)C^{12}$. The experimental arrangements were the same as used in the previously reported work on the deuteron disintegration of nitrogen.[6] The protons striking the aluminum foil separating the target gas from the cyclotron tank had an energy of 0.70_8 Mev. According to the measurements of Parkinson, Herb, Bellamy and Hudson[7] the stopping power of aluminum for protons between 0.7 and 0.4 Mev is about 8 percent less than for Po alphas which were used for calibrating the foils. Therefore the foil used, of 0.86_8 cm air equivalent according to the calibration, had an actual equivalent of 0.80 cm air (15°C, 760 mm). The target of 30 percent N^{14} and 70 percent N^{15} had a thickness of 0.046 cm of air at 0°C, 760 mm Hg. The energy of the protons in the center of the target chamber was then 0.36 Mev. The ionization chamber with a collimating face subtended 0.0088 steradians of the total solid angle about the target volume.

In order to be certain that the $N^{15}(p,\alpha)C^{12}$ reaction was the one taking place the range of the alphas was measured and found to be 2.5_7 cm (15°C, 760 mm). The range to be expected from the Q value, 4.79 Mev, calculated from mass values is 2.37 cm. From the Q value observed by Burcham and Smith,[5] *viz.*, 5.00 Mev, a range of 2.50 cm would be expected. This is a sufficiently good check considering the uncertainty in the value for the proton energy. A target of N^{14} alone gave no alphas. This last fact and the reasonable check of the range make it virtually certain that the alphas came from the $N^{15}(p,\alpha)C^{12}$ reaction.

The yield was obtained by taking a number distance curve with a thyratron bias low enough to count all alpha-particles having 3 mm or more of their range in the ionization chamber. The current of protons ($\sim 0.3\mu a$) striking the target was integrated by means of a circuit described by Herb, Kerst and McKibben.[8] The total yield in 4π solid angle was 2.3×10^{-8} alpha per proton at 0.36 Mev with a target containing 3.78×10^{19} N^{15} atoms/cm^3 at 0°C, 760 mm Hg and 0.046 cm thick (air equivalent at 0°C, 760 mm). From these figures the cross section of the $N^{15}(p,\alpha)C^{12}$ reaction is calculated to be 1.3×10^{-26} cm^2 at 0.36 Mev.

Theoretically, we may safely assume that the p,α reaction is by far the most probable reaction which can be caused by the collision of a proton with N^{15}. Then its cross section should be[9]

$$\sigma = \pi\lambda\!\!\!^{-2} 2\pi\kappa b e^{-2G} S, \qquad (1)$$

where $\lambda\!\!\!^{-}$ is the wave-length of the incident protons, κ the absolute value of its "wave number" at the surface of the nucleus, b the range of the nuclear forces, e^{-2G} the Gamow penetrability factor, and S a factor taking into account the effect of orbital momenta different from zero. For 0.36 Mev, we have $\lambda\!\!\!^{-}=7.6\times10^{-13}$ cm, $2\pi\kappa b=1.7_8$ and $e^{2G}=430$, assuming a nuclear radius $R=1.5\times10^{-13}\times16^{\frac{1}{3}}=3.8\times10^{-13}$ cm which corresponds to a barrier height of 2.6 Mev. S can be calculated from the rules given by Bethe[10] and comes out about 1.25. Therefore the theoretical cross section from (1) is 0.9×10^{-26} cm^2, in very satisfactory agreement with the rather rough experimental value.

For a comparison with other astrophysical reactions, it may be most convenient to calculate the "effective width" Γ used in reference 1 Eq. (11). From the measured cross section we obtain $\Gamma=1.0\times10^7$ ev which classes $N^{15}(p,\alpha)C^{12}$ among the most probable nuclear reactions. The lifetime of a N^{15} nucleus at the center of the sun is then only about 20 years, provided no resonance effects influence the cross section. Moreover, the branching ratio between the reactions $N^{15}(p,\alpha)C^{12}$ and $N^{15}(p,\gamma)O^{16}$ is probably of the order 10^6 rather than 10^4 as assumed in reference 1 (p. 446), which means that in each completed carbon cycle only about one nucleus in a million is lost to the cycle. An account of the astrophysical consequences will be published in the *Astrophysical Journal*.

We wish to thank Professor H. C. Urey for the sample of N^{15} gas.

M. G. HOLLOWAY
H. A. BETHE

Department of Physics,
Cornell University,
Ithaca, New York,
March 13, 1940.

[1] H. A. Bethe, Phys. Rev. **55**, 434 (1939).
[2] R. B. Roberts and N. P. Heydenburg, Phys. Rev. **53**, 374 (1938).
[3] P. I. Dee, S. C. Curran and V. Petržílka, Nature **141**, 642 (1938).
[4] S. C. Curran and J. E. Struthers, Nature **145**, 224 (1940).
[5] This reaction was reported, but no cross section measured by Burcham and Smith, Nature **143**, 795 (1939).
[6] M. G. Holloway and B. L. Moore, Phys. Rev. **56**, 705 (1939).
[7] D. B. Parkinson, R. G. Herb, J. C. Bellamy and C. M. Hudson, Phys. Rev. **52**, 75 (1937).
[8] R. G. Herb, D. W. Kerst, and J. L. McKibben, Phys. Rev. **51**, 691 (1937).
[9] H. A. Bethe, a continuum theory of the compound nucleus, to appear shortly in the *Physical Review*.
[10] H. A. Bethe, Rev. Mod. Phys. **9**, 178 (1937).

Further Experiments on Fission of Separated Uranium Isotopes*

Recently[1] we bombarded with slow neutrons small quantities of uranium isotopes which had been separated by means of a mass spectrometer. Measurement of the fission rates from the samples gave strong support to the view that it is U^{235} (or possibly U^{234}) rather than U^{238} which undergoes fission under slow neutron bombardment.

This conclusion has now been verified with considerably larger samples of separated uranium isotopes. In addition, it has been possible to obtain tests of several samples of partially separated U^{235} and U^{234}. In the new work the uranium ion currents were increased by a factor of about ten times by increasing the electron current bombarding the UBr_4 vapor by a factor of ten. The U^{238} ions were collected on an insulated platinum plate (1×15 mm) and the current to this plate measured with an electrometer tube amplifier. The U^{235} and U^{234} ions were collected in the first set of samples on a single grounded platinum plate and in the second set on a pair of grounded plates. The dispersion of the apparatus is such that for infinitely great resolving power, ions differing in mass by one unit would fall along sharp parallel lines on the collector separated by 0.75 mm. From a measure of the variation of the current to the insulated collector with energy of ions, it was possible to determine the actual spread of the ion beam and hence the overlap of adjacent isotopes. It was concluded that for a region 0.75 mm wide, centered about the U^{234} position, one would collect approximately 25 percent as many U^{235} ions as in an equally wide strip centered about the U^{235} position. As the ion peaks are nearly symmetrical the converse also holds. That the resolution was good enough to separate U^{234} and U^{235} was not apparent in the earlier work as the insulated collection plate was considerably wider (2.0 mm).

Slow neutron tests.—The separated isotopes were first tested by placing in an ionization chamber connected to a linear amplifier, and bombarding with neutrons from the Columbia cyclotron which had been slowed in paraffin.

TABLE I. *Slow neutron tests of separated* U^{238}, U^{235} *and* U^{234}.

	U^{238}	U^{235}	U^{234}
Sample set No. 1: Mass $U^{238}=3.1\mu g$			
alphas/min. expected	1.1	0.05	1.1
alphas/min. observed	1.0±0.1	0.25±0.05	0.75±0.1
fissions/min.	0.1±0.1	4.4 ±0.2	1.5 ±0.1
fission/alpha ratio	0.1	18.	2.
Sample Set No. 2: Mass $U^{238}=4.4\mu g$*			
alphas/min. expected	1.6	0.07	1.6
alphas/min. observed	2.3±0.1	0.63±0.1	2.2±0.2
fissions/min.	0.5±0.2	10.3 ±0.5	7.8±0.5
fission/alpha ratio	0.22	16.	3.5

* Considerable difficulty in obtaining large ion currents was encountered in this run. As a result, a great deal of testing and adjustment was necessary. Unfortunately, no record of the time or currents was kept while adjustments were being made. The mass of the U^{238} target was thus larger than 4.4μg. This would account for a good share of the discrepancy between the expected and observed alpha-counts. The resolution of the apparatus was definitely poorer in this run than the number one run.

TABLE II. *Fast neutron tests of separated* U^{238}.

	U^{238} No. 2	U^{238} No. 3
alphas/min.	2.3±0.1	5.5±0.2
fissions/min. without Cd	0.5±0.1	1.4±0.2
fissions/min. with Cd	0.5±0.1	1.4±0.2

For the first set of samples, where the U^{234} and U^{238} were deposited on the same plate with some overlapping, the alpha-particle and fission counts were made by covering each of the sample regions in turn with aluminum foil 0.008 cm thick.

Table I shows (*a*) the number of alpha-particles/min. to be expected on the basis of the masses of the uranium isotopes deposited as calculated from the mass spectrometer ion currents assuming complete separation, (*b*) the observed number of alpha-particles/min., (*c*) the number of fissions/min., and (*d*) the fission/alpha-ratio, for the various isotope samples. The background has been subtracted.

The number of alpha-particles/min. observed is in agreement with the expected number within the limits of error. The amount of overlapping of U^{234} and U^{235} is likewise close to that calculated from the resolution of the mass spectrometer.

The number of fissions/min. observed and the fission/alpha ratios show conclusively that U^{235} is responsible for at least seventy-five percent of the slow neutron fission observed in unseparated U. Since U^{234} is present only to 1 part in 17,000, it cannot be excluded that U^{234} does undergo some slow neutron fission, but the total contribution of U^{234}, if any, is small.

Fast neutron tests.—Further tests were made of U^{238} to see if the small numbers of fissions observed from it in the slow neutron tests, were due to fast neutrons. Measurements were made without paraffin, and with and without Cd surrounding the fission chamber, on the U^{238} sample from set No. 2 and also on a much larger sample, No. 3 (18.9 micrograms), subsequently collected under improved conditions. The data are recorded in Table II.

These results indicate that U^{238} undergoes fast neutron fission only. Furthermore, the number of fissions/microgram of U^{238} observed under these neutron intensity conditions, is sufficient to account for practically all the fast neutron fission observed from unseparated U.

The aid of the Research Corporation to Columbia University is gratefully acknowledged. The collection of the isotopes was supported by a grant from the University of Minnesota Graduate School.

A. O. NIER

Department of Physics,
University of Minnesota,
Minneapolis, Minnesota,

E. T. BOOTH
J. R. DUNNING
A. V. GROSSE

Department of Physics,
Columbia University,
New York, New York,
April 3, 1940.

* Publication assisted by the Ernest Kempton Adams Fund for Physical Research of Columbia University.

[1] Nier, Booth, Dunning and Grosse, Phys. Rev. 57, 546 (1940).

Shower Production by Mesotrons in Different Materials[1]

The apparatus used has already been described[2] and comprises a number of Geiger counter trays, each forming a sensitive area 20 by 20 cm, mounted in a vertical column and arranged in relation to the associated electrical circuits in such manner that the apparatus is only allowed to record when a ray passes through all of the trays. Below the top tray is placed a block of lead 18 cm thick, or its mass equivalent in other materials, so that all records by the apparatus are initiated by a ray which is capable of passing through at least this thickness of material. When a ray passes through all of the trays, any shower rays accompanying it are recorded separately by the individual counters which they excite, the record being a photograph of spots of light from the mirrors of a number of electroscopes—one for each counter. The whole apparatus is mounted below a 30-foot column of water contained in a large water tank.

With the above apparatus the authors measured the numbers of one-ray showers, two-ray showers, three-ray showers, etc., produced in lead last August, and the *present experiments extend the measurements to lead, tin, iron, and magnesium.*

In dealing with the various materials, it was necessary to have a thickness sufficiently great to insure that shower production through mesotrons had attained equilibrium. Thus, it was necessary to have the thickness comparable with or greater than the range of the electrons. In order that one might be free from complications involved in variation of mesotron intensity by different absorptions in the different elements, it was arranged that, in the case of each element, the total equivalent thickness as regards mass absorption should be the same, the balance being adjusted for convenience in each case by the choice of a suitable thickness of lead above the material under examination.

Figure 1 shows the results. Horizontally are plotted the atomic numbers of the elements concerned. The ordinates represent the numbers of showers, of the kind cited, associated with the passage of 1000 mesotrons through the apparatus.

The two-electron, and perhaps the three-electron, showers showed frequency of occurrence which is independent of the atomic number within the limits of accuracy of the experiments; but the one-electron showers show a marked dependence upon atomic number, a dependence sufficiently strong to dominate the situation even if we should plot a curve representing the total number of shower rays associated with 1000 mesotrons. These results are not in harmony with the elementary conclusions from Bhabha's theory, which predicts results practically independent of atomic number. As shown in our former paper,[1] however, the data for the actual numbers of showers agree, as regards order of magnitude, with the theoretical predictions.

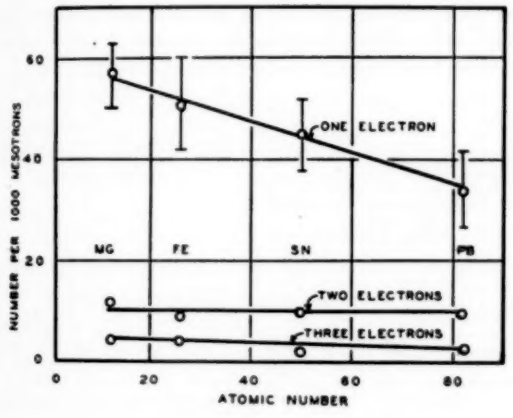

FIG. 1.

It is a curious fact that the regularity of the graphs for the actual data is greater than one might expect on the basis of the statistical uncertainty indicated in the usual way by the vertical. This is a matter which may have a rather profound significance in relation to processes involved.

W. F. G. SWANN
W. E. RAMSEY

Bartol Research Foundation,
The Franklin Institute,
Swarthmore, Pennsylvania,
March 26, 1940.

[1] Presented at the New York Meeting of the American Physical Society, February 23–24, 1940 (Phys. Rev. **57**, 554(A) (1940)).
[2] W. F. G. Swann and W. E. Ramsey, Phys. Rev. **56**, 378 (1939); W. F. G. Swann, Rev. Mod. Phys. **11**, 242 (1939).

Fission of the Separated Isotopes of Uranium*

Samples of the separated isotopes of uranium have been prepared with a mass spectrograph. UCl_4 was vaporized in a furnace, and the electron source for ion formation was placed inside the furnace. The upper entrance slit of the analyzer was also mounted on the furnace to avoid condensation of UCl_4. With a beam current of U^{235+} of 6×10^{-8} amp., about 1.8 microgram of U^{235} was collected on a Pt strip in three hours. The corresponding amounts of $U^{234+235}$ were collected on an adjacent Pt strip. A third Pt strip, mounted on the opposite side of the U^{235} collector, showed no measurable α-emission. The α-count for the U^{235} sample was 0.6 ± 0.1 per minute, and for the $U^{235+234}$ sample 0.6 ± 0.1 per minute.

The fission of the separated isotopes was tested by bombarding with slow neutrons from the Columbia cyclotron. The $U^{234+235}$ sample gave 3.7 ± 0.4 fissions/minute, and the U^{238} sample gave 0.1 ± 0.1 fission/minute. This shows definitely that U^{238} is not responsible for slow neutron fission in uranium, and confirms the results previously reported.[1]

K. H. KINGDON
H. C. POLLOCK

Research Laboratory,
General Electric Company,
Schenectady, New York,

E. T. BOOTH
J. R. DUNNING

Columbia University,
New York, New York,
March 20, 1940.

* Publication assisted by the Ernest Kempton Adams Fund for Physical Research of Columbia University.
[1] Nier, Booth, Dunning and Grosse, Phys. Rev. **57**, 546 (1940).

Collisions of Alpha-Particles with Chlorine Nuclei

The cloud tracks of about 700,000 thorium (C+C′) alpha-particles have been photographed with a stereoscopic camera. A large-diameter cloud chamber filled with methyl-chloride and helium was used. In addition to the range and velocity measurements obtained for carbon recoil nuclei,[1] forty-one selected forks ascribed to collisions of alpha-particles with chlorine nuclei have been analyzed, the results of which are presented here in Fig. 1. The analysis was carried out with the same procedure as that used for the carbon collisions by one of us (G. A. W.), the value 36 for the atomic weight of chlorine being used throughout.

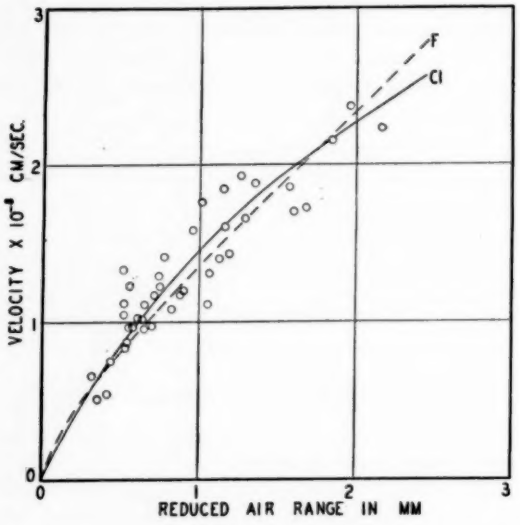

FIG. 1. Range-velocity curve for chlorine recoil atoms in methyl-chloride and helium.

The range-velocity curve for recoil fluorine nuclei as obtained by Feather[2] is included for comparison (broken curve). No outstanding similarity is observed in the shape of the fluorine and chlorine curves for the region of recoil ranges considered, although such might have been expected from Anthony's[3] observations. The range-velocity curve for chlorine obtained from that for fluorine by the empirical relation given by Blackett and Lees[4] gives poor agreement with the present results.

WILBUR HANSEN
GERALD A. WRENSHALL

Sloane Physics Laboratory,
Yale University,
New Haven, Connecticut,
March 26, 1940.

[1] G. A. Wrenshall, to appear soon in the *Physical Review*.
[2] N. Feather, Proc. Roy. Soc. **A141**, 194–209 (1933).
[3] R. L. Anthony, Phys. Rev. [2] **50**, 726–732 (1936).
[4] P. M. S. Blackett and D. S. Lees, Proc. Roy. Soc. **A134**, 658–671 (1932).

A New Radioactive Isotope of Masurium, $_{43}Ma^{101}$*

An accurate study of the 24-min. period produced in molybdenum by bombardment with slow neutrons made it clear that this period should be analyzed into two. This point was first noticed in a very short exposure, in which the decay curve showed a distinct convex curvature.

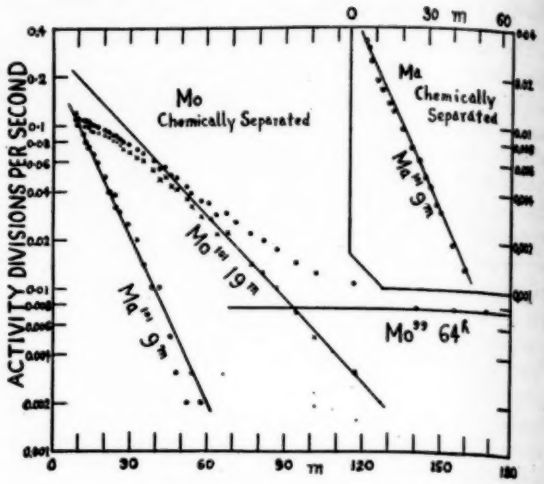

FIG. 1. The decay curves obtained for the chemically separated masurium and molybdenum fractions.

A very quick chemical separation of the molybdenum sample into the masurium fraction and the molybdenum fraction after a slow neutron bombardment, enabled us to find a new masurium isotope, Ma^{101} which emits β-rays of about 1.14×10^6 ev in energy (K-U upper limit) with a half-life of 9 ± 1 min., while the mother isotope Mo^{101} decays with a half-life of 19 ± 1 min. emitting β-rays of 1.78×10^6 ev in energy. The decay curves for the chemically separated molybdenum and masurium fractions are given in Fig. 1.

Another masurium isotope Ma^{99} has been found by Seaborg and Segrè,[1] the half-life of which is 6 hours but it emits very soft β-rays.[2,3] For the investigation of some special chemical nature of masurium, it would be much more convenient to use Ma^{101} rather than Ma^{99} because it is produced very strongly by bombardment with slow neutrons and also it emits energetic β-rays.

We are indebted to Dr. Y. Nishina and Professor K. Kimura for their valuable help and discussions. The assistance given by Mr. Matsuura, Mr. Saito and Mr. Mori is highly appreciated. We wish to acknowledge the financial support given by the Japan Society for the Promotion of Scientific Research, Oji Paper Manufacturing Company, Mitsui Ho-Onkwai Foundation, Tokyo Electric Light Company and Japan Wireless Telegraph Company.

R. SAGANE
S. KOJIMA
G. MIYAMOTO
M. IKAWA

Department of Physics,
Department of Chemistry,
Tokyo Imperial University,
Tokyo, Japan,
March 1, 1940.

* Reported at the meeting held on December 13, 1939 at the Institute of Physical and Chemical Research.
[1] G. T. Seaborg and E. Segrè, Phys. Rev. **55**, 808 (1939).
[2] By bombardment with protons, four periods, 0.5 min., 31 min., 53 min. and 110 hr. have been found, but not much has been reported yet. Du Bridge, Barnes, Buck and Strain, Phys. Rev. **53**, 447 (1938); Sherr, Henderson, White, Delsasso and Ridenour, Phys. Rev. **53**, 948 (1938); Ewing, Perry and McCreary, Phys. Rev. **59**, 1136 (1939).
[3] By bombardment with deuterons, several long periods have been reported. C. Perrier and E. Segrè, J. Chem. Phys. **5**, 712 (1937); Nature **140**, 193 (1937); B. N. Cacciapuoti and E. Segrè, Phys. Rev. **52**, 1252 (1937); B. N. Cacciapuoti, Phys. Rev. **55**, 110 (1938).

On the Dynamics of Complex Fission

We wish to report preliminary results of an investigation of the large amplitude distortions of a nucleus undergoing fission. The nucleus is assumed to have a uniform charge and mass density and a constant volume for all distortions. The radius vector r is expanded in a series of Legendre polynomials $r=R(1+\Sigma a_n P_n)$, and the values of a_0 and a_1 are adjusted to insure constancy of the volume and center of gravity. An estimate of the quantum excitation energies shows that only the first five harmonics need be considered. The potential energy of distortion, including all terms so far evaluated, is given by

$$\begin{aligned}\Delta E=4\pi R^2O\{&0.4(1-x)a_2^2+(0.7143-0.4082x)a_3^2\\&+(1-0.3704x)a_4^2+(1.2727-0.3306x)a_5^2\\&-(0.03810+0.07619x)a_2^3-(0.07619+0.2503x)a_2a_3^2\\&-(0.1143+0.3429x)a_2^2a_4-(0.05195+0.2226x)a_3^2a_4\\&-(0.1732+0.6702x)a_2a_3a_5-(0.2171-0.2563x)a_2^4\\&-(1.3615-1.0934x)a_2^2a_3^2+(0.09350+0.03206x)a_2^5\},\end{aligned}$$

where $2x=(3\varepsilon^2e^2/5R)/(4\pi R^2O)$ and O is the surface tension.

The following conclusions may be drawn from this formula. (1) There are large coupling terms between odd and even harmonics. These provide a possible explanation of the marked asymmetry of fission.[1] Bohr and Wheeler[2] have neglected these coupling terms. (2) The coupling between a_2 and a_4 is such as to give an equatorial bulge to the drop when it is on the road to fission.[3] The drop is pinched in near both poles; this would lead to ternary fission were it not for the excitation of the third harmonic which causes one of the preformed droplets to come off first, leaving a residual fragment which has not a sufficiently high excitation energy for its low charge number to divide further. However, it seems possible that such a ternary fission may occasionally be observed, in view of the fact that the saddle point for this mode of fission corresponds to $a_3=0$, and moreover, appears to lie at very low energies. Thus, whether fission occurs principally through the coupling of a_2 and a_3 or through the coupling of a_2 and a_4, in either case the fragments are of unequal sizes. According to the experiments, it is very improbable that the nucleus should divide into nearly equal fragments.[1, 4] (3) The coupling between a_2 and a_3 leads to an energy surface which has been investigated for a wide range in x. We have assumed a_3 to be of the order of a_2^2 and taken all terms in ΔE up through the fifth order in a_2. For $x=0.75$ we find a saddle point at $a_2=0.66$, $a_3=0.30$ with an activation energy $E_f=13$ Mev (assuming the surface energy of uranium to be 500 Mev); for $x=0.85$ there is a saddle point with $a_2=0.65$, $a_3=0.25$ and $E_f=6$ Mev. For such large amplitudes, the terms considered can give only a rough description of the fission process; moreover, theoretical uncertainties in the values of the nuclear radius and surface tension make any exact estimate impossible. These results are nevertheless of the right order of magnitude to explain the observed fission of uranium. (4) The energy surface for the a_2-a_4 coupling has been investigated for terms up through the fourth order in a_2 assuming that a_4 is of the order of a_2^2. For $x=0.75$ there is a saddle point at $a_2=0.47$, $a_4=0.057$ with $E_f=4.4$ Mev and for $x=0.85$ we find one at $a_2=0.31$, $a_4=0.029$ with $E_f=1.1$ Mev. (5) With all the mutual coupling terms for a_2, a_3 and a_4 included, there are two roots of the extremalizing equations which are of interest. One of these corresponds to $a_3=0$ and reproduces the results already stated in (4). The other leads to a reduction of the amplitudes and activation energies evaluated in (3). We have not yet included a sufficient number of terms to give a significant estimate of this effect, but it appears to be of the order of several Mev. In view of this fact and especially because of the modifications that may arise with the inclusion of higher order terms, we cannot conclude that the a_2-a_4 mode of fission requires less activation energy than the a_2-a_3 mode. (6) An estimate of the particle sizes to be expected from the a_2-a_3 mode of fission can be made by using the relative amplitudes of a_1, a_2 and a_3 at the saddle point. The two fission products have approximately 0.4 and 0.6 the mass of the original nucleus, this result being insensitive to the value of x. For the a_2-a_4 mode of fission the particle sizes are roughly in the ratio of 1:3 for binary fission and 1:2:1 for ternary fission. The first of these is consistent with the experimental energy peaks.[1]

Finally we want to emphasize that certain conclusions of this note are subject to possible modification due to the inclusion of higher order terms which are probably not small. A more detailed discussion of the dynamics of fission will be published shortly.[5]

R. D. PRESENT
J. K. KNIPP

Purdue University,
Lafayette, Indiana,
April 1, 1940.

[1] Booth, Dunning and Slack, Phys. Rev. **55**, 981 (1939); M. H. Kanner and H. H. Barschall, Phys. Rev. **57**, 372 (1940).
[2] N. Bohr and J. A. Wheeler, Phys. Rev. **56**, 426 (1939).
[3] In contradiction to the statement of Bohr and Wheeler, reference 2, p. 433, that a_4 contributes a concavity about the equatorial belt such as to lead continuously to a dumb-bell shaped figure. We do not check the higher order coefficients of their Eq. (22) and we note further that Eq. (23) is inconsistent in sign and magnitude with Eq. (22).
[4] L. A. Turner, Rev. Mod. Phys. **12**, 1 (1940), cf. table on p. 23.
[5] Related biophysical problems are being considered.

Radio Isotopes of Chromium

We have investigated the induced radioactivities of chromium by the aid of our cyclotron. The results are summarized as follows:

(I) *Deuteron bombardment.* The exposure of chromium metal to about 100 microampere hours of 3-Mev deuterons yields chemically identified chromium isotopes of half-lives 1.6 hours and about 14 days.

(II) *Slow neutron bombardment.* In this case activity induced in chromium was very weak. The following periods were established: 2.8 hr., 14 hr., 1.7 hr. The purity of the sample was chemically tested and Al (1.1 percent), Si (0.17 percent), Fe (0.7 percent), Mn(>0.02 percent) were shown as impurities. Therefore the 2.8-hour activity seems to be due to Si^{31} (2.5 hours) or Mn^{56} (2.5 hours), and the 14-hour activity is probably due to Na^{24} produced in aluminum impurity by the reaction Al-n-α-Na, as a considerable number of fast neutrons were always among slow neutrons. The period 1.7 hours is very near to the

period 1.6 hours observed in the case of deuteron bombardment, and therefore can probably be ascribed to an isotope of chromium, but unfortunately no chemical identification was done because of very weak intensity.

(III) *Fast neutron bombardment.* Periods of 3–4 hours, 14 hours and about 12 days were observed. In this case the activities were very weak. The 3–4-hour activity is very likely due to V^{50} (3.7 hours) according to the reaction Cr^{50}-n-p. The 14-hour activity is probably Na^{24} as in the case of slow neutron bombardment. The period 12 days is probably due to the same activity (14 days), as was observed in the case of deuteron bombardment.

Now chromium has four stable isotopes Cr^{50}, Cr^{52}, Cr^{53}, Cr^{54}. According to the above results we can attribute the 1.6-hour activity to Cr^{55}, and the longer period (about 14 days) activity to Cr^{51}.

A more detailed account of this work will be given later in the *Scientific Papers of the Institute of Physical and Chemical Research.*

In conclusion we wish to express our best thanks to Dr. Y. Nishina for his kind interest.

TOSHIO AMAKI
TAKEO IIMORI
ASAO SUGIMOTO

Nuclear Research Laboratory,
Institute of Physical and Chemical Research,
Tokyo, Japan,
January 10, 1940.

Spectroscopic Evidence for the B_2 Molecule

Modern valence theories lead one to expect that a molecule formed from two boron atoms should be stable.[1] The stability of B_2H_6 also suggests that a stable bond between two boron atoms is possible. But no evidence for the existence of the B_2 molecule has yet been reported. The observation of a B_2 spectrum, apart from showing that B_2 exists, also would be of interest because it would make possible a determination of the spin and the statistics of the boron nuclei.

We have therefore tried to observe a B_2 spectrum in a discharge through helium of about 10 mm pressure to which a trace of BCl_3 was added. Under these conditions we have been able to find between 3300 and 3170A a system of new bands having a simple fine structure (P and R branches only). The following considerations prove definitely that the emitter of these bands is the B_2 molecule whose existence is thus established for the first time.

(1) A clear intensity alternation is observed in the two bands that are least overlapped by others, the even-numbered lines being the strong ones. This shows definitely that the carrier of the spectrum is a homonuclear molecule.

(2) Each band is accompanied by a weaker isotopic band, whose intensity and displacement from the main band is accountable only on the assumption that the main bands are due to $B^{11}B^{11}$, the weaker bands to $B^{11}B^{10}$. The $B^{11}B^{10}$ bands, as is to be expected, do not show any intensity alternation. There are indications also of bands due to $B^{10}B^{10}$.

Only two sequences of the new system, $\Delta v=0$ and $\Delta v=+1$, have thus far been observed. A preliminary vibrational analysis yields the following formula for the band heads:

$$\nu=30546.1+(929.3v-2.75v^2)-(1035.2v''-9.58v''^2).$$

A preliminary rotational analysis yields $B_0''=1.205$ cm^{-1}, $B_0'=1.155$ cm^{-1} and consequently for the internuclear distances $r_0''=1.595\times10^{-8}$ cm, $r_0'=1.628\times10^{-8}$ cm.

A rough estimate leads to a value of the intensity ratio of the strong and weak lines between 2 : 1 and 1.5 : 1 which would mean that the spin of the B^{11} nucleus is very probably $I=\frac{3}{2}$. However, more accurate intensity measurements are necessary to fix definitely this value. By such measurements we also hope to determine the spin of the B^{10} nucleus.

The fact that the bands have only one P and one R branch shows that they represent a $\Sigma-\Sigma$ transition. Since the lines with even values of J are the strong ones it follows, if Fermi statistics is assumed for the B^{11} nucleus, that the lower state is a Σ_g state and the upper state Σ_u^-. From the electron configuration one would expect the ground state of B_2 to be $^3\Sigma_g^-$ and a $^3\Sigma_u^-\rightarrow{}^3\Sigma_g^-$ transition to be a strong one. It seems very likely that the new bands are this transition, the triplet splitting being too small for detection. It is significant to find that the assumption of Fermi statistics for the B^{11} nuclei leads to reasonable results since it is the statistics one would expect for this nucleus on the basis of modern nuclear theory.

When nitrogen was added to the discharge in He and BCl_3 two new band systems were found, one around 3600A, the other around 3225A. The former can be assigned definitely, the latter probably to the BN molecule whose spectrum has not been previously observed. When hydrogen was added two new electronic transitions of the BH molecule were found at 3415 and at 3100A.

A more detailed report of our experiments will be submitted to the *Canadian Journal of Research.*

This investigation has been supported by a grant from the Penrose fund of the American Philosophical Society and by the National Research Council of Canada. To both organizations we would like to express our thanks.

A. E. DOUGLAS
G. HERZBERG

Department of Physics,
University of Saskatchewan,
Saskatoon, Saskatchewan, Canada,
March 25, 1940.

[1] See, for example, G. Herzberg, *Molecular Spectra and Molecular Structure I* (Prentice-Hall, New York, 1939), p. 392.